Model analysis, Parameter Estimation and Control of a Synchronous Generator

PhD thesis

DOI: 10.18136/PE.2015.583

Written by: Attila Fodor

Supervisors: Dr. Katalin Hangos, Dr. Attila Magyar

University of Pannonia
Doctoral School of Information Science and Technology

2015

Model analysis, Parameter Estimation and Control of a Synchronous Generator

Értekezés doktori (PhD) fokozat elnyerése érdekében
a Pannon Egyetem Informatikai Tudományok
Doktori Iskolájához tartozóan

Írta:
Fodor Attila

Konzulens: Dr. Hangos Katalin, Dr. Magyar Attila

Elfogadásra javaslom (igen / nem)

(aláírás)

A jelölt a doktori szigorlaton .....%-ot ért el

Veszprém .....
a Szigorlati Bizottság elnöke

Az értekezést bírálóként elfogadásra javaslom:

Bíráló neve: ..... (igen / nem)

(aláírás)

Bíráló neve: ..... (igen / nem)

(aláírás)

A jelölt az értekezés nyilvános vitáján .....%-ot ért el

Veszprém, ...
a Bíráló Bizottság elnöke

A doktori (PhD) oklevél minősítése .....

.....
Az EDHT elnöke

Contents

Acknowledgement

The author of this dissertation wishes to acknowledge the continuous support and help of his supervisors, Prof. Katalin Hangos and Dr. Attila Magyar. I could not have accomplished this dissertation without their work and patience.

Furthermore, the author wishes to thank to the actual and the former teachers and colleagues in the Department of Electrical Engineering and Information Systems and previously in Department of Automation for their continuous support and companionship.

Expressions of gratitude and apology are directed to my wife, my family and my colleagues and friends, who patiently endured the long working hours.

We acknowledge the financial support of this work by the Hungarian State and the European Union under the TAMOP-4.2.2.A-11/1/ KONV-2012-0072 project.

This work was also supported in part by the Hungarian Research Fund through grant 83440.

Abstract

Global warming caused by greenhouse gases and the constantly growing use of electricity of the industry is forcing power plants operator's engineers to achieve the higher efficiency of the power plants. In many cases, increasing the efficiency can be achieved by modernization of the control system, as it is done in the MVM Paks Nuclear Power Plant.

The dissertation deals with the synchronous generator used in nuclear power plants, thermal power plants and hydropower plants, presents the design of an advanced controller for its power control together with the necessary preliminary steps.

The basis of the design is the state-space model of the synchronous generator. Simple but effective model analysis methods were proposed for model verification and for preliminary parameter selection in parameter estimation of the synchronous generator. Based on the result of the sensitivity analysis, it is possible to define 4 groups of parameters. Based on this results 9 parameters were selected to parameter estimation.

A parameter estimation method using passive industrial measurement was also proposed for a synchronous generator that uses passive measurement of power changing transients. The quality of the parameter estimation was characterized using the quality, the fit and the dependence of the error function on the parameters. The confidence region was also estimated from the level sets of the error function.

Based on the model and the parameter estimation a servo version of a Linear Quadratic Regulator (LQR) has been proposed for control of the industrial synchronous generator operating in MVM Paks NPP. The proposed LQ-servo controller was verified by simulation using step changes in active power. Based on the simulation the developed LQ-servo controller provides better control than the existing PID controllers in MVM Paks NPP.

Abstract

Az üvegházhatású gázok okozta globális felmelegedés és az ipar folyamatosan növekedő villamos energiafelhasználása arra kényszeríti az erőműveket üzemeltető mérnököket, hogy minél nagyobb hatásfokot próbáljanak elérni az erőművekben. A hatásfok növelését sok esetben az irányítástechnikai rendszer korszerűsítésével is el lehet érni, mint ahogyan azt a MVM Paksi Atomerőművében is teszik. A dolgozat az atom-, hő- és vízerőművekben használt berendezés, a szinkron generátorhoz használható szabályozó tervezését és annak lépéseit mutatja be.

A kutatásaim során egy fizikai törvényeken alapuló állapottér modellt használtam. A modell analízis egyszerű eszközeit használva elvégeztem a szinkron generátor modelljének verifikációját és stabilitás vizsgálatát. Elvégeztem a modell paramétereinek az érzékenységvizsgálatát, annak eredményeit felhasználva 4 csoportba soroltam a szinkron generátor modelljének a paramétereit. Ezeket felhasználva a paraméterek közül meghatároztam azokat a paramétereket, amelyeket becsülni lehet.

Passzív ipari mérések alapján elvégeztem a MVM Paksi Atomerőmű egyik szinkron generátorának a paraméterbecslését terhelési tranziens felhasználásával. A paraméterbecslés jóságát ellenőriztem az illeszkedés és a paraméterek függvényében is, közelítő konfidencia intervallumokat határoztam meg a hibafüggvény szinthalmazaiból.

A modellt és a becsült paramétereket felhasználva egy observer alapú LQ-servo (Linear Quadratic) szabályozót terveztem a Paksi Atomerőmű generátorához. A megtervezett szabályozó stabilitását szimulácókkal ellenőriztem. A szimulációk alapján a megtervezett új LQ-servo szabályozó jobb szabályozásra képes, mint a jelenleg használt PID szabályozók.

Abstrakt

Ingenieure, die Kraftwerke betreiben, werden durch die globale Erwärmung, die wegen der Treibhausgase und des ständig wachsenden Stromverbrauchs in der Industrie entsteht, gezwungen, höhere Effizienz der Kraftwerke zu erreichen. Die Effizienzerhöhung kann in vielen Fällen durch die Modernisierung der Prozessleittechnik erreicht werden, wie das in MVM Kernkraftwerk Paks getan wird.

Die Dissertation zeigt die Ausrüstung, die in Kern-, Heiz- und Wasserkraftwerken verwendet wird, bzw. die Schritte der Systemplanung eines Regulators, welcher zu den Synchrongeneratoren gebraucht werden kann. Während meiner Forschungen wurde ein Zustandsraummodell verwendet, das auf physischen Gesetzen basierte. Die Verifikation des Synchrongenerators und die Stabilitätsuntersuchung wurden durch die einfachen Methoden der Modellanalyse durchgeführt.

Nachdem die Sensitivitätsanalyse durchgeführt worden war, ließen sich anhand deren Ergebnisse 4 Parametergruppen des Synchrongenerators definieren. Mit dieser Methode wurden die messbaren Parameter bestimmt. Die Parameterschätzung eines Synchrongenerators wurde durch passive Industriemessungen im Kernkraftwerk Paks mit Verwendung Belastungstransienten durchgeführt. Die Qualität der Parameterschätzung wurde auch in der Funktion der Passung und der Parameter kontrolliert. Annähernde konfidentielle Intervalle wurden aus den Niveaumengen der Fehlerfunktion definiert.

Ein LQ-Servo-Regulator (Linear Quadratic) wurde mit Hilfe des Modells und der geschätzten Parameter zum Atomkraftwerksgenerator geplant. Die Stabilität des geplanten Regulators wurde durch die Simulationstechnik kontrolliert. Der entwickelte LQ-Servo-Regulator ermöglicht aufgrund der Simulationen bessere Regelungen als die vorhandenen PID-Regler.

Chapter 1

Introduction

1.1 Motivation and background

Mankind wanted to use the possibility of the rotation long-long time ago, using the technical advancement of the age. An example of this is the wheel, the horse-mill of the antiquity and other applications (see: [69] and [15]). The rotating actuation can be easily applied using electricity in the rotating electrical machines (e.g.: induction machine, synchronous machine, direct-current machine). This principle is used even today for the electrical generators in power plants [47].

Rotating electrical machines, electrical motors and generators form a basic class of units in electrical engineering, and present a challenge in control-oriented applications because of their inherent nonlinearities. Although control-related methods, such as dynamic modeling, model analysis, parameter estimation, controller design and diagnosis is a traditional and well investigated area in both the classical linear and the advanced nonlinear systems and control theory, but these challenges and the practical importance of the electrical rotating machines call for a continuous advancing of their control using the recent results in systems and control theory (see e.g. [38], [39] and [40]).

This work is focused a class of rotating electrical machines, the so called synchronous machines, where both the synchronous motors and generators are of great practical importance. A number of fundamental books and papers deal with the control problems of induction motors (see e.g. [90], [93] and [94]), but the modeling, model analysis and control design problems of synchronous generators are much less investigated, maybe because of their restricted application area. These generators are widely used in industrial power plants, where the safety-critical nature of their operation makes the use of advanced control approaches difficult, and thus very rare.

Unfortunately, the use of advanced control methods for a nonlinear system (see e.g. [38] and [9]) requires the effective utilization of the specialities of the system to be controlled and that of the control task, otherwise the general purpose methods lead to infeasible or practically intractable problems. Therefore, an interdisciplinary holistic approach was adopted to carry out the model analysis, parameter estimation and controller design of an industrial synchronous generator to overcome this obstacle.

Beside of the traditional, well-established and robust linear controller design pre-

sented in this thesis, the first steps to explore the applicability of advanced nonlinear techniques have also been made in a follow-up research [O7].

1.2 Synchronous generators as dynamic systems and their control

Nuclear power plants are important energy providers worldwide. They produce energy mainly in the form of electrical energy, the transportation and distribution of which is performed by using large-scale electrical power grid. This grid should be operated in a balanced way taking the time varying power demand of the consumers into account. From the viewpoint of the power grid the electric power generation of nuclear power is characterized by the operation of the electrical generators.

It is obvious, since the final stage of the power production in a nuclear power plant (NPP) includes a synchronous generator (SG) that is driven by a turbine. A synchronous generator operating in a NPP and its controller is the subject of the present thesis.

Besides the active power produced by a power plant, other characteristics are also of great importance. Most notably the reactive power and the frequency of the produced energy are also essential. The importance of the reactive power is indicated by the fact that insufficient reactive power of the system may result in voltage collapse. Therefore, it is widely accepted that the consumers of the reactive power should pay for it and the producers of the reactive power are enumerated [29]. Therefore, the power controllers of nuclear power plants should also take the production of the reactive power into account.

Because of the above described requirements on the operation of the large-scale electrical power grids, power plants should not only be able to follow the time-varying active and reactive power demand of the consumers and the central dispatch center, but also keep the quality indicators (frequency, waveform, total harmonic distortion) of the grid on the expected level. This can be achieved by applying proper control methods based on dynamic models of plant (see e.g. [11], [56]) and the involved generators.

1.2.1 SG modeling and analysis in the literature

Because of the specialities and great practical importance of synchronous generators in power plants, their modeling for control purposes is well investigated in the literature. Besides of the basic textbooks (see e.g. [7]) that develop general purpose dynamic models for SGs, there are several papers that describe the modeling and use the developed models for the design of various controllers, see e.g. [55, 25].

Two SG models are presented and analyzed in [13]. One model is developed in the (d, q) natural reference frame and the other one is referred to the (d, q) stator reference frame. The models are validated using a 75 kVA salient-pole synchronous machine with damper windings. In [66] a new method of SG modeling is presented taking an infinite inner resistance into account, and a statistical technique for determining the parameters of the synchronous machine is proposed.

The SG models in [97], [98], [65], [26] are linear models, which do not consider the mechanical motion equation. This implies that they do not describe neither the rotor position nor the loading angle (δ). However, the loading angle is important system variable because the SG may fall out of sync if the loading angle exceeds 90^o.

A simplified linear mathematical model of a SG with an excitation system is presented in [64], and the stability of the model is investigated by simulation. Angular velocity of the machine is assumed to be constant in this model, hence it is not able to calculate the load angle (δ).

A suitable method for time-domain identification of the parameters of a laboratory size synchronous machine (380 V, 3 kVA) is presented in [97] that uses a hybrid state space model. The angular velocity of the SG has been fixed to the synchronous speed in the model. A load rejection test of a combined resistive/inductive load is performed for the parameter identification.

Because of the highly nonlinear nature of the dynamic models of synchronous machines, the need for applying methods of modern systems and control theory have also appeared in the literature recently.

In [98] a simple linear time-invariant state space model of a SG is developed for load-rejection tests and the model was tested in a laboratory size generator (1.5 kVA).

A third order nonlinear state space model of a synchronous generator has also been proposed in [27], where field voltage was considered as input, active output power and rotor angle were considered as outputs.

A square-root unscented Kalman filter has been applied recently to simultaneously estimate state variables and unknown generator parameters in [45]. Here a third order model with field voltage input has been considered that has been equipped with suitable measurement and output equations.

1.2.2 Generator controllers in the literature

Several excellent books were fully devoted to the control of induction motors (IM) (see. e.g.: [90], [91], [94] and [93]). The modeling, stability and the control of the synchronous generator is a less investigated area than the induction motor because of its limited use.

Third-order nonlinear models are commonly used in control theory for the stability analysis of both open loop and closed loop synchronous machines (SM). The ability of these models to describe the electrical machine dynamics has been tested experimentally in [8] using a 7 kVA lab-scale SG.

In addition to conventional control tasks related to synchronous generators in power plants, special purpose SG control studies are also reported. The behavior of a SG during short-circuit is investigated in [30]. This article reports the short-circuit characteristics of a stand-alone turbo-generator driven by separately excited DC motors, the applied model of the SG is similar to that used in this paper.

A sliding mode controller is proposed in [88] using a non-linear SG model, where the stability of the controlled model is also analyzed.

A new approach to SG output voltage control is presented in [65] applying H_∞

control theory, where the control strategy was based on the classical modeling of the SG. A technique to determine the effect of the field-voltage circuit during the load-rejection test of a large-rating salient-pole SG was presented in [26].

The presence of reactive power may cause overload effects on the line, circuit breakers, transformers, relays, but it cannot be transformed into mechanical power. In addition, the presence of reactive power requires to increase the dimension of cables used in the transmission line. Therefore the management of reactive power generation and consumption is well investigated in the literature. A recent paper [23] proposes reactive power compensation using a fuzzy logic controlled synchronous machine. Reactive power management is also a critical issue when dealing with the planning and operation of power networks. Its use for transmission line fault location and power system protection is described in [103].

A recent study [5] proposes a coordinated reactive power planning strategy among induction generators. According to this strategy, the total reactive power capability is obtained first and the limitations on deliverable power are deduced from it for each operation point.

An optimal reactive power flow incorporating static voltage stability is computed in [102] based on a multi-objective adaptive immune algorithm. The algorithm solves the optimal reactive power flow problem incorporating voltage stability.

In a power system, voltage stability margin improvement can and should also be done by regulating generator voltages, transformer tap settings and capacitor or reactor rated reactive powers. For this purpose, a reactive power rescheduling method with generator ranking has been proposed in [78].

Seen from a holistic view, electrical power systems should operate in an economic way with minimum possible operating cost and under normal operating conditions. To ensure this, a preventive controller for power systems has been presented in [96]. It encompasses many types of control actions, including generation rescheduling, load curtailment and network switching reactive compensation.

1.2.3 Controllers in nuclear power plants

Interesting advanced control applications can also be found in nuclear power plants. A robust strategy to cascade control of a TOPAZ II nuclear system has been presented in [4]. The control strategy is based on linearizing feedback control endowed with a modeling error estimator via a reduced order observer. The proposed strategy results in a control scheme which comprises a cascade approach. In the start-up regime this cascade operates two loops of control.

In [19], a MIMO reactor controller has been presented using soft computing methods. An on-line intelligent core controller for load following operations has been designed in this paper, based on a heuristic control algorithm, using a valid and updatable recurrent neutral network.

In [86], the performance of some control strategies for a power manoeuvering event was evaluated. The reactor-leading strategy showed a relatively weak performance although the reactor power followed the external power demand well. The turbine-leading strategy, that is widely used for commercial nuclear power plants, concluded to be still adoptable for a power control strategy.

1.3 The power control problem in a pressurized water NPP

MVM Paks NPP, where the investigated generators work, is located in Hungary, and operates four pressurized water (VVER-440/213 type) reactors with a total nominal electrical power of 2000 MW (see. [2]). Each reactor is equipped with two turbine-generator units that work in parallel. The turbo generator is a specific synchronous generator with a special cooling system.

Our study is concerned with the power control of MVM Paks NPP. In this section a brief overview of the plant from the generators point of view is given first, then a description of the power changing operations follows.

1.3.1 The role of the SG in the plant technology

The SG is located in the secondary circuit of a unit in MVM Paks NPP (see Fig. 1 for the flowchart the secondary circuit). Every nuclear unit operates six steam generators with capacity 450 t/h with a temperature of 260 °C and a pressure of 46 bar that interface the primary and secondary circuits [80], [31], [46]. These six steam generators are connected to two turbo-generators, three to each.

Every nuclear unit operates two independent secondary coolant circuits, that are controlled by independent control systems. In the first stage of the secondary coolant circuit there are three steam generators that provide steam for the turbines. There are three turbines in each secondary coolant circuit (one high pressure and two low pressure ones), attached to one synchronous generator and one exciter machine set on the same axis.

1.3.2 The power control system

The power control of a unit in MVM Paks NPP is performed by three loosely coupled controllers: the power controller of the reactor, the turbine power controller and the generator exciter controller. While the reactor power controller is mainly responsible for taking care of the total power, the turbine controller regulates the frequency and the generator controller deals with maintaining the proper ratio of the active and reactive power.

The detailed model-based analysis of the reactor power controller of a unit in MVM Paks NPP is reported in [35], that uses a simple dynamic model of the primary circuit based on first engineering principles.

As the generator controller operates relatively independently of the other two controllers involved in the power control, we aim at optimally re-design the generator controller using a simple control-oriented dynamic model in order to be able to maintain the desired active and reactive power level even under power changing operation conditions.

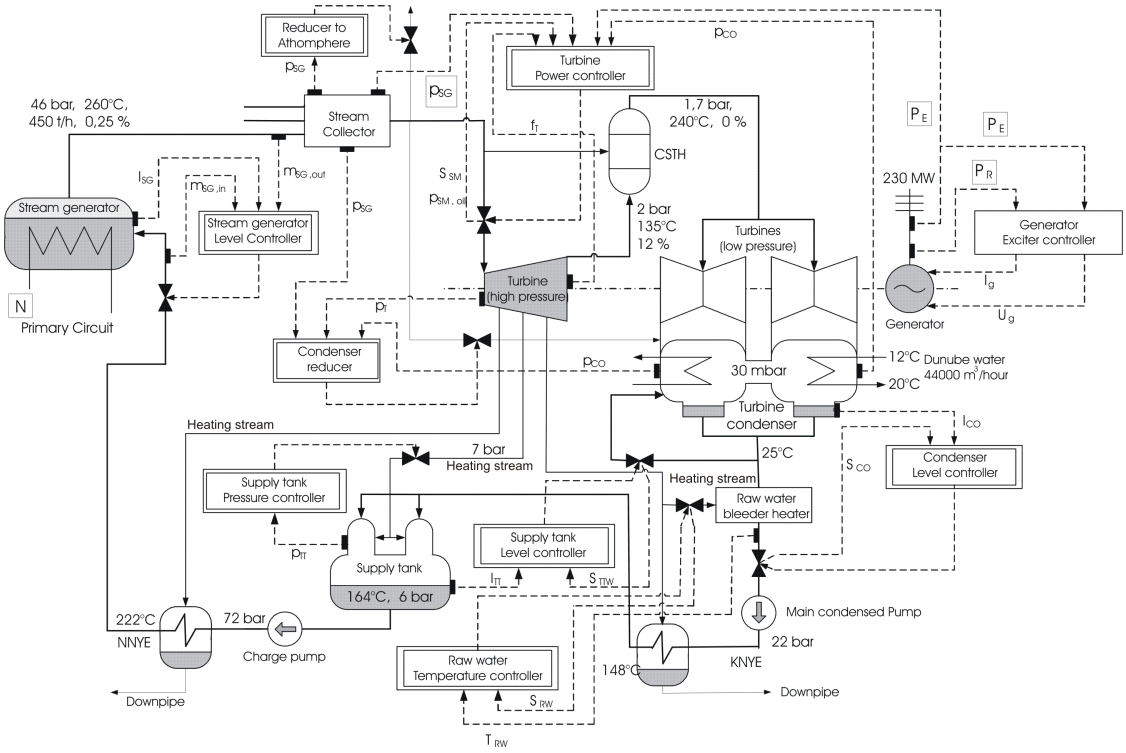

Figure 1: The schematic figure of the secondary circuit. Both the main operating units and the main controllers are shown.

1.3.3 Power changing operations

In Figure 2 the time varying output of a nuclear power plant, MVM Paks NPP is depicted during load changing transients. It can be seen that the reactive power (q_{out}) is also changing in the same way as the active power (p_{out}). Since a unit in the NPP of interest contains two generators, the same signals belonging to the two generators are both depicted.

It can be seen in Figure 2 that the reactive powers (q_{out}) of the SG are changing during the power switching. It can also be seen that the active power (p_{out}) of the generators follow the neutron flux which follows the control rod position of the nuclear reactor.

In the case presented by Figure 2 the active power was controlled by a classical PI controller with the manipulated input being the exciter voltage (v_F). On the other hand, no reactive power control policy was used in the NPP, therefore the *reactive power follows the change of the active power*.

1.4 Aim and structure of the thesis

The literature about synchronous generator control (see the first part of Section 1.2), however, does not take the special circumstances found in nuclear power plants into account, where load torque and exciter current are the measurable input variables (although load torque is only measured indirectly through the turbine steam load), and the important measurable output variables are the active and reactive power.

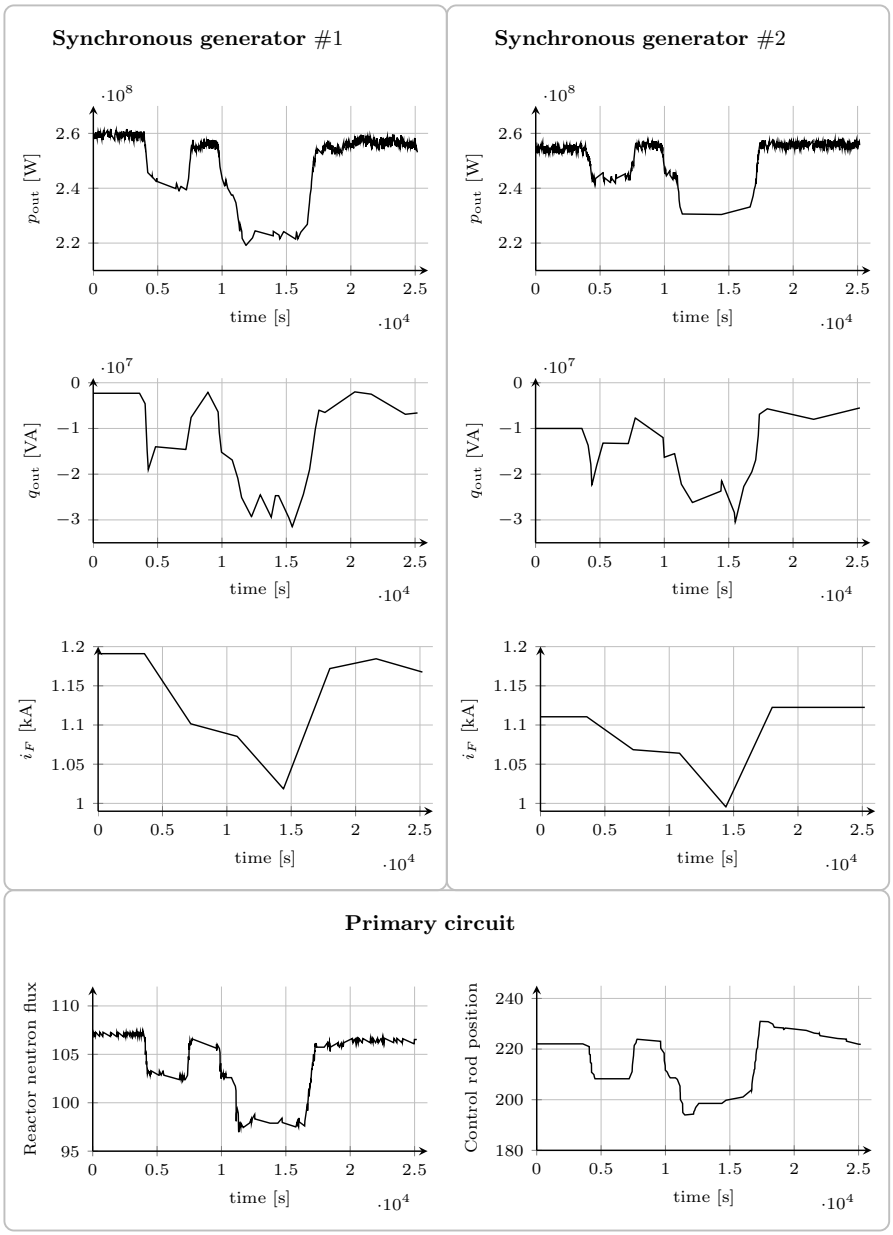

Figure 2: Effective and reactive power (p_{out} and q_{out}) and the exiting current (i_F) of two generators attached to the same reactor, the neutron flux and control rod position of the reactor during load changing transients. The close connection between the neutron flux and p_{out} is apparent. Because of the simple controller structure q_{out} follows p_{out}.

In addition, these papers do not describe the mechanical motion related to the SG, thus there is no possibility to give any information about the angular velocity and the loading angle, that are important state variables under industrial operating conditions. These facts require to develop special dynamic models for large industrial synchronous generators operating in nuclear power plants. Based on these models, model-based re-design of the generator controller can be applied so that it is able to control the active and reactive power of the power plant simultaneously. For controller design, however, the developed model should be verified against engineering intuition and its parameters estimated using measured data from the real power plant.

The first step of this work was to propose a simple dynamic model of a SG in a nuclear power plant for control studies (see Chapter 2), where the model development is largely based on [7], [6] and [17]. This chapter contains also the description and initial values of the parameters of the model.

Chapter 3 shows the model verification, as well as the methods and the results of the parametric sensitivity analysis (see Chapter 3). Based on the result of the sensitivity analysis, the parameters to be estimated could be determined. The sensitivity analysis was thus a preparatory step for the model parameter estimation.

In Chapter 4, an optimization-based method is proposed for estimating the model parameters from industrial measured data.

The final aim of this work was to design a MIMO servo controller that keeps the active power of a SG at the desired level, and performs reactive power reference tracking using the reactive power demand from the central dispatch center. The controller design and verification is described in Chapter 5.

Finally, the conclusion and the further work are presented in Chapter 6. This chapter summarizes the results, contains the list of own publications, and the thesis points.

The appendix of the dissertation contains the list of abbreviations and notations.

Chapter 2

The synchronous generator model

In this chapter the state-space model for a synchronous generator is described that will be used for stability analysis, parameter estimation and controller design.

The model development is largely based on [7], [6] and [17] but the special circumstances of the generator operation in the considered nuclear power plant have also been taken into account.

There are several synchronous machine (SM) models in the literature (e.g.: Coultes and Watson [24], Wamkeue at al. [99], [97] and [98], Loukianov at al. [55], Dehkordi at al. [28], Semlyen et al. [85], Mouni at al. [66] and [65], Tu et al. [89], Achilles et al. [3], Hansen et al. [42], Ramtharan et al. [77], Milano [62], Perdana [71], Gonzalez-Longatt et al. [36], Dehghani [27], Nanou et al. [67]) but the special requirements (the presence of active and reactive power equations the need for modeling amortisseur or dumper windings) called for an extension of the usual models. There are a few extended dynamics model in the literature [7], [6], [55], that required further improvements and classification.

It is important to note, however, that large industrial synchronous generators operating in other (e.g. hydro, gas or coal powered) types of power plant have similar operating conditions and grid requirements, therefore the resulting dynamical model is also applicable there.

Only the basic steps of the model development and the resulting model equations are described here using the notation list can be found in the Appendix (see Section 7.2).

2.1 The electrical submodel

For constructing the synchronous generator model, the following assumptions are made:

1. a symmetric tri-phase stator winding system in machine is assumed,
2. the machine has one field coil,
3. there are two amortisseur or damper windings in the machine,
4. all of the windings are magnetically coupled,

5. the flux linkage of the winding is the function of the rotor position,

6. the spatial distribution of the stator fluxes and apertures wave are considered to be sinusoidal,

7. stator and rotor permeability are assumed to be infinite

8. all the losses due to wiring, saturation, and slots can be neglected.

According to assumptions 4. and 5. the actual terminal voltage v of the windings can be written in the form

$$v = \pm \sum_{j=1}^{J} (r_j i_j) \pm \sum_{j=1}^{J} (\dot{\lambda}_j), \tag{1}$$

where i_j are the currents, r_j are the winding resistances, and λ_j are the flux linkages. The positive directions of the stator currents point out of the synchronous generator terminals.

Thereafter, the two stator electromagnetic fields, both traveling at rotor speed, were identified by decomposing each stator phase current under steady state into two components, one in phase with the electromagnetic field and the other phase shifted by 90^o. With the aboves, one can construct an airgap field with its maximum aligned to the rotor poles (d axis), while the other is aligned to the q axis (between poles).

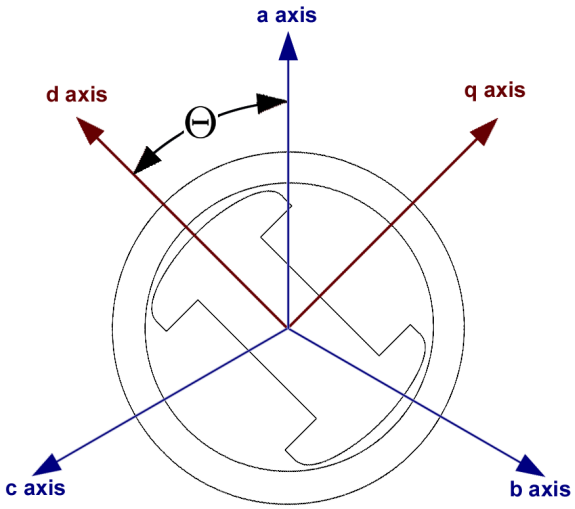

Figure 3: The abc and $0dq$ frames of the generator. The $0dq$ coordinate of frame is fixed to the rotor, abc coordinate frame is fixed the stator flux.

This change in the coordinates is called the Park's transformation [70] that gives

$$i_d = \frac{2}{3}\left[i_a \cos(\Theta) + i_b \cos\left(\Theta - \frac{2\pi}{3}\right) + i_c \cos\left(\Theta - \frac{4\pi}{3}\right)\right] \tag{2}$$

$$i_q = \frac{2}{3}\left[i_a \sin(\Theta) + i_b \sin\left(\Theta - \frac{2\pi}{3}\right) + i_c \sin\left(\Theta - \frac{4\pi}{3}\right)\right], \tag{3}$$

where i_a, i_b and i_c are the phase currents and Θ is the angle between the phase current i_a and the current i_d. During the eduction the angles are computed in radian. The Park's transformation uses three variables as d and q axis components (i_d and i_q) and the last one is the stationary current component (i_0), which is proportional to the zero-sequence current. By denoting vectors by boldface and matrices with capital boldface letters can write the new current components from the relationship

$$\boldsymbol{i}_{0dq} = \boldsymbol{P}\,\boldsymbol{i}_{abc}, \tag{4}$$

where the current vectors are

$$\boldsymbol{i}_{0dq} = \begin{bmatrix} i_0 & i_d & i_q \end{bmatrix}^T \quad \text{and} \quad \boldsymbol{i}_{abc} = \begin{bmatrix} i_a & i_b & i_c \end{bmatrix}^T, \tag{5}$$

and the Park's transformation matrix is

$$\boldsymbol{P} = \sqrt{\frac{2}{3}} \begin{bmatrix} \frac{1}{\sqrt{2}} & \frac{1}{\sqrt{2}} & \frac{1}{\sqrt{2}} \\ \cos(\Theta) & \cos(\Theta - \frac{2\pi}{3}) & \cos(\Theta - \frac{4\pi}{3}) \\ \sin(\Theta) & \sin(\Theta - \frac{2\pi}{3}) & \sin(\Theta - \frac{4\pi}{3}) \end{bmatrix}. \tag{6}$$

All flux components correspond to an electromagnetic field (EMF), the generator EMF is primarily along the rotor q axis. The angle between this EMF and the output voltage is the machine torque angle δ, where the phase a is the reference voltage of the output voltage. The angular position of the d axis (in radian) is in the form

$$\Theta = \omega_r t + \delta + \pi/2, \tag{7}$$

where ω_r is the rated synchronous angular frequency. Finally, the following voltage and linkage equations can be written

$$\boldsymbol{v}_{0dq} = \boldsymbol{P}\,\boldsymbol{v}_{abc} \quad \text{and} \quad \boldsymbol{\lambda}_{0dq} = \boldsymbol{P}\,\boldsymbol{\lambda}_{abc}, \tag{8}$$

where the voltage vectors $\boldsymbol{v}_{0dq} = \begin{bmatrix} v_0 & v_d & v_q \end{bmatrix}^T$ and $\boldsymbol{v}_{abc} = \begin{bmatrix} v_a & v_b & v_c \end{bmatrix}^T$, and the linkage flux vectors $\boldsymbol{\lambda}_{0dq} = \begin{bmatrix} \lambda_0 & \lambda_d & \lambda_q \end{bmatrix}^T$ and $\boldsymbol{\lambda}_{abc} = \begin{bmatrix} \lambda_a & \lambda_b & \lambda_c \end{bmatrix}^T$ are constructed similarly to (5).

There exists also an inverse of the Park's transformation matrix (6) that is used to obtain

$$\boldsymbol{i}_{abc} = \boldsymbol{P}^{-1}\,\boldsymbol{i}_{0dq}. \tag{9}$$

Finally, the the following active power equations can be obtained:

$$\begin{aligned} p = v_a i_a + v_b i_b + v_c i_c = \boldsymbol{v}_{abc}^T \boldsymbol{i}_{abc} = (\boldsymbol{P}^{-1}\boldsymbol{v}_{0dq})^T\,(\boldsymbol{P}^{-1}\boldsymbol{i}_{0dq}) = \\ = \boldsymbol{v}_{0dq}^T (\boldsymbol{P}^{-1})^T\,\boldsymbol{P}^{-1}\boldsymbol{i}_{0dq} = \boldsymbol{v}_{0dq}^T \boldsymbol{P}\boldsymbol{P}^{-1}\boldsymbol{i}_{0dq} = \boldsymbol{v}_{0dq}^T \boldsymbol{i}_{0dq} = \\ = v_d i_d + v_q i_q + v_0 i_0 \end{aligned} \tag{10}$$

2.1.1 The flux linkage equations

The generator consists of six coupled coils. The coils with indices a, b and c are the stator phases coils, F is the field coil, D is the d-axis amortisseur and Q is the q-axis amortisseur. The linkage equations can be written in the following form

$$\left[\begin{array}{c} \lambda_a \\ \lambda_b \\ \lambda_c \\ \hline \lambda_F \\ \lambda_D \\ \lambda_Q \end{array}\right] = \left[\begin{array}{ccc|ccc} L_{aa} & L_{ab} & L_{ac} & L_{aF} & L_{aD} & L_{aQ} \\ L_{ba} & L_{bb} & L_{bc} & L_{bF} & L_{bD} & L_{bQ} \\ L_{ca} & L_{cb} & L_{cc} & L_{cF} & L_{cD} & L_{cQ} \\ \hline L_{Fa} & L_{Fb} & L_{Fc} & L_{FF} & L_{FD} & L_{FQ} \\ L_{Da} & L_{Db} & L_{Dc} & L_{DF} & L_{DD} & L_{DQ} \\ L_{Qa} & L_{Qb} & L_{Qc} & L_{QF} & L_{QD} & L_{QQ} \end{array}\right] \left[\begin{array}{c} i_a \\ i_b \\ i_c \\ \hline i_F \\ i_D \\ i_Q \end{array}\right] = \left[\begin{array}{cc} \boldsymbol{L}_{ss} & \boldsymbol{L}_{sR} \\ \boldsymbol{L}_{Rs} & \boldsymbol{L}_{RR} \end{array}\right] \left[\begin{array}{c} \boldsymbol{i}_{abc} \\ \boldsymbol{i}_{FDQ} \end{array}\right], \tag{11}$$

where L_{xy} is the coupling inductance of the coils x and y, $\boldsymbol{L}_{RR}$ is the rotor-rotor, $\boldsymbol{L}_{ss}$ is the stator-stator, $\boldsymbol{L}_{sR}$ and $\boldsymbol{L}_{Rs}$ are the stator-rotor inductances. It is important to note that the inductances are time varying since Θ is a function of time.

The stator self inductances are given by

$$\begin{aligned} L_{aa} &= L_s + L_m \cos(2\Theta) \\ L_{bb} &= L_s + L_m \cos(2(\Theta - \tfrac{2\pi}{3})) \\ L_{cc} &= L_s + L_m \cos(2(\Theta + \tfrac{2\pi}{3})), \end{aligned} \tag{12}$$

where L_s is the self inductance and L_m is the mutual inductance.

The rotor self inductances are written as: $L_{FF} = L_F$ and $L_{DD} = L_D$ and $L_{QQ} = L_Q$.

The stator mutual inductances are given by

$$\begin{aligned} L_{ab} = L_{ba} &= -M_s - L_m \cos(2(\Theta - \tfrac{\pi}{6})) \\ L_{bc} = L_{cb} &= -M_s - L_m \cos(2(\Theta - \tfrac{\pi}{2})) \\ L_{ca} = L_{ac} &= -M_s - L_m \cos(2(\Theta + \tfrac{5\pi}{6})), \end{aligned} \tag{13}$$

where M_s and L_m is mutual inductances.

The rotor mutual inductances are $L_{FD} = L_{DF} = M_R$ and $L_{FQ} = L_{QF} = 0$ and $L_{DQ} = L_{QD} = 0$.

The stator to rotor mutual inductances are given by: (From phase windings to the field windings)

$$\begin{aligned} L_{aF} = L_{Fa} &= M_F \cos(\Theta) \\ L_{bF} = L_{Fb} &= M_F \cos(\Theta - \tfrac{2\pi}{3}) \\ L_{cF} = L_{Fc} &= M_F \cos(\Theta + \tfrac{2\pi}{3}) \end{aligned} \tag{14}$$

The stator to rotor mutual inductances are given by: (From phase windings to the damper windings direct axis)

$$\begin{aligned} L_{aD} = L_{Da} &= M_D \cos(\Theta) \\ L_{bD} = L_{Db} &= M_D \cos(\Theta - \tfrac{2\pi}{3}) \\ L_{cD} = L_{Dc} &= M_D \cos(\Theta + \tfrac{2\pi}{3}) \end{aligned} \tag{15}$$

The stator to rotor mutual inductances are given by: (From phase windings to the damper quadrature direct axis)

$$\begin{aligned} L_{aQ} = L_{Qa} &= M_Q \cos(\Theta) \\ L_{bQ} = L_{Qb} &= M_Q \cos(\Theta - \tfrac{2\pi}{3}) \\ L_{cQ} = L_{Qc} &= M_Q \cos(\Theta + \tfrac{2\pi}{3}) \end{aligned} \tag{16}$$

The time-varying inductances can be simplified by referring all quantities to a rotor frame of reference through Park's Transformation:

$$\begin{bmatrix} \boldsymbol{P} & \boldsymbol{0} \\ \boldsymbol{0} & \boldsymbol{I}_3 \end{bmatrix} \begin{bmatrix} \boldsymbol{\lambda}_{abc} \\ \boldsymbol{\lambda}_{FDQ} \end{bmatrix} = \begin{bmatrix} \boldsymbol{P} & \boldsymbol{0} \\ \boldsymbol{0} & \boldsymbol{I}_3 \end{bmatrix} \begin{bmatrix} \boldsymbol{L}_{ss} & \boldsymbol{L}_{sR} \\ \boldsymbol{L}_{Rs} & \boldsymbol{L}_{RR} \end{bmatrix} \cdot \cdot \begin{bmatrix} \boldsymbol{P^{-1}} & \boldsymbol{0} \\ \boldsymbol{0} & \boldsymbol{I}_3 \end{bmatrix} \begin{bmatrix} \boldsymbol{P} & \boldsymbol{0} \\ \boldsymbol{0} & \boldsymbol{I}_3 \end{bmatrix} \begin{bmatrix} \boldsymbol{i}_{abc} \\ \boldsymbol{i}_{FDQ} \end{bmatrix} \tag{17}$$

The matrix $\boldsymbol{P}$ is the Park's transformation matrix in (6), $\boldsymbol{I}_3$ is the 3×3 unit matrix and $\boldsymbol{\lambda}_{FDQ} = \begin{bmatrix} \lambda_F & \lambda_D & \lambda_Q \end{bmatrix}^T$. This way, we obtain the following transformed flux linkage equations

$$\begin{bmatrix} \lambda_0 \\ \lambda_d \\ \lambda_q \\ \lambda_F \\ \lambda_D \\ \lambda_Q \end{bmatrix} = \begin{bmatrix} L_0 & 0 & 0 & 0 & 0 & 0 \\ 0 & L_d & 0 & kM_F & kM_D & 0 \\ 0 & 0 & L_q & 0 & 0 & kM_Q \\ 0 & kM_F & 0 & L_F & M_R & 0 \\ 0 & kM_D & 0 & M_R & L_D & 0 \\ 0 & 0 & kM_Q & 0 & 0 & L_Q \end{bmatrix} \begin{bmatrix} i_0 \\ i_d \\ i_q \\ i_F \\ i_D \\ i_Q \end{bmatrix}, \tag{18}$$

where the new constants are defined by the following equations:

$$\begin{aligned} L_d &= L_s + M_s + \tfrac{3}{2} L_m \\ L_q &= L_s + M_s - \tfrac{3}{2} L_m \\ L_0 &= L_s - 2M_s \\ k &= \sqrt{\tfrac{2}{3}} \end{aligned} \tag{19}$$

2.1.2 The voltage equations

The equivalent circuit of the synchronous machine is depicted in Figure 4.

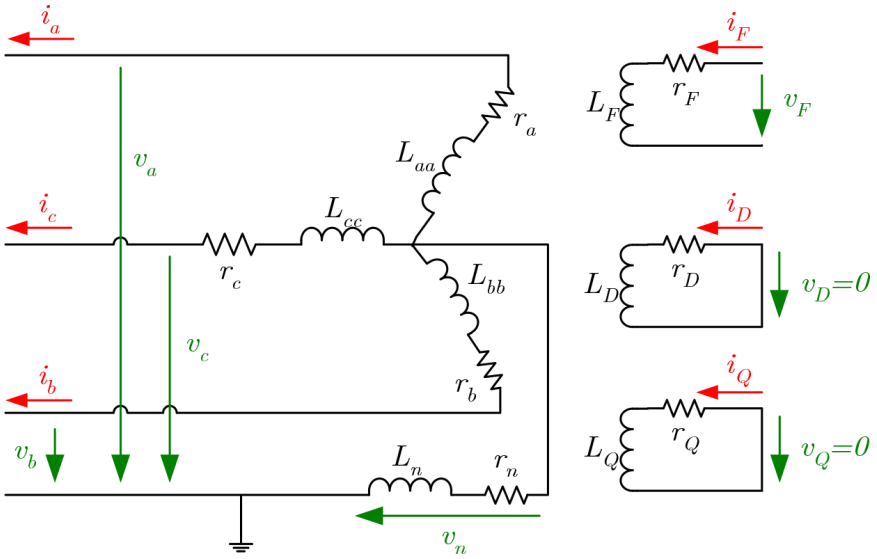

Figure 4: The simplified equivalent circuit of the stator and rotor circuits. The voltages v_D and v_Q are zero, because the ammortisseur windings are short-circuited.

Using the notations of Figure 4 the general matrix-vector form of Kirchoff's voltage law is

$$\boldsymbol{v} = -\boldsymbol{r}\boldsymbol{i} - \dot{\boldsymbol{\lambda}} + \boldsymbol{v}_n, \tag{20}$$

and its particular form is

$$\begin{bmatrix} \boldsymbol{v}_{abc} \\ \boldsymbol{v}_{FDQ} \end{bmatrix} = -\begin{bmatrix} \boldsymbol{R}_{abc} & \boldsymbol{0} \\ \boldsymbol{0} & \boldsymbol{R}_{FDQ} \end{bmatrix} \begin{bmatrix} \boldsymbol{i}_{abc} \\ \boldsymbol{i}_{FDQ} \end{bmatrix} - \begin{bmatrix} \dot{\boldsymbol{\lambda}}_{abc} \\ \dot{\boldsymbol{\lambda}}_{FDQ} \end{bmatrix} + \begin{bmatrix} \boldsymbol{v}_n \\ \boldsymbol{0} \end{bmatrix}, \tag{21}$$

where $\boldsymbol{v}_{FDQ} = [v_F \quad v_D \quad v_Q]$, $\boldsymbol{i}_{FDQ} = [i_F \quad i_D \quad i_Q]$, $\boldsymbol{R}_{abc} = \begin{bmatrix} r_a & 0 & 0 \\ 0 & r_b & 0 \\ 0 & 0 & r_c \end{bmatrix}$ and $\boldsymbol{R}_{FDQ} = \begin{bmatrix} r_F & 0 & 0 \\ 0 & r_D & 0 \\ 0 & 0 & r_Q \end{bmatrix}$.

In what follows, the voltage equations will be expressed in the dq coordinate system. Expanding Eq. (21) leads to the matrix equation

$$\begin{bmatrix} v_a \\ v_b \\ v_c \\ -v_F \\ 0 \\ 0 \end{bmatrix} = -\begin{bmatrix} r_a & 0 & 0 & 0 & 0 & 0 \\ 0 & r_b & 0 & 0 & 0 & 0 \\ 0 & 0 & r_c & 0 & 0 & 0 \\ 0 & 0 & 0 & r_F & 0 & 0 \\ 0 & 0 & 0 & 0 & r_D & 0 \\ 0 & 0 & 0 & 0 & 0 & r_Q \end{bmatrix} \begin{bmatrix} i_a \\ i_b \\ i_c \\ i_F \\ i_D \\ i_Q \end{bmatrix} - \begin{bmatrix} \dot{\lambda}_a \\ \dot{\lambda}_b \\ \dot{\lambda}_c \\ \dot{\lambda}_F \\ \dot{\lambda}_D \\ \dot{\lambda}_Q \end{bmatrix} + \begin{bmatrix} \boldsymbol{v}_n \\ \boldsymbol{0} \end{bmatrix} \tag{22}$$

where the $\boldsymbol{v}_n$ is the neutral voltage

$$\boldsymbol{v_n} = -r_n \begin{bmatrix} 1 & 1 & 1 \\ 1 & 1 & 1 \\ 1 & 1 & 1 \end{bmatrix} \begin{bmatrix} i_a \\ i_b \\ i_c \end{bmatrix} - L_n \begin{bmatrix} 1 & 1 & 1 \\ 1 & 1 & 1 \\ 1 & 1 & 1 \end{bmatrix} \begin{bmatrix} \dot{i}_a \\ \dot{i}_b \\ \dot{i}_c \end{bmatrix} \tag{23}$$

$$\boldsymbol{v_n} = -\boldsymbol{R}_n \boldsymbol{i}_{abc} - \boldsymbol{L}_{nm} \dot{\boldsymbol{i}}_{abc} \tag{24}$$

where $\boldsymbol{L}_{nm} = \begin{bmatrix} L_n & L_n & L_n \\ L_n & L_n & L_n \\ L_n & L_n & L_n \end{bmatrix}$ and $\boldsymbol{R}_n = \begin{bmatrix} r_n & r_n & r_n \\ r_n & r_n & r_n \\ r_n & r_n & r_n \end{bmatrix}$.

Transforming the left hand side of Eq. (21) to the dq frame is done with Park's transformation:

$$\begin{bmatrix} \boldsymbol{P} & \boldsymbol{0} \\ \boldsymbol{0} & \boldsymbol{I}_3 \end{bmatrix} \begin{bmatrix} \boldsymbol{v}_{abc} \\ \boldsymbol{v}_{FDQ} \end{bmatrix} = \begin{bmatrix} \boldsymbol{v}_{0dq} \\ \boldsymbol{v}_{FDQ} \end{bmatrix} \tag{25}$$

The first step is to express the voltage of the resistances in the d-q frame using Ohm's law.

$$\begin{aligned} &\begin{bmatrix} \boldsymbol{P} & \boldsymbol{0} \\ \boldsymbol{0} & \boldsymbol{I_3} \end{bmatrix} \begin{bmatrix} \boldsymbol{R}_{abc} & \boldsymbol{0} \\ \boldsymbol{0} & \boldsymbol{R}_{FDQ} \end{bmatrix} \begin{bmatrix} \boldsymbol{i}_{abc} \\ \boldsymbol{i}_{FDQ} \end{bmatrix} = \\ &= \begin{bmatrix} \boldsymbol{P} & \boldsymbol{0} \\ \boldsymbol{0} & \boldsymbol{I}_3 \end{bmatrix} \begin{bmatrix} \boldsymbol{R}_{abc} & \boldsymbol{0} \\ \boldsymbol{0} & \boldsymbol{R}_{FDQ} \end{bmatrix} \begin{bmatrix} \boldsymbol{P}^{-1} & \boldsymbol{0} \\ \boldsymbol{0} & \boldsymbol{I}_3 \end{bmatrix} \begin{bmatrix} \boldsymbol{P} & \boldsymbol{0} \\ \boldsymbol{0} & \boldsymbol{I}_3 \end{bmatrix} \begin{bmatrix} \boldsymbol{i}_{abc} \\ \boldsymbol{i}_{FDQ} \end{bmatrix} = \\ &= \begin{bmatrix} \boldsymbol{P}\boldsymbol{R}_{abc}\boldsymbol{P}^{-1} & \boldsymbol{0} \\ \boldsymbol{0} & \boldsymbol{R}_{FDQ} \end{bmatrix} \begin{bmatrix} \boldsymbol{i}_{0dq} \\ \boldsymbol{i}_{FDQ} \end{bmatrix} = \begin{bmatrix} \hat{\boldsymbol{R}}_{abc} & \boldsymbol{0} \\ \boldsymbol{0} & \boldsymbol{R}_{FDQ} \end{bmatrix} \begin{bmatrix} \boldsymbol{i}_{0dq} \\ \boldsymbol{i}_{FDQ} \end{bmatrix} \end{aligned} \tag{26}$$

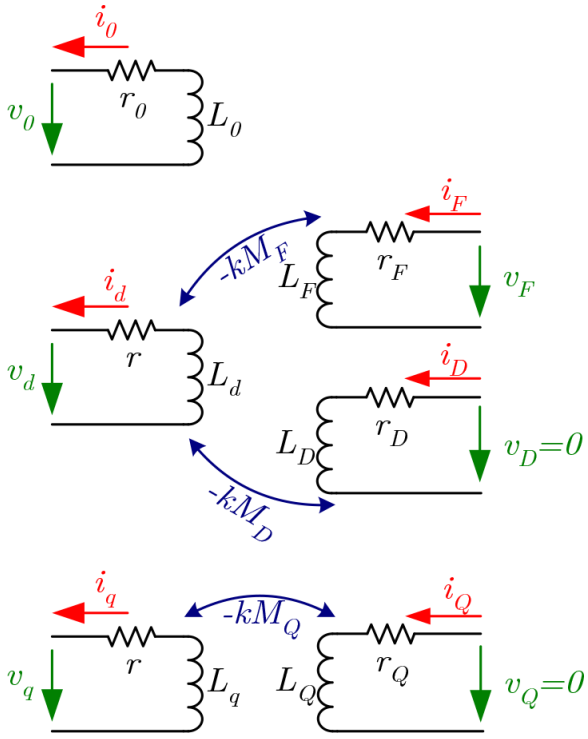

Figure 5: The simplified equivalent circuit of the transformed stator and rotor circuits

As it was assumed, the machine has symmetrical tri-phase stator windings ($r_a = r_b = r_c = r$), so the resistance matrix $\hat{\boldsymbol{R}}_{abc}$ is in the following diagonal form:

$$\hat{\boldsymbol{R}}_{abc} = \boldsymbol{R}_{abc} = \begin{bmatrix} r & 0 & 0 \\ 0 & r & 0 \\ 0 & 0 & r \end{bmatrix} \tag{27}$$

The second step is to compute the time derivatives of the fluxes as

$$\begin{bmatrix} \boldsymbol{P} & \boldsymbol{0} \\ \boldsymbol{0} & \boldsymbol{I}_3 \end{bmatrix} \begin{bmatrix} \dot{\boldsymbol{\lambda}}_{abc} \\ \dot{\boldsymbol{\lambda}}_{FDQ} \end{bmatrix} = \begin{bmatrix} \boldsymbol{P}\dot{\boldsymbol{\lambda}}_{abc} \\ \dot{\boldsymbol{\lambda}}_{FDQ} \end{bmatrix}. \tag{28}$$

Using the fact, that $\boldsymbol{P}$ is time dependent (through Θ), $\boldsymbol{P}\dot{\boldsymbol{\lambda}}_{abc}$ can be expressed as:

$$\boldsymbol{P}\dot{\boldsymbol{\lambda}}_{abc} = \dot{\boldsymbol{\lambda}}_{0dq} - \dot{\boldsymbol{P}}\boldsymbol{\lambda}_{abc} = \dot{\boldsymbol{\lambda}}_{0dq} - \dot{\boldsymbol{P}}\boldsymbol{P}^{-1}\boldsymbol{\lambda}_{0dq} \tag{29}$$

It is easy to see from Eq. (29), that expression $\dot{\boldsymbol{P}}\boldsymbol{P}^{-1}\boldsymbol{\lambda}_{0dq}$ has the following form:

$$\dot{\boldsymbol{P}}\boldsymbol{P}^{-1}\boldsymbol{\lambda}_{0dq} = \omega \begin{bmatrix} 0 & 0 & 0 \\ 0 & 0 & -1 \\ 0 & 1 & 0 \end{bmatrix} \begin{bmatrix} \lambda_0 \\ \lambda_d \\ \lambda_q \end{bmatrix} = \begin{bmatrix} 0 \\ -\omega\lambda_q \\ \omega\lambda_d \end{bmatrix} \tag{30}$$

The final step is to obtain the neutral voltage of Eq. (24) using Park's transformation

$$\boldsymbol{v}_{0dq} = \boldsymbol{P}\boldsymbol{v}_n = -\boldsymbol{P}\boldsymbol{R}_n\boldsymbol{P}^{-1}\boldsymbol{P}\boldsymbol{i}_{abc} - \boldsymbol{P}\boldsymbol{L}_{nm}\boldsymbol{P}^{-1}\boldsymbol{P}\dot{\boldsymbol{i}}_{abc} =$$

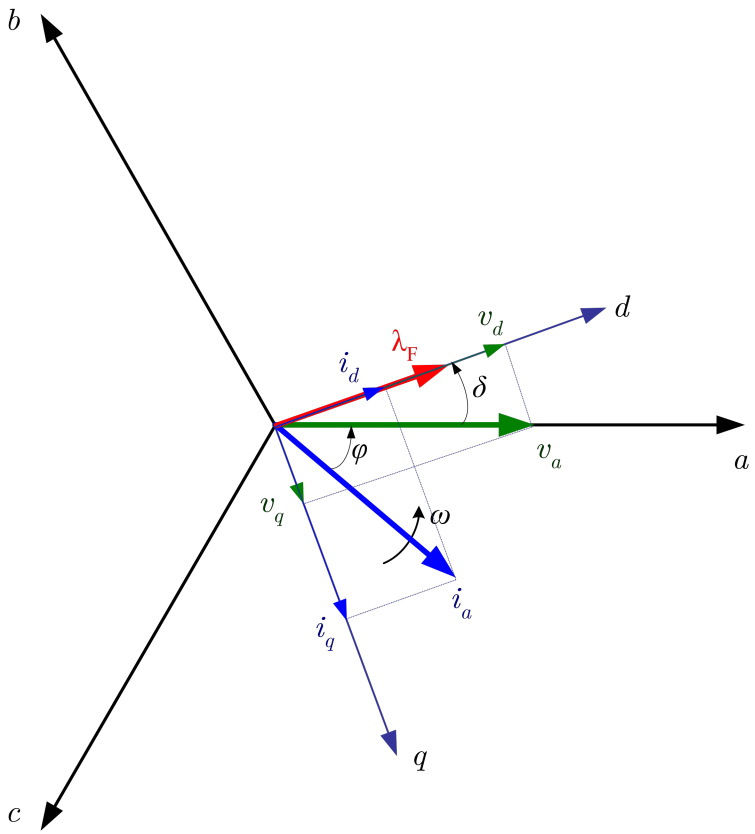

Figure 6: The voltages, currents and the flux of the synchronous machine in *abc* and *dq* coordinate system, where φ is the phase offset, δ is the load angle and ω represents the angular velocity of the EMF.

$$-\boldsymbol{P}\boldsymbol{R}_n\boldsymbol{P}^{-1}\boldsymbol{i}_{0dq}-\boldsymbol{P}\boldsymbol{L}_{nm}\boldsymbol{P}^{-1}\dot{\boldsymbol{i}}_{0dq}=\begin{bmatrix}-3r_ni_0\\0\\0\end{bmatrix}-\begin{bmatrix}-3L_n\dot{i}_0\\0\\0\end{bmatrix}. \tag{31}$$

Summarizing the previous steps, the voltage equations can be expressed in the dq frame as

$$\begin{bmatrix}\boldsymbol{v}_{0dq}\\\boldsymbol{v}_{FDQ}\end{bmatrix}=-\begin{bmatrix}\boldsymbol{R}_{0dq}&\boldsymbol{0}\\\boldsymbol{0}&\boldsymbol{R}_{FDQ}\end{bmatrix}\begin{bmatrix}\boldsymbol{i}_{0dq}\\\boldsymbol{i}_{FDQ}\end{bmatrix}-\begin{bmatrix}\dot{\boldsymbol{\lambda}}_{0dq}\\\dot{\boldsymbol{\lambda}}_{FDQ}\end{bmatrix}+\begin{bmatrix}\dot{\boldsymbol{P}}\boldsymbol{P}^{-1}\boldsymbol{\lambda}_{0dq}\\\boldsymbol{0}\end{bmatrix}+\begin{bmatrix}\boldsymbol{v}_{0dq}\\\boldsymbol{0}\end{bmatrix}, \tag{32}$$

where $\boldsymbol{n}_{0dq}$ is the voltage drop from the neutral network and ω is the angular velocity.

Using Eq. (18) and (32) the voltage equations can be rearranged in the form:

$$\begin{bmatrix}v_0\\v_d\\v_F\\v_D=0\\v_q\\v_Q=0\end{bmatrix}=-\begin{bmatrix}r+3r_n&0&0&0&0&0\\0&r&0&0&\omega L_q&\omega kM_Q\\0&0&r_F&0&0&0\\0&0&0&r_D&0&0\\0&-\omega L_d&-\omega kM_F&-\omega kM_D&r&0\\0&0&0&0&0&r_Q\end{bmatrix}\begin{bmatrix}i_0\\i_d\\i_F\\i_D\\i_q\\i_Q\end{bmatrix}-$$
$$-\begin{bmatrix}L_0+3L_n&0&0&0&0&0\\0&L_d&kM_F&kM_D&0&0\\0&kM_F&L_F&M_R&0&0\\0&kM_D&M_R&L_D&0&0\\0&0&0&0&L_q&kM_Q\\0&0&0&0&kM_Q&L_Q\end{bmatrix}\begin{bmatrix}\dot{i}_0\\\dot{i}_d\\\dot{i}_F\\\dot{i}_D\\\dot{i}_q\\\dot{i}_Q\end{bmatrix} \tag{33}$$

Equation (33) shows more clearly the decoupling of the circuits. In balanced condition voltage v_0 is equal to 0, i.e. this component may be omitted as follows

$$\begin{bmatrix}v_d\\v_F\\v_D=0\\v_q\\v_Q=0\end{bmatrix}=-\begin{bmatrix}r&0&0&\omega L_q&\omega kM_Q\\0&r_F&0&0&0\\0&0&r_D&0&0\\-\omega L_d&-\omega kM_F&-\omega kM_D&r&0\\0&0&0&0&r_Q\end{bmatrix}\begin{bmatrix}i_d\\i_F\\i_D\\i_q\\i_Q\end{bmatrix}-$$
$$\begin{bmatrix}L_d&kM_F&kM_D&0&0\\kM_F&L_F&M_R&0&0\\kM_D&M_R&L_D&0&0\\0&0&0&L_q&kM_Q\\0&0&0&kM_Q&L_Q\end{bmatrix}\begin{bmatrix}\dot{i}_d\\\dot{i}_F\\\dot{i}_D\\\dot{i}_q\\\dot{i}_Q\end{bmatrix} \tag{34}$$

Then Eq. (34) can be written in the following block matrix form, using the simplified notation

$$\begin{bmatrix}\boldsymbol{v}_{dq}\\\boldsymbol{v}_{FDQ}\end{bmatrix}=-\begin{bmatrix}\boldsymbol{R}&\boldsymbol{0}\\\boldsymbol{0}&\boldsymbol{R}_R\end{bmatrix}\begin{bmatrix}\boldsymbol{i}_{dq}\\\boldsymbol{i}_{FDQ}\end{bmatrix}-\begin{bmatrix}\dot{\boldsymbol{\lambda}}_{dq}\\\dot{\boldsymbol{\lambda}}_{FDQ}\end{bmatrix}+\begin{bmatrix}\boldsymbol{S}\\\boldsymbol{0}\end{bmatrix}+\begin{bmatrix}\boldsymbol{v}_{0dq}\\\boldsymbol{0}\end{bmatrix}, \tag{35}$$

where $\boldsymbol{R}=\begin{bmatrix}r&0\\0&r\end{bmatrix}$, $\boldsymbol{R_R}=\begin{bmatrix}r_F&0&0\\0&r_D&0\\0&0&r_Q\end{bmatrix}$ and $\boldsymbol{S}=\begin{bmatrix}-\omega\lambda_q\\\omega\lambda_d\end{bmatrix}$.

The voltage equation (34) can also be presented in a more compact form

$$\boldsymbol{v}_{dFDqQ} = -\boldsymbol{R}_{RS\omega}\boldsymbol{i}_{dFDqQ} - \boldsymbol{L}\dot{\boldsymbol{i}}_{dFDqQ}, \tag{36}$$

where $\boldsymbol{v}_{dFDqQ}$, $\boldsymbol{i}_{dFDqQ}$, $\dot{\boldsymbol{i}}_{dFDqQ}$ $\boldsymbol{R}_{RS\omega}$ and $\boldsymbol{L}$ are the following objects:

$$\boldsymbol{v}_{dFDqQ} = \begin{bmatrix} v_d & v_F & v_D & v_q & v_Q \end{bmatrix}^T \tag{37}$$

$$\boldsymbol{i}_{dFDqQ} = \begin{bmatrix} i_d & i_F & i_D & i_q & i_Q \end{bmatrix}^T \tag{38}$$

$$\dot{\boldsymbol{i}}_{dFDqQ} = \begin{bmatrix} \dot{i}_d & \dot{i}_F & \dot{i}_D & \dot{i}_q & \dot{i}_Q \end{bmatrix}^T \tag{39}$$

$$\boldsymbol{R}_{RS\omega}(\omega) = \begin{bmatrix} r & 0 & 0 & \omega L_q & \omega k M_Q \\ 0 & r_F & 0 & 0 & 0 \\ 0 & 0 & r_D & 0 & 0 \\ -\omega L_d & -\omega k M_F & -\omega k M_D & r & 0 \\ 0 & 0 & 0 & 0 & r_Q \end{bmatrix} \tag{40}$$

$$\boldsymbol{L} = \begin{bmatrix} L_d & kM_F & kM_D & 0 & 0 \\ kM_F & L_F & M_R & 0 & 0 \\ kM_D & M_R & L_D & 0 & 0 \\ 0 & 0 & 0 & L_q & kM_Q \\ 0 & 0 & 0 & kM_Q & L_Q \end{bmatrix} \tag{41}$$

2.1.3 The dynamic model equations

The time derivatives $\frac{i_d}{dt}$, $\frac{i_F}{dt}$, $\frac{i_D}{dt}$, $\frac{i_q}{dt}$ and $\frac{i_Q}{dt}$ can easily be expressed from Eq. (34):

$$\begin{bmatrix} \dot{i}_d \\ \dot{i}_F \\ \dot{i}_D \\ \dot{i}_q \\ \dot{i}_Q \end{bmatrix} = -\boldsymbol{L}^{-1}\boldsymbol{R}_{\boldsymbol{RS\omega}}(\omega) \begin{bmatrix} i_d \\ i_F \\ i_D \\ i_q \\ i_Q \end{bmatrix} - \boldsymbol{L}^{-1} \begin{bmatrix} -v_d \\ v_F \\ 0 \\ -v_q \\ 0 \end{bmatrix} \tag{42}$$

It is important to note, that matrix $\boldsymbol{R}_{RS\omega}(\omega)$ is a function of the rotational speed (ω).

2.1.4 Connecting the synchronous generator to an infinitely large network

The synchronous generator which connected to an infinity huge electrical network is depicted in Fig. 7. The resistance R_e and inductance L_e represent the output transformer of the synchronous generator and the transmission-line.

Using the notation of Fig. 7 the voltage of the generator can be written as:

$$\begin{bmatrix} v_a \\ v_b \\ v_c \end{bmatrix} = \begin{bmatrix} v_{\infty a} \\ v_{\infty b} \\ v_{\infty c} \end{bmatrix} + R_e\boldsymbol{I}_3 \begin{bmatrix} i_a \\ i_b \\ i_c \end{bmatrix} + L_e\boldsymbol{I}_3 \begin{bmatrix} \dot{i}_a \\ \dot{i}_b \\ \dot{i}_c \end{bmatrix} \tag{43}$$

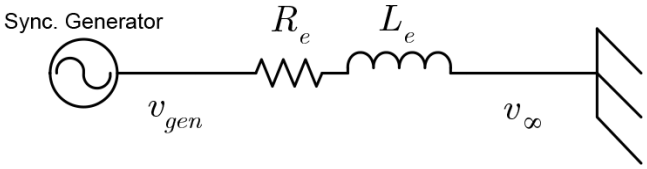

Figure 7: Synchronous machine connected to an infinite bus, where v_∞ is the magnitude of the RMS phase voltage of the grid and v_{gen} is the magnitude of the RMS phase voltage of the SG.

In matrix form Eq. (43) looks like

$$\boldsymbol{v}_{abc} = \boldsymbol{v}_{\infty abc} + R_e \boldsymbol{I}_3 \boldsymbol{i}_{abc} + L_e \boldsymbol{I}_3 \dot{\boldsymbol{i}}_{abc}. \tag{44}$$

We can write it in $0dq$ coordinate system we get the following:

$$\boldsymbol{v}_{0dq} = \boldsymbol{P}\boldsymbol{v}_{abc} = \boldsymbol{P}\boldsymbol{v}_{\infty abc} + R_e \boldsymbol{I}_3 \boldsymbol{i}_{0dq} + L_e \boldsymbol{I}_3 \dot{\boldsymbol{i}}_{0dq} \tag{45}$$

The three phase voltages of the bus are the

$$\boldsymbol{v}_{\infty abc} = \sqrt{2} v_\infty \begin{bmatrix} \cos(\omega_r t + \alpha) \\ \cos(\omega_r t + \alpha - \frac{2\pi}{3}) \\ \cos(\omega_r t + \alpha + \frac{2\pi}{3}) \end{bmatrix}, \tag{46}$$

where v_∞ is the magnitude of the RMS phase voltage of the grid and $\alpha = \delta + \pi/2$.

In $0dq$ coordinate system:

$$\boldsymbol{v}_{\infty 0dq} = \boldsymbol{P}\boldsymbol{v}_{\infty abc} = \sqrt{3} v_\infty \begin{bmatrix} 0 \\ -\sin(\delta - \alpha) \\ \cos(\delta - \alpha) \end{bmatrix} \tag{47}$$

The $\boldsymbol{i}_{0dq}$ currents can be computed as:

$$\boldsymbol{P}\dot{\boldsymbol{i}}_{abc} = \dot{\boldsymbol{i}}_{0dq} - \dot{\boldsymbol{P}}\boldsymbol{i}_{abc} = \dot{\boldsymbol{i}}_{0dq} - \dot{\boldsymbol{P}}\boldsymbol{P}^{-1}\boldsymbol{i}_{0dq} \tag{48}$$

$$\boldsymbol{v}_{0dq} = v_\infty \sqrt{3} \begin{bmatrix} 0 \\ -\sin(\delta - \alpha) \\ \cos(\delta - \alpha) \end{bmatrix} + R_e \boldsymbol{i}_{0dq} + L_e \dot{\boldsymbol{i}}_{0dq} - \omega L_e \begin{bmatrix} 0 \\ -i_q \\ i_d \end{bmatrix} \tag{49}$$

Revisiting the voltage equation (Eq. (36)) of the SG, the effect of the network can be represented by replacing the $\boldsymbol{R}_{RS\omega(\omega)}$ and the $\boldsymbol{L}$ matrix. The new $\tilde{\boldsymbol{R}}_{RS\omega(\omega)}$ and the $\tilde{\boldsymbol{L}}$ matrices consist of the R_e resistance and L_e inductance. $\tilde{R} = r + R_e$, $\tilde{L}_d = L_d + L_e$ and $\tilde{L}_q = L_q + L_e$.

With this change the new voltage equation in simplified matrix form is the following:

$$\boldsymbol{v}_{dFDqQ} = -\tilde{\boldsymbol{R}}_{RS\omega}(\omega)\boldsymbol{i}_{dFDqQ} - \tilde{\boldsymbol{L}}\dot{\boldsymbol{i}}_{dFDqQ} \tag{50}$$

Where $\boldsymbol{R}_{RS\omega}(\omega)$ and $\tilde{\boldsymbol{L}}$ are the following matrices:

$$\tilde{\boldsymbol{R}}_{RS\omega}(\omega) = \begin{bmatrix} r+R_e & 0 & 0 & \omega L_q & \omega k M_Q \\ 0 & r_F & 0 & 0 & 0 \\ 0 & 0 & r_D & 0 & 0 \\ -\omega L_d & -\omega k M_F & -\omega k M_D & r+R_e & 0 \\ 0 & 0 & 0 & 0 & r_Q \end{bmatrix} \tag{51}$$

$$\tilde{\boldsymbol{L}} = \begin{bmatrix} L_d+L_e & kM_F & kM_D & 0 & 0 \\ kM_F & L_F & M_R & 0 & 0 \\ kM_D & M_R & L_D & 0 & 0 \\ 0 & 0 & 0 & L_q+L_e & kM_Q \\ 0 & 0 & 0 & kM_Q & L_Q \end{bmatrix} \tag{52}$$

After it, $\dot{\boldsymbol{i}}_d$, $\dot{\boldsymbol{i}}_F$, $\dot{\boldsymbol{i}}_D$, $\dot{\boldsymbol{i}}_q$ and $\dot{\boldsymbol{i}}_Q$ can be expressed from Eq. (50):

$$\dot{\boldsymbol{i}}_{dFDqQ} = -\tilde{\boldsymbol{L}}^{-1}\tilde{\boldsymbol{R}}_{RS\omega}(\omega)\boldsymbol{i}_{dFDqQ} - \tilde{\boldsymbol{L}}^{-1}\boldsymbol{v}_{dFDqQ} \tag{53}$$

This is the current state space model of the SG in the $0dq$ frame.

2.2 The mechanical submodel

From Newton's second law for rotation we are able to write the speed and torque equation for the SG as

$$2H\omega_B\dot{\omega} = T_{acc}, \tag{54}$$

where the H is the inertia constant, T_{acc} is the accelerating torque and ω_B is the angular velocity base unit used for normalization. We can write the time and the rotation speed in

$$t_u = \omega_B t \quad \text{and} \quad \omega_u = \frac{\omega}{\omega_B}. \tag{55}$$

After it the normalized swing equation can be written as

$$2H\omega_B\frac{\omega_u}{dt_u} = T_{acc}. \tag{56}$$

The expression $2H\omega_B$ can be substituted by a new constant

$$\tau_j = 2H\omega_B. \tag{57}$$

The accelerating torque can be expressed using the following three components

$$T_{acc} = T_{mech} - T_{electr} - T_{damp}, \tag{58}$$

where T_{mech} is the mechanical torque, T_{electr} is the electrical torque and the T_{damp} is the damping torque. The damping torque is in the form

$$T_{damp} = D\omega, \tag{59}$$

where D is a damping constant.

The electrical torque can be derived from the flux and the current of the machine

$$T_{electr} = \frac{1}{3}(\lambda_d i_q - \lambda_q i_d). \tag{60}$$

To compute the electrical torque the direct and quadrature part of the stator flux have to be written from the Eq. (18):

$$\lambda_d = L_d i_d + kM_F i_F + kM_D i_D \tag{61}$$

$$\lambda_q = L_q i_q + kM_Q i_Q \tag{62}$$

Using Eqs. (60), (61) and (62) the electrical torque is

$$T_{electr} = \frac{1}{3}\begin{bmatrix} L_d i_q & kM_F i_q & kM_D i_q & -L_q i_d & -kM_Q i_d \end{bmatrix} \begin{bmatrix} i_d \\ i_F \\ i_D \\ i_q \\ i_Q \end{bmatrix}. \tag{63}$$

Substituting Eq. (57), (59) and (63) to (56) the speed of the synchronous machine can be obtained as

$$\dot{\omega} = -\frac{L_q i_q i_d}{3\tau_j} - \frac{kM_F i_q i_F}{3\tau_j} - \frac{kM_D i_q i_D}{3\tau_j} + \frac{L_q i_d i_q}{3\tau_j} + \frac{kM_Q i_d i_Q}{3\tau_j} - \frac{D\omega}{\tau_j} + \frac{T_{mech}}{\tau_j}, \tag{64}$$

$$\dot{\omega} = \begin{bmatrix} \frac{-L_d i_q}{3\tau_j} & -\frac{kM_F i_q}{3\tau_j} & -\frac{kM_D i_q}{3\tau_j} & \frac{L_q i_d}{3\tau_j} & \frac{kM_Q i_d}{3\tau_j} & -\frac{D}{\tau_j} \end{bmatrix} \begin{bmatrix} i_d \\ i_F \\ i_D \\ i_q \\ i_Q \\ \omega \end{bmatrix} + \frac{T_{mech}}{\tau_j}, \tag{65}$$

which will serve as the sixth state equation in the SG state space model.

2.3 The electro-mechanical state space model

The complete electro-mechanical model of the synchronous generator that is the basis of the following steps of model analysis, parameter estimation and controller design is to be constructed in this section. Merging Eq. (53) and (65) results in the following electro-mechanical model:

$$\begin{bmatrix} \dot{i}_d \\ \dot{i}_F \\ \dot{i}_D \\ \dot{i}_q \\ \dot{i}_Q \\ \dot{\omega} \end{bmatrix} = \left[\begin{array}{ccccc|c} & & \tilde{\boldsymbol{L}}^{-1}\tilde{\boldsymbol{R}}_{RS\omega}(\omega) & & & \begin{matrix}0\\0\\0\\0\\0\end{matrix} \\ \hline -\frac{L_d i_q}{3\tau_j} & -\frac{kM_F i_q}{3\tau_j} & -\frac{kM_D i_q}{3\tau_j} & \frac{L_q i_d}{3\tau_j} & \frac{kM_Q i_d}{3\tau_j} & -\frac{D}{\tau_j} \end{array}\right] \cdot \begin{bmatrix} i_d \\ i_F \\ i_D \\ i_q \\ i_Q \\ \omega \end{bmatrix} +$$

$$\left[\begin{array}{ccccc|c} & & \tilde{\boldsymbol{L}}^{-1} & & & \begin{matrix}0\\0\\0\\0\\0\end{matrix} \\ \hline 0 & 0 & 0 & 0 & 0 & \frac{1}{\tau_j} \end{array}\right] \cdot \left[\begin{array}{c} -v_d \\ v_F \\ 0 \\ -v_q \\ 0 \\ T_{mech} \end{array}\right] \tag{66}$$

On the other hand the load angle (δ) of the synchronous generator is

$$\delta = \delta_0 + \int_{t_0}^{t} (\omega - \omega_r) dt, \tag{67}$$

which can be included in the electro-mechanical model by differentiating Eq. (67) with respect to time:

$$\dot{\delta} = \omega - 1 \tag{68}$$

Note, that normalized units are used (see Section 2.4). Inserting the load angle (Eq. (68)) to the state space model (Eq. (66)) of the machine the following (nonlinear) state space model is obtained:

$$\left[\begin{array}{c} \dot{i}_d \\ \dot{i}_F \\ \dot{i}_D \\ \dot{i}_q \\ \dot{i}_Q \\ \dot{\omega} \\ \dot{\delta} \end{array}\right] = \left[\begin{array}{ccccc|cc} & & \tilde{\boldsymbol{L}}^{-1}\tilde{\boldsymbol{R}}_{RS\omega}(\omega) & & & \begin{matrix}0&0\\0&0\\0&0\\0&0\\0&0\end{matrix} \\ \hline -\frac{L_d i_q}{3\tau_j} & -\frac{kM_F i_q}{3\tau_j} & -\frac{kM_D i_q}{3\tau_j} & \frac{L_q i_d}{3\tau_j} & \frac{kM_Q i_d}{3\tau_j} & -\frac{D}{\tau_j} & 0 \\ 0 & 0 & 0 & 0 & 0 & 1 & 0 \end{array}\right] \cdot \left[\begin{array}{c} i_d \\ i_F \\ i_D \\ i_q \\ i_Q \\ \omega \\ \delta \end{array}\right] +$$

$$\left[\begin{array}{ccccc|cc} & & \tilde{\boldsymbol{L}}^{-1} & & & \begin{matrix}0&0\\0&0\\0&0\\0&0\\0&0\end{matrix} \\ \hline 0 & 0 & 0 & 0 & 0 & \frac{1}{\tau_j} & 0 \\ 0 & 0 & 0 & 0 & 0 & 0 & 1 \end{array}\right] \cdot \left[\begin{array}{c} -v_d \\ v_F \\ 0 \\ -v_q \\ 0 \\ T_{mech} \\ -1 \end{array}\right] \tag{69}$$

2.3.1 The state equations of the model

The state space model Eq. (69) can be expressed in the following general form:

$$\dot{\boldsymbol{x}} = \boldsymbol{A}(\boldsymbol{x})\boldsymbol{x} + \boldsymbol{B}\boldsymbol{u} \tag{70}$$

$$\boldsymbol{y} = h(\boldsymbol{x}, \boldsymbol{u}) \tag{71}$$

where Eq. (70) is the state equation and the Eq. (71) is the output equation. The above state space model is nonlinear in both the state and output equations, but it is input-affine.

In the general form vector $\boldsymbol{x}$ represents the vector of the state variables which is in the following form:

$$\boldsymbol{x} = \left[\begin{array}{c|cc} \boldsymbol{i}_{dFDqQ} & \omega & \delta \end{array}\right]^T = \left[\begin{array}{ccccccc} i_d & i_F & i_D & i_q & i_Q & \omega & \delta \end{array}\right]^T \tag{72}$$

Vector $\boldsymbol{u}$ denotes the input vector of the input variables, with the following elements:

$$\boldsymbol{u} = \left[\; -\boldsymbol{v}_{dFDqQ} \; \middle| \; T_{mech} \quad -1 \; \right]^T =$$

$$= \left[\; -v_d \quad v_F \quad v_D = 0 \quad -v_q \quad v_Q = 0 \quad T_{mech} \quad -1 \; \right]^T. \tag{73}$$

For later use we separate the elements of the input vector to manipulable and disturbance elements. The manipulable input vector of the model is

$$\boldsymbol{u}_{man} = \left[\; v_F \quad T_{mech} \; \right]^T \tag{74}$$

and the disturbance ($\boldsymbol{d}$) input is the following

$$\boldsymbol{d} = \left[\; v_d \quad v_D = 0 \quad v_q \quad v_Q = 0 \quad -1 \; \right]^T. \tag{75}$$

2.3.2 The output equations of the model

The output active power of the three phase machine in the $0dq$ frame can be expressed as

$$p_{out} = \boldsymbol{v}_{0dq}^T \boldsymbol{i}_{0dq}^T = v_d i_d + v_q i_q + v_0 i_0 \tag{76}$$

Assuming steady-state for the stationary components ($v_0 = i_0 = 0$), (76) simplifies to active power (p_{out}), reactive power (q_{out}) and output current

$$p_{out} = v_d i_d + v_q i_q$$

$$q_{out} = v_d i_q - v_q i_d.$$

$$i_{out} = \sqrt{i_d^2 + i_q^2} \tag{77}$$

Equations (77) are the *output equations* of the generator's state-space model. Observe, that these equations *are bi-linear in the state and input variables.* The output vector also include the following variables

$$\boldsymbol{y} = [p_{out} \quad q_{out} \quad i_d \quad i_q \quad i_{out} \quad \omega \quad i_F]^T. \tag{78}$$

2.4 Model parameters

The parameters are described only for phase a since the machine is assumed to have symmetrical tri-phase stator windings i.e. the other two phases have the same parameters. The stator mutual inductances of phase a are

$$L_{ab} = L_{ba} = -M_s - L_m \cos(2(\Theta - \frac{\pi}{6})) \tag{79}$$

where M_s is a given constant. The rotor mutual inductances are

$$\begin{array}{rcl} L_{FD} & = & L_{DF} = M_R, \\ L_{FQ} & = & L_{QF} = 0 \\ L_{DQ} & = & L_{QD} = 0 \end{array} \tag{80}$$

The phase to rotor mutual inductances are given by: (from phase windings to the field windings)

$$L_{aF} = L_{Fa} = M_F \cos(\Theta), \tag{81}$$

where the parameter M_F is given.

The stator to rotor mutual inductance for phase a (from phase windings to the direct axis of the damper windings) is

$$L_{aD} = L_{Da} = M_D \cos(\Theta), \tag{82}$$

with a given parameter M_D.

The phase a stator to rotor mutual inductances are given by: (From phase windings to the damper quadrature direct axis)

$$L_{aQ} = L_{Qa} = M_Q \cos(\Theta) \tag{83}$$

The parameters L_d, L_q, M_D, M_F, M_R and M_D used by the state space model (Eqs. (69) and (77)) are defined as

$$\begin{array}{l} L_d = L_s + M_s + \frac{3}{2}L_m \\ L_q = L_s + M_s - \frac{3}{2}L_m \\ M_D = \frac{L_{AD}}{k} \\ M_F = \frac{LAD}{k} \\ M_R = L_{AD} \\ M_Q = \frac{L_{AQ}}{k} \\ k = \sqrt{\frac{2}{3}} \end{array} \tag{84}$$

The elements of the equivalent circuit corresponding to the parameters L_F, L_D, L_Q, L_d, L_q, M_F, M_D, M_Q, r_F, r_D and r_Q, can be seen in Figure 4.

Using the initial assumption of symmetrical tri-phase stator windings (i.e. $r_a = r_b = r_c = r$) we get the resistance of stator windings of the generator, while r_F represents the resistance of the rotor windings, r_D and r_Q represent the resistance of the d and q axis circuit.

The resistance R_e and inductance L_e represent the output transformer of the synchronous generator and the transmission-line.

Since the variables in their natural units have a few orders of magnitude difference in their values, the equations are normalized using a base value (corresponding to the normal range of the variables). This way all signals are measured in normalized units (p.u.).

The parameters of the synchronous generator were obtained from the literature [7]. The stator base quantities, the rated power, output voltage, output current and the angular frequency are:

$$\begin{array}{rcl} s_B & = & 160 \text{ MVA}/3 = 53.333 \text{ MVA} \\ v_B & = & 15 \text{ kV}/\sqrt{3} = 8.66 \text{ kV} \\ i_B & = & 6158 \text{ A} \\ \omega_B & = & 2\pi f \text{ rad/s} = 2\pi 60\text{Hz rad/s} \end{array} \tag{85}$$

The time, flux, resistance and inductance quantities are calculated as:

$$\begin{array}{rcl} t_B & = & 1/\omega_B = 2.626 \text{ ms} \\ \lambda_B & = & v_B t_B = 22.972 \text{ Vs} \\ R_B & = & v_B/i_B = 1.406\ \Omega \\ L_B & = & v_B/(i_B/t_B) = 3.73 \text{ mH} \end{array} \tag{86}$$

The parameters of the synchronous machine [7] and the external network [7] in per units are:

$$\begin{array}{lll} L_d = 1.700 & l_d = 0.150 & L_{MD} = 0.02838 \\ L_q = 1.640 & l_q = 0.150 & L_{MQ} = 0.2836 \\ L_D = 1.605 & l_F = 0.101 & r = 0.001096 \\ L_Q = 1.526 & l_D = 0.055 & r_F = 0.00074 \\ L_F = 1.651 & l_Q = 0.036 & r_D = 0.0131 \\ L_{AQ} = 1.490 & r_Q = 0.054 & R_e = 0.2 \\ L_{AD} = 1.550 & L_e = 1.640 & D = 2.004 \\ V_\infty = 0.828 & & \end{array} \tag{87}$$

During the model analysis the above parameter set were used and this parameter set was used as the initial values for parameter estimation.

Chapter 3

Model analysis

In this section the model analysis of the state-space model of a synchronous generator is described. The model analysis results serve as preliminary investigations for model parameter estimation and controller design, but they are important tools for model verification, too.

Static and dynamic sensitivity analysis has been applied to determine the model parameters to be estimated. The main goal of the analysis was choosing the non-sensitive and the sensitive parameters from the parameters of the synchronous generator.

3.1 Characterization of the nonlinear model

The state space model of the synchronous generator deriver from engineering priciples (Eq. (69)) was expressed in the general form (Eqs. (70) and (71)). It is seen that the matrix $\boldsymbol{A}(\boldsymbol{x})$ is a function of the state vector ($\boldsymbol{x}$) and the output vector ($h(\boldsymbol{x}, \boldsymbol{u})$) is a nonlinear function of the state vector ($\boldsymbol{x}$), and the input vector ($\boldsymbol{u}$). The state space model of the synchronous generator is nonlinear in both the state and output equations, but it is input-affine. Observe, that these equations *are bi-linear in the state and input variables.*

It is also seen that one of the working criteria of the synchronous generator is that the angular velocity (ω) of the generator must be the synchronous angular velocity of the electrical network. Because of this reason during the simulations the angular velocity (ω) of the generator should be controlled. In open loop environment the synchronous generator is not operable, therefore the synchronous generator cannot be analyzed in open loop circumstances. This implies that in the linearized model the angular velocity (ω) of the synchronous generator is constant and the loading angle (δ) is not present.

3.2 The measurement methods in the Paks NPP

This subsection presents briefly the measurement methods in the Paks NPP which we used in model analysis, parameter estimation and controller design.

In the Paks nuclear power plant there are two independent data acquisition methods, one equidistant and one event oriented.

The VERONA system has been developed for the full scale core monitoring of the Hungarian Paks NPP. Services of the system satisfy virtually all operational core monitoring needs arising at the time. This data acquisition system monitors only some relevant data for the operation of the SGs in the plant, but these data are available in every sampling interval with a fixed sampling rate 2 sec. Display monitors are situated in the main control room and in the main computer room of all units. No connection among the units, nor with any other site (e.g. management) is available. Display screens with numerical, colored and graphical information serve the operator with all data relevant to the status of the core (see [1]).

Unlike the VERONA system with its fixed sampling rate, in the secondary circuit the data acquisition method is not equidistant, but event based. The computer stores only the data and the time when the change in the measured signals exceeds pre-selected limits individually set of each signals.

Finally, it should be emphasized, that because of operational and safety reasons, no experiment design with artificial disturbed inputs was permitted, and the plant was always under control, therefore only passive data were available for the parameter estimation. In order to promote sufficient excitation, measured data from load changng transients were used.

3.3 Model verification through analysis of dynamic properties

The model verification is an important step in developing a dynamic model, when one compares the qualitative dynamic properties of the model against engineering expectations. The stability of the open loop model, as well as disturbance rejection and reference tracking properties of the partially controlled model (i.e. the model with only the angular velocity controller) were investigated in order to perform the verification of dynamic model described in Chapter 2.

The disturbance rejection properties of the model have been investigated in such a way that a single SG was connected to an infinite bus that models the electrical network. Simulation analysis was used to investigate the disturbance rejective properties of the SG against load disturbance from the electrical network.

Furthermore, local stability analysis of the SG model has been performed around its physically meaningful equilibrium to find out whether the model is locally asymptotically stable.

3.3.1 The dynamic model for verification

The model equations (Eqs. (69) and (77)) developed in Section 2.3 were verified by simulation against engineering intuition using parameter values of a similar generator taken from the literature [7].

The dynamic properties of the generator have been investigated in such a way that a single synchronous generator was connected to an infinite bus that models

the electrical network. In addition, simple PI controllers were applied to the SG in the usual way as described below.

In the control scheme two classical PI controllers were applied that ensure stability of the equilibrium point under small perturbations [25]. The controlled outputs are the active power (p_{out}) and speed (ω), while the manipulated inputs are exciter voltage (v_F) and mechanical torque (T_{Mech}). The proportional parameter (P) of the PI controller of the speed is 0.05 and the integrator time (I) is 0.1 in per units, while the proportional and integrator parameters of the active power controller are 0.003 and 0.03, respectively.

3.3.2 The effect of changes in exciter voltage

First, the response of the speed controlled generator has been tested under step-like changes of the exciter voltage. The simulation results are shown in Fig. 8, where the exciter voltage v_F and the torque angle (δ) are shown together with the d and q components of the current.

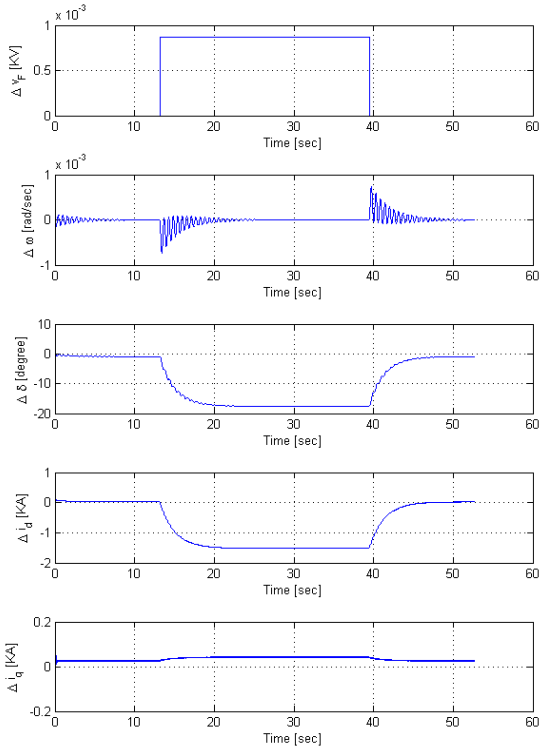

Figure 8: Response to the exciter voltage step change of the controlled generator (Δ means the deviation form the steady-state value)

When we increase the exciter voltage (v_F) we wait for the decreasing of the loading angle (δ) (see: [48], [37], [16] and [7]), it is seen in Fig. 8. It is also seen in the picture that the quadrature component of the stator current (i_q) does not show

any effect during the simulation because the exciter coil and the quadrature coil are not coupled magnetically.

In order to quantify numerically the magnitude of the deviation caused by the step-like change, the normalized cost function of the speed controller (C_{speed}) was used, that is calculated from the set value and the process value:

$$C_{speed} = \frac{\sqrt{\sum (\omega_{sv} - \omega_{pv})^2}}{n_{sample}}, \tag{88}$$

where ω_{sv} is the set value, ω_{pv} is the simulated process value and n_{sample} is the number of the sample points. The value of the cost function is $9.182 \cdot 10^{-7}$.

3.3.3 The effect of disturbances from the network

The effect of disturbances from the electrical network is modeled by using a noise from the infinite bus that appears in v_q. The transient behavior of the electrical power system ranges from the dynamics of lightning surges ($10^{-7} - 10^{-2}$ Hz, in time domain: $100 - 10^7$ sec) to that generator dispatch and load load following ($5 \cdot 10^3 - 5 \cdot 10^4$ Hz, in time domain: $2 \cdot 10^{-5} - 2 \cdot 10^{-4}$ sec), see in [6]

In order to investigate the effects of disturbances, step-like changes in the setpoint of the active power has been applied. Fig. 9. shows the simulation results. Here again, both the effective and the reactive power follow the setpoint changes well, and the controlled system is stable. In addition, the controller rejects the disturbances well.

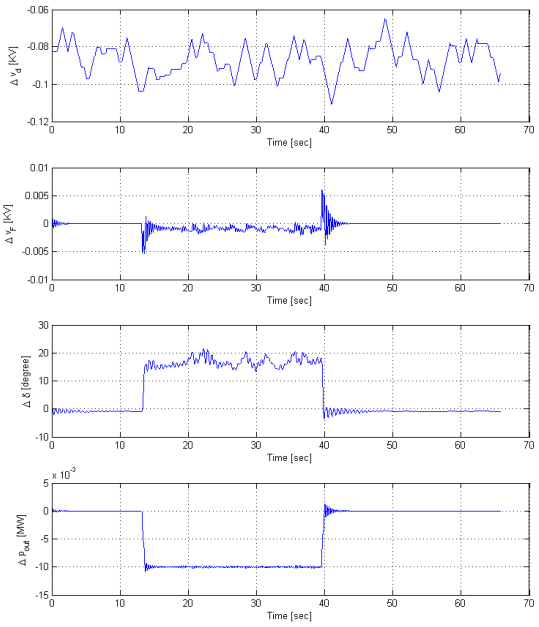

Figure 9: The effect of the network disturbances

The normalized cost function of the speed controller is calculable from the set value and the process value of the speed. The value of the cost function (Eq. (88)) of the speed controller is $2.101 \cdot 10^{-5}$.

Here again, the normalized cost function ($C_{ActivePower}$) of the active power controller was used to characterize the effect, that is calculated from the set value and the process value:

$$C_{ActivePower} = \frac{\sqrt{\sum (P_{sv} - P_{pv})^2}}{n_{sample}}, \tag{89}$$

where P_{sv} is the set value, P_{pv} is the simulated process value and n_{sample} is the number of the sample points. The value of the cost function of the active power controller is $2.414 \cdot 10^{-6}$.

More details on the effect of disturbances from the electrical network and the setpoint following of the SG are reported in [O2], [O3] and [O4].

3.3.4 Changing the active power of the generator

The response of the controlled SG has been tested under real measured active power changes of MVM Paks NPP that occurred in the setpoint of the active power. The simulation results can be seen in Fig. 10, where the simulated and the measured signals are shown. Measured signals are plotted on the right hand side of the figure while simulated signals are on the left side. Time is expressed in base time (t_B), so it can be calculated that the total simulation time is 7.7 hours.

Based on the above results it is apparent that both the active and the reactive power follow the setpoint changes, and the controlled system is stable. It is seen that both the simulated active power (p_{out}) and speed (ω) follow the setpoint changes well and the waveform of the exciter voltage (v_F) and the reactive power (q_{out}) are similar to the measured signals. Unfortunately the quality of measured exciter voltage (v_F) and reactive power (q_{out}) signals are poor compared to other signals because their measurement record consists of about 10-15 samples in the measured period. It is apparent that the dynamic behavior of the measured and the simulated exciter voltage (v_F) and the reactive power (q_{out}) signals are similar. The reason of the difference is the fact that the parameters used in the simulation are obtained only from a similar SG. The parameter estimation that was performed later and described in Chapter 4 has led to a better match.

3.3.5 Local stability analysis

Numerous studies on stability analysis of SG model are reported in the literature (Park [70], Anderson et al. [6], Barakat et al. [13], Mon and Aung [64], Prempraneerach et al. [72] and [21], Wamkeue at al. [99], Achilles et al. [3], Fernandez et al. [33], Basek et al. [14], Gonzalez-Longatt et al. [36], Arjona et al. [8], Basak et al. [14], Nanou et al. [67] Dehghani [27]), but none of them analyzed the stability as a function of the model parameters of the synchronous generator.

The steady-state values of the state variables can be obtained from the steady-state version of state equations (Eq. (69) and (77)) using the parameters given in Section 2.4. Equation (22) implies that the expected value of i_D and i_Q is 0, that

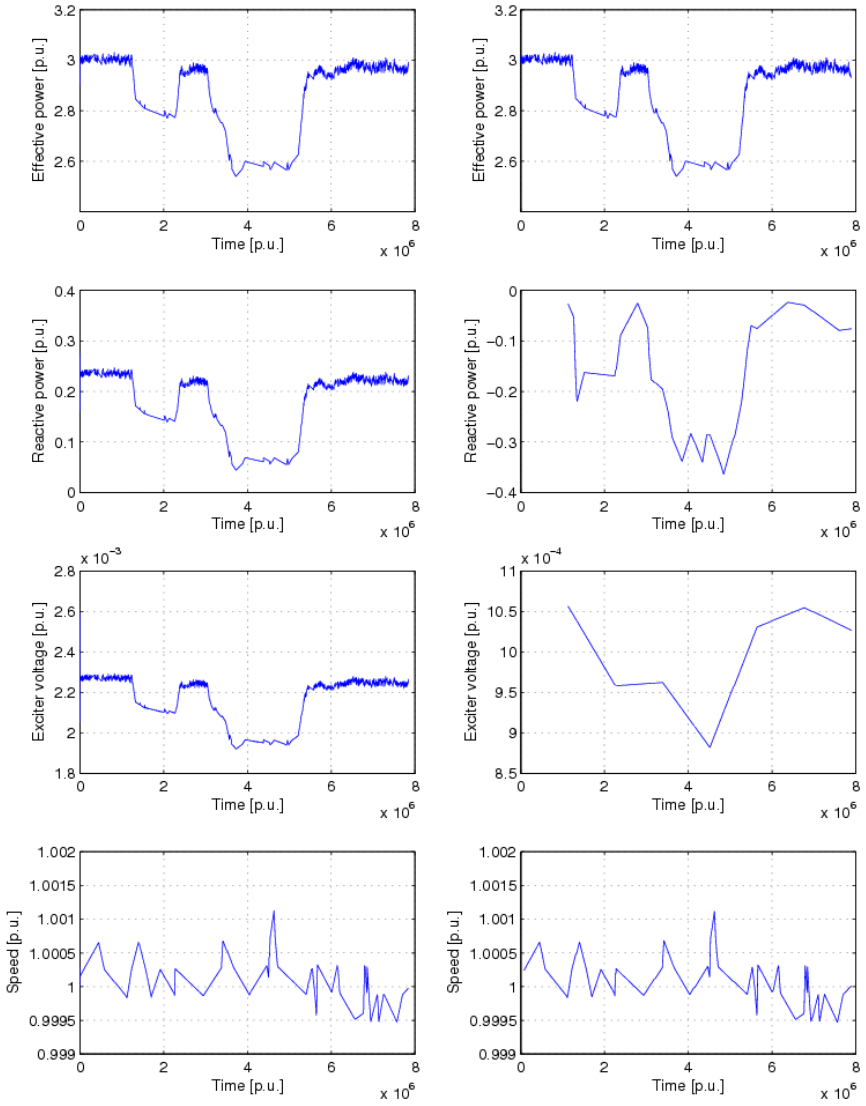

Figure 10: Changing the active power of the generator (Simulated and the measured signals)

coincide with the engineering intuition because the time derivatives of λ_D and λ_Q are 0. During normal operation the angular velocity (ω) of the generator must be the synchronous angular velocity (ω_r) which is equal 1 p.u. and every value of the state variables must be real.

During the model linearization the equilibrium point is determined first, that is substituted into the Jacobi matrix of the model (see [38]). It is important to emphasize, that the state equations for the angular velocity and the load angle will disappear from the state space model (Eq. (69)), because of the constant singular velocity assumption (it is set to the synchronous value 1 p.u.), therefore the linearized model is not suitable for any real control of an industrial SG.

As the model is nonlinear there are 9 possible equilibrium points of the system. From these there are only three cases, when the value of the state variables are real, in the remaining physically not plausible cases the state variable values have imaginary parts, too.

In the first case of equilibrium points (Eq. (90)) every value of the state variables is acceptable and physically plausible, this is the one we use in the following:

$$\begin{aligned} \omega &= 0.9990691 \\ i_d &= -1.9132609 \\ i_q &= 0.66750001 \\ i_F &= 2.97899982 \\ i_D &= -8.6242856 \cdot 10^{-9} \\ i_Q &= -5.3334899 \cdot 10^{-10} \end{aligned} \tag{90}$$

In the second case of equilibrium points (Eq. (91)) the angular velocity and the direct component of the stator current i_d of the generator are not plausible:

$$\begin{aligned} \omega &= 0.4320402945 \cdot 10^{-2} \\ i_d &= 62.12454774 \\ i_q &= 1.076826124 \\ i_F &= 2.978997177 \\ i_D &= -1.618398209 \cdot 10^{-7} \\ i_Q &= 2.380089275 \cdot 10^{-9} \end{aligned} \tag{91}$$

In the third case of equilibrium points (Eq. (92)) the angular velocity of the generator is not plausible:

$$\begin{aligned} \omega &= 0.4992888874 \\ i_d &= -1.637093230 \\ i_q &= 1.329936877 \\ i_F &= 2.978996329 \\ i_D &= -2.007337004 \cdot 10^{-7} \\ i_Q &= 9.388711640 \cdot 10^{-10} \end{aligned} \tag{92}$$

The state matrix $\boldsymbol{A}$ of the locally linearized state-space model $\dot{\boldsymbol{x}} = \boldsymbol{A}\boldsymbol{x} + \boldsymbol{B}\boldsymbol{u}$ has the following numerical value in this equilibrium:

$$\boldsymbol{A} = \begin{bmatrix} -0.0361 & 0.0004 & 0.0142 & -3.4851 & -2.5455 & -2.3285 \\ 0.0124 & -0.0049 & 0.0772 & 1.2011 & 0.8773 & 0.8025 \\ 0.0228 & 0.0044 & -0.0964 & 2.2057 & 1.6110 & 1.4737 \\ 3.5855 & 2.6464 & 2.6464 & -0.0361 & 0.0901 & 1.0247 \\ -3.5009 & -2.5839 & -2.5839 & 0.0352 & -0.1234 & -1.0005 \\ -8 \cdot 10^{-6} & -0.0002 & -0.0002 & -0.0008 & -0.0005 & -0.0011 \end{bmatrix} \tag{93}$$

The eigenvalues of the above state matrix are:

$$\begin{array}{ll} \lambda_{1,2} = -3.619088 \cdot 10^{-2} \pm & \text{j}0.997704 \\ \lambda_3 = -0.100024 & \lambda_4 = -1.67235 \cdot 10^{-3} \\ \lambda_5 = -4.724291 \cdot 10^{-4} & \lambda_6 = -0.123426 \end{array} \tag{94}$$

It is apparent that the real part of the eigenvalues are negative but their magnitudes are small, thus the system is on the boundary of the stability domain. Furthermore, the two first eigenvalues are complex with a relatively large imaginary part, that indicates the presence of an oscillatory component in the response.

The time-constants of the synchronous generator can be calculated from Eq. (94). The time-constants (in p.u.) of the above state-space model are:

$$\begin{array}{l} T_1 = 8.13 \\ T_2 = 10.0 \\ T_3 = 27.62 \\ T_4 = 598 \\ T_5 = 2118 \end{array} \tag{95}$$

The effect of the change in the values of the input variables (v_d, v_q, v_F and T_m) to the equilibrium point of the SG was also investigated. The values of the equilibrium points and the time constants are collected in Tables 1, 2 and 3.

It is seen that the model is sensitive to the modification of the following inputs: network voltage components (v_d and v_q), exciter voltage (v_F) and the mechanical torque (T_m). As the d and q components of the voltage of the generator (v_d and v_q) are related to the voltage of the infinity huge electrical network (v_∞) and the loading angle (δ) as

$$v_\infty^2 = v_d^2 + v_q^2 \ . \tag{96}$$

The synchronous generator is sensitive to the changing of the voltage of the electrical network, too.

3.4 Sensitivity analysis for parameter estimation

The aim of this section to perform preliminary investigations for model parameter estimation by forming parameter groups according to the system's sensitivity on them.

Name	Nominal value (p.u.)	Change v_d (+10%)	Change v_d (-10%)	Change v_q (10%)	Change v_q (-10%)
ω	0.9997	0.631	1.0822	0.9991	0.9990
i_d	-1.91	-1.75	-1.908	-1.897	-1.948
i_q	0.667	1.156	0.5569	0.6673	0.6679
i_F	2.978	2.978	2.9789	2.9789	2.9789
i_D (10^{-9})	-8.62	-74.11	76.244	-200.89	-200.9
i_Q (10^{-10})	-5.33	5.49	-7.783	-224.08	-10.66
Physically acceptable	Yes	No	No	Yes	Yes
$\lambda_{1,2}$ (10^{-2})	-3.61 $\pm$j99.7			-3.5 $\pm$j99.7	-35.0 $\pm$j99.7
λ_3	-0.100			-0.1234	-0.1234
λ_4	$-1.67 \cdot 10^{-3}$			$-0.4688 \cdot 10^{-3}$	$-0.4806 \cdot 10^{-3}$
λ_5	$-4.72 \cdot 10^{-4}$			$-0.168 \cdot 10^{-2}$	$-0.164 \cdot 10^{-3}$
λ_6	-0.123			-0.0297	-0.0299
Stable?	Yes	-	-	Yes	Yes
T_1	8.13			8.103	8.103
T_2	10.0			28.55	28.55
T_3	27.62			33.67	33.44
T_4	598			595	2080
T_5	2118			2133	6097

Table 1: The equilibrium points and the time constants as functions of the generator input voltage components (v_d and v_q)

Name	Nominal value (p.u.)	Change v_F (+10%)	Change v_F (+10%)	Change V_F (-10%)
ω	0.9997	0.644	0.853	0.853
i_d	-1.91	-1.99	-2.095	-2.095
i_q	0.667	1.035	0.783	0.7838
i_F	2.978	3.277	3.277	3.276
i_D	$-8.62 \cdot 10^{-9}$	$-1.08 \cdot 10^{-7}$	$-1.08 \cdot 10^{-7}$	$-1.08 \cdot 10^{-7}$
i_Q	$-5.33 \cdot 10^{-10}$	$3.19 \cdot 10^{-10}$	$-3.54 \cdot 10^{-10}$	$-3.54 \cdot 10^{-10}$
Physically acceptable	Yes	No	No	No

Table 2: The equilibrium points as functions of the exciter voltage (v_F)

Name	Nominal value (p.u.)	Change T_m (+10%)	Change T_m (-10%)
ω	0.9997	1.249	-
i_d	-1.91	-1.91	-
i_q	0.667	0.534	-
i_F	2.978	2.978	-
i_D	$-8.62 \cdot 10^{-9}$	$-2.01 \cdot 10^{-7}$	-
i_Q	$-5.33 \cdot 10^{-10}$	$-1.26 \cdot 10^{-9}$	-
Physically acceptable	Yes	No	-

Table 3: The equilibrium points as functions of the mechanical torque (T_m)

The parameters of the model used for controlled design purposes were given and discussed in Section 2.4 together with their typical nominal values taken from the literature. The developed model has 23 parameters, 19 of them belong closely to the SG, the remaining four characterize the controllers. This number is too high for any engineering parameter estimation method that can handle dynamic models nonlinear in its parameters. Therefore, the need arises to select those "influential" parameters for parameter estimation that effect significantly the dynamic response of the SG, and thus the measured data may have sufficient information for their estimation.

There are a few sensitivity analysis results in the literature (e.g.: Caracotsios and Stewart [21], Prempraneerach et al. [73] and [72]) but none of them analyzes the change of the model parameters of the synchronous generator.

Simple ways of parametric sensitivity analysis were therefore carried out to determine the parameters that can be reliably estimated using both preliminary and estimation error based sensitivities.

3.4.1 Frequently used methods in sensitivity analysis

There is a vast amount of literature that investigate the various type of sensitivities of the linear and non-linear systems with differential analysis methods, for example [41].

The continuous sensitivity equations (variational equations) are a possible approach for computations of derivative. They are defined in the context of the variations, see in [18]. Riley at al. [79] utilize the linearity of the sensitivity equations to express the Adams-Moulton formula. For sensitivity computations Maly and Petzold [58], Caracotsios and Steward [22] developed and used the Backwards Differentiation Formula (BDF).

Using the continuous adjoint equations is also one way to compute the sensitivity function, this is the method of adjoint sensitivity analysis [41]. The first-order and second-order adjoint equations for the computation of the Hessian have been presented by Haug and Ehle in [44]. The first-order adjoint equations for the differential-algebraic problem have been derived by Cao et al. [20].

The sensitivity analysis of the non-smooth systems has been presented by Hannemann-Tamás in [41]. The non-smooth dynamical systems can be derived in three types, according to Leine and Nijmeijer (see in [52]). Existence and uniqueness conditions of index reduction techniques for non-smooths system have been analyzed by Mehrmann and Wunderlich in [59]. The forward sensitivity equations for implicite index-1 DAE systems have been derived by Galan et al. in [34]. The equations associated with ordinary differential equations by means of a Lagrangian approach have been derived by Ruban in [81].

In general, neither the state equations nor the forward sensitivity or adjoint equations can be solved analytically. Instead, some numerical integration method has to be applied see in [41]. RADAU5 and several more linearly and linearly-implicit Runge-Kutta methods to so-called discrete tangent-linear and discrete adjoint sensitivity analysis have been extended by Sandu and Miehe, see in [83]. Schlegel et al. [84] has demonstrated to be computationally efficient for forward sensitivity analysis. One step-methods applied to semi-explicit DAE systems of index 1, result in differential discrete adjoints, in contrast to multi-step methods, see in [82].

3.4.2 The dynamic model of the SG used for the analysis

As it has been mentioned before, control schemes of synchronous machines are commonly based on a non- linear model with two classical PI controllers that ensure stability of the equilibrium point under small perturbations [25].

One controlled output is the active power (p_{out}) with the manipulated input being the exciter voltage (v_F), while the angular velocity (ω) is controlled by manipulating the mechanical torque T_{Mech} (indirectly through the steam flow rate to the turbine).

As each PI controller has two parameters, our model includes the parameters of the *exciter voltage controller* (P and I), and that of the *angular velocity controller* (P_ω and I_ω).

3.4.3 The aim and the method of the sensitivity analysis

The preliminary sensitivity analysis was used to pre-select those parameters that have no or negligible influence on the model outputs. Here we performed dynamic simulations with the nominal values of the parameters, and by changing them one-by-one 10% up and down from their nominal values, we repeated the simulations and observed the differences in the output. This way we have concluded that the model output is not sensitive to the inductances l_d, l_q, l_D, l_Q, L_{MD}, L_{MQ} and L_Q, therefore they could be excluded from the set of the parameters to be estimated, and their value was fixed to ensure the stability of the model.

On the other hand, the preliminary sensitivity analysis revealed two model parameters, the inductances L_{AD} and L_D, that affect critically the stability of the closed loop model. There was only a very narrow region in their physically meaningful domain, where the stability of the model could be guaranteed. Therefore, these parameters were also excluded from the set of parameters to be estimated.

Linkage inductances l_d, l_q, l_D, l_Q, L_{MD} and L_{MQ} are not used by the current model, only by the flux model. It is not expected that the output and the state

variables of system change when these parameters are perturbed, see Fig. 11. As it was expected, the model is insensitive for these parameters. Note, that the linkage inductance parameters are only used for calculating the fluxes of the generator.

The sensitivity of the model to the controller parameters P and I and the dumping constant D has also been investigated. Since the PI controller controls ω modifying the value of D the controller keeps ω at synchronous speed. This is why the output and the steady state value of the system variables do not change (as it is apparent in Fig 12) even for a considerably large change of D.

Sensitivity analysis of the resistance of the stator and the resistance of the transmission line led to the same result. A $\pm 20\%$ perturbation in them resulted in a small change in currents i_d, i_q and i_F, this causes the change of the effective and the reactive power of the generator, as it is shown in Fig. 13.

The analysis of the rotor resistance r_F showed, that the $\pm 20\%$ perturbation of r_F kept the quadratic component of the stator current (i_q) constant, but currents i_d and i_F were changed. The output of the generator also changed, as it is shown in Fig. 14.

The sensitivity of the model states and outputs to the inductance of the rotor (L_F) and the inductance of the direct axis (L_D) has also been analyzed. The results show only a moderate reaction in i_d and i_F to the parameter perturbations, and the equilibrium state of the system kept unchanged. However, decreasing the value of the parameters to the 90 percent of their nominal value destabilized the system. The results of a $\pm 9\%$ perturbation in L_F are shown in Fig. 15. A small perturbation of the outputs is noticeable.

Finally, the sensitivity of the model (Eqs. (69) and (77)) to the linkage inductance L_{AD} has been examined. When the parameter has been changed by $\pm 5\%$, currents i_d and i_F changed only a little. On the other hand, the steady-state of the system has shifted as it can be seen in Fig. 16. A parameter variation of 5% destabilized the system.

3.4.4 Results and conclusion of the sensitivity analysis

As a result of the sensitivity analysis, it is possible to define the following groups of parameters:

- Not sensitive
  inductances l_d, l_q, l_D, l_Q, L_{MD}, L_{MQ}, L_{AQ}, L_Q, damping constant D and the controller parameters P and I. Since the state space model of interest is insensitive for them, the values of these parameters cannot be determined from measurement data using any parameter estimation method.

- Sensitive
  - Less: resistances of the stator r and the transmission-line R_e.
  - More: resistance r_F of the rotor and the inductance of transmission-line L_e. These parameters are candidates for parameter estimation.

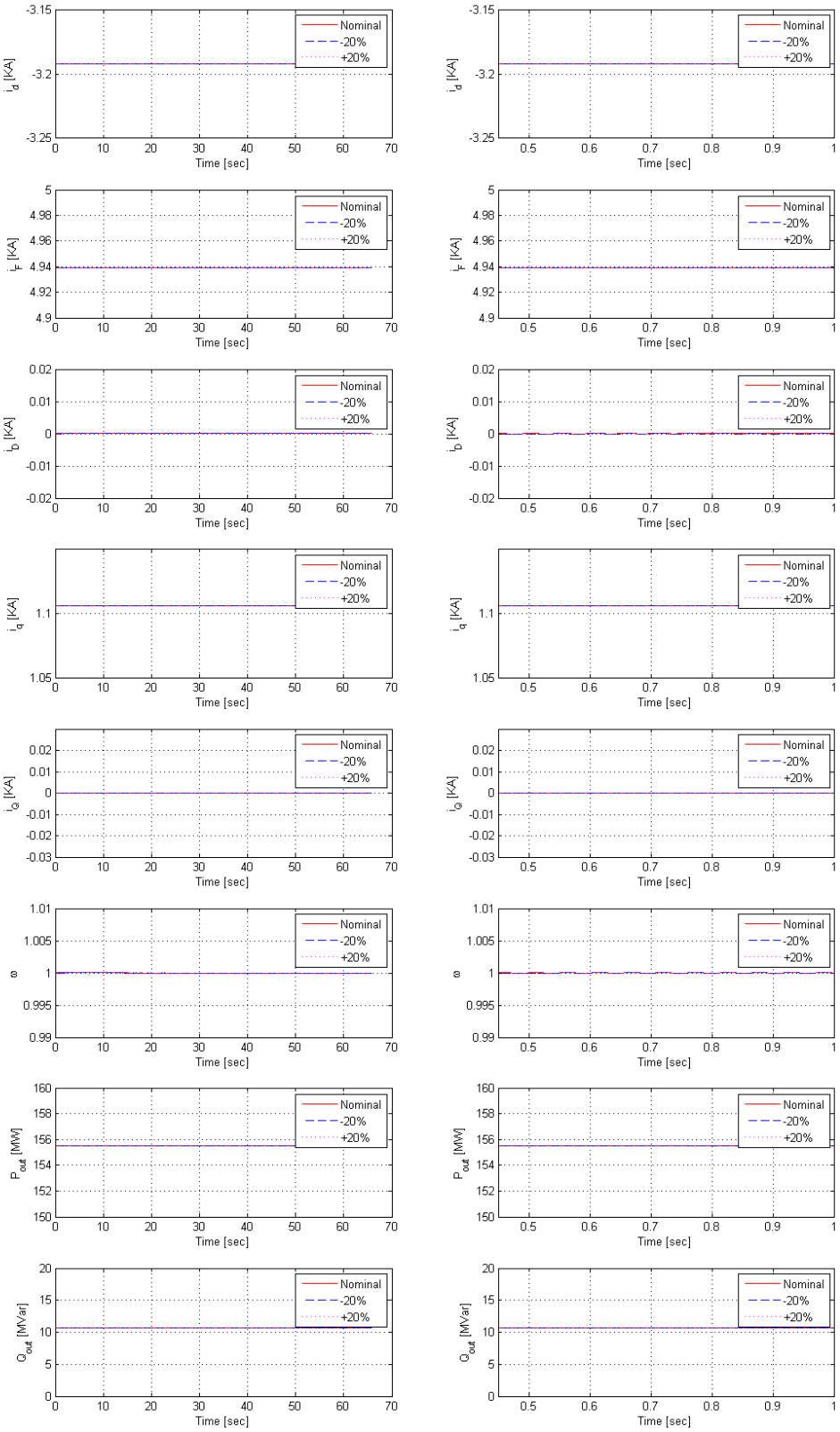

Figure 11: The model states and outputs for a $\pm 20\%$ change of l_d, on right hand side can see the transient after the parameter changing

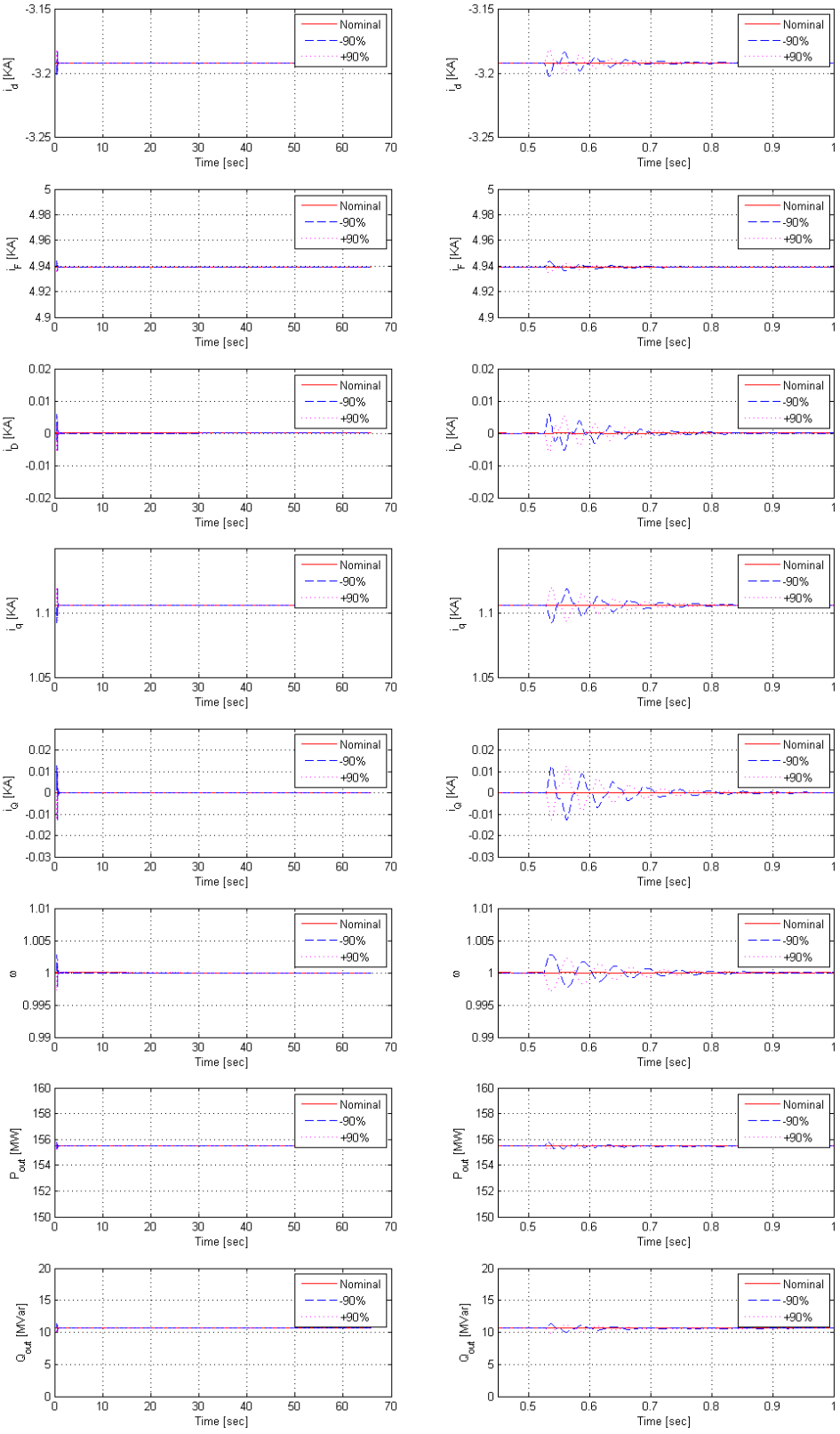

Figure 12: The model states and outputs for a $\pm 90\%$ change of D, on right hand side can see the transient after the parameter changing

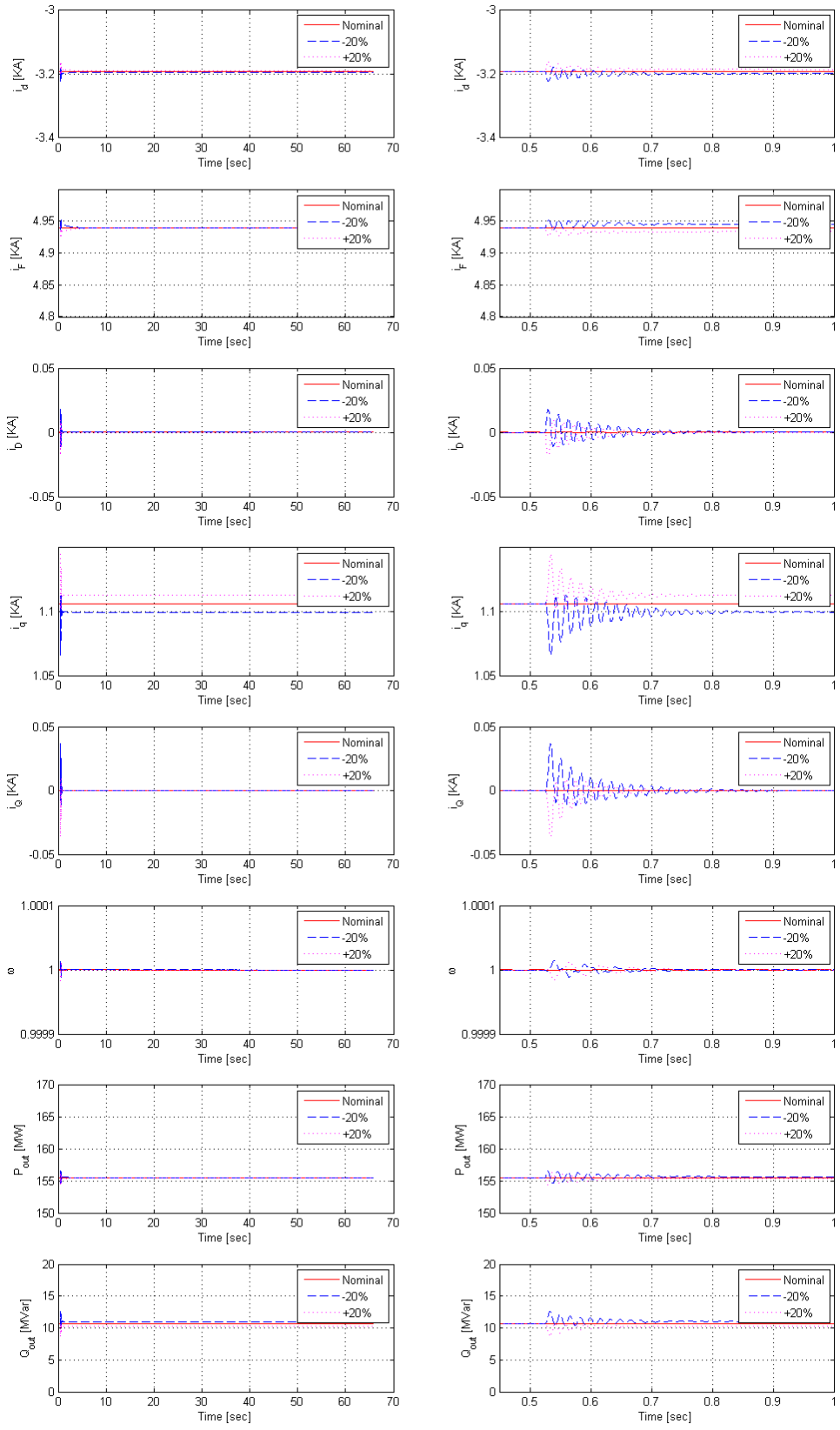

Figure 13: The model states and outputs for a ±20% change of r_{resist}, on right hand side can see the transient after the parameter changing

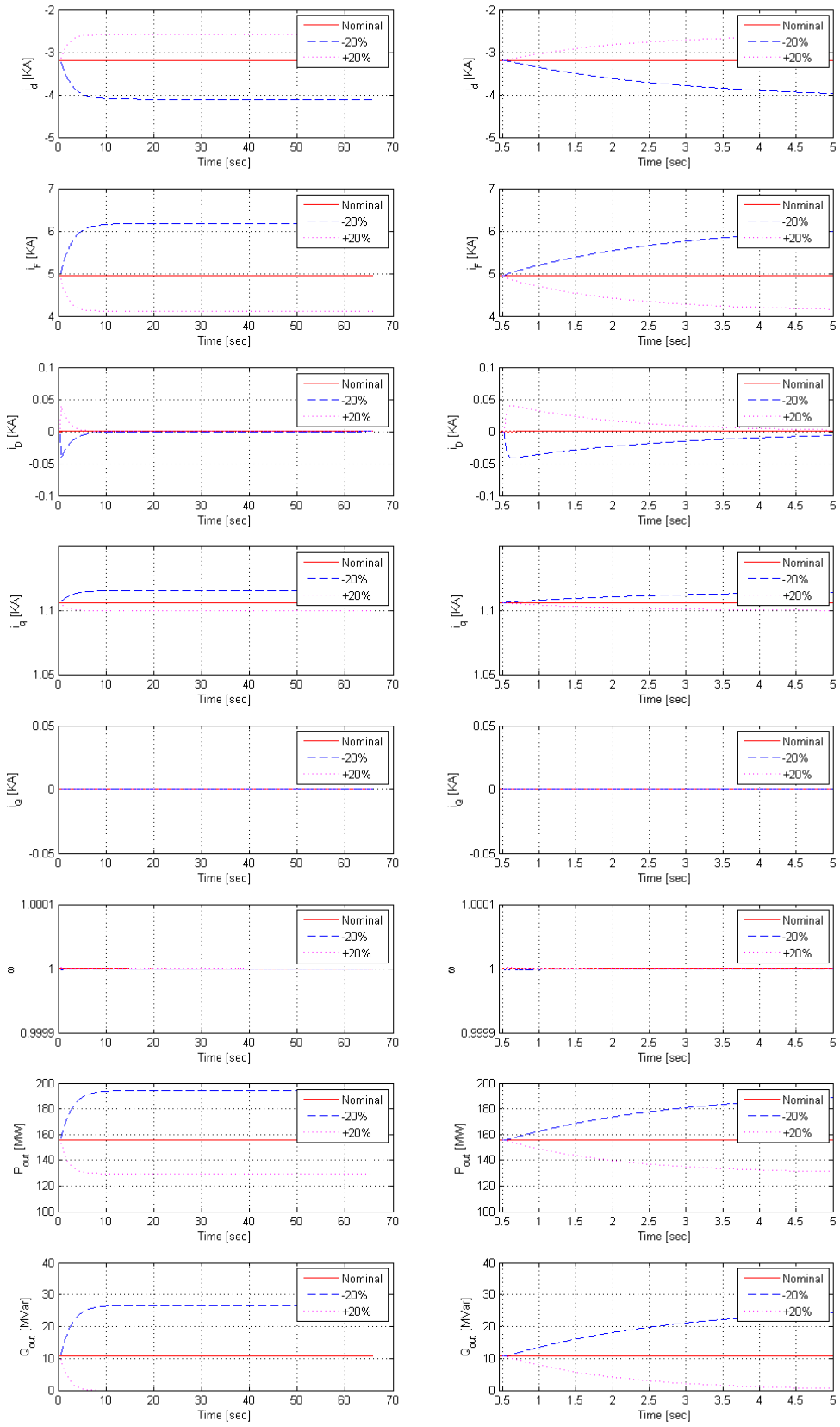

Figure 14: The model states and outputs for a ±20% change of r_F, on right hand side can see the transient after the parameter changing

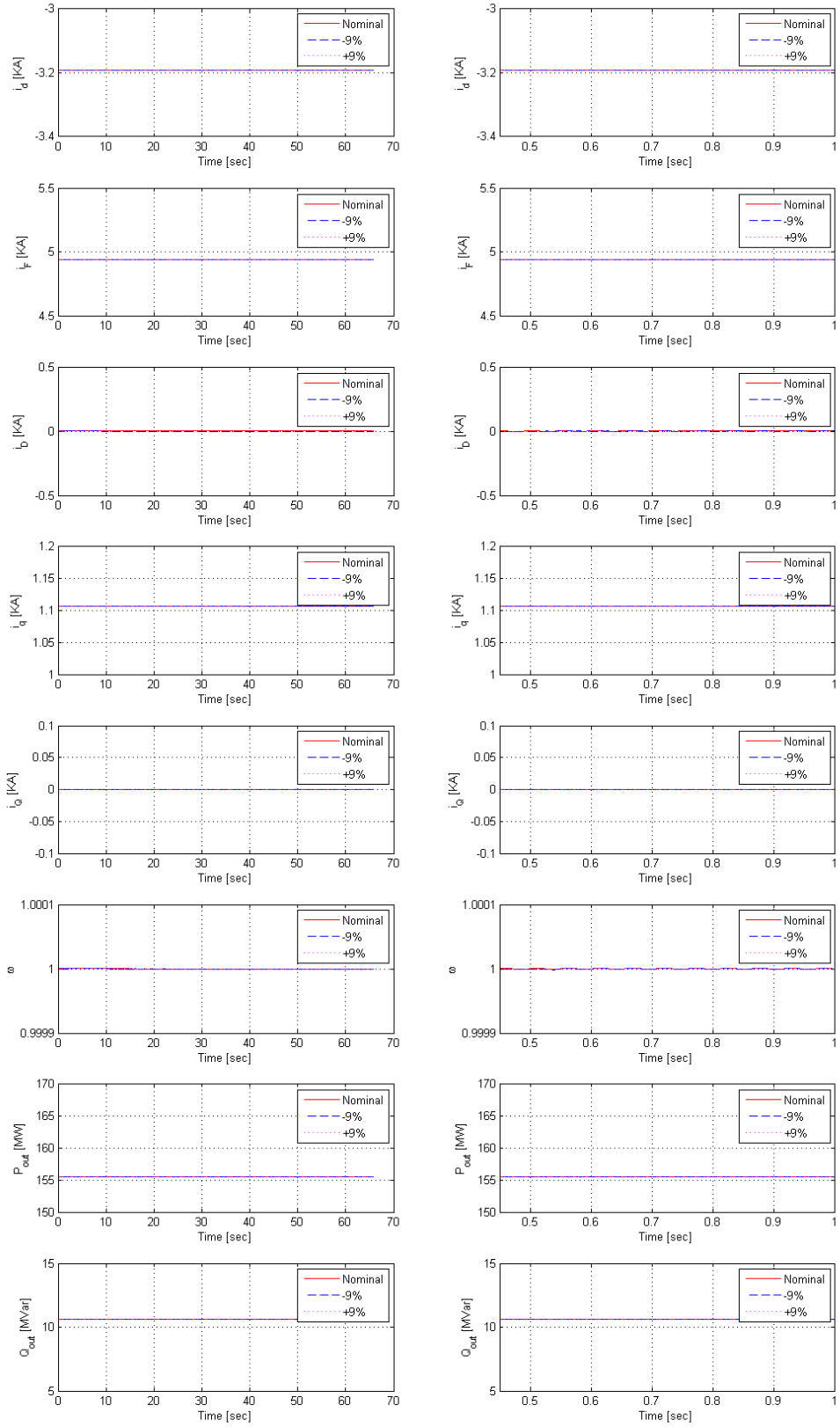

Figure 15: The model states and outputs for a ±9% change of L_F, on right hand side can see the transient after the parameter changing

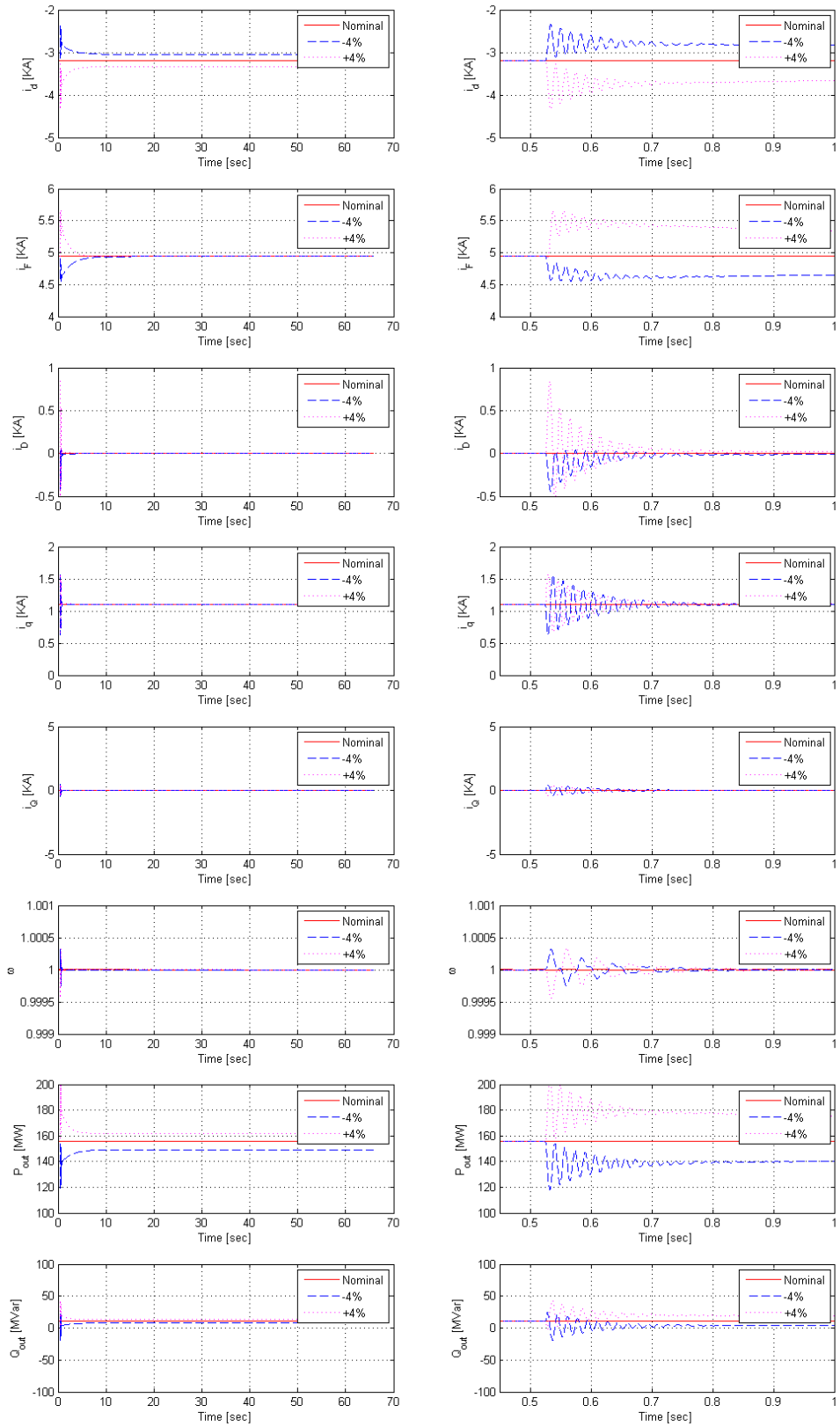

Figure 16: The model states and outputs for a ±4% change of L_{AD}, on right hand side can see the transient after the parameter changing

- Critically sensitive
  linkage inductance L_{AD}, inductances L_D and L_F. These parameters can be estimated very well.

Based on the results of the sensitivity analysis we can choose the parameters for the parameter estimation and we can choose the initial value and the limits for the parameters. As the system is on the boundary of the stability domain, when we change the value of critically sensitive parameters in a great extent the system will be unstable because the real part of some eigenvalues of the model will be positive.

3.5 Summary

The simple bilinear dynamic model of an industrial size synchronous generator operating in a nuclear power plant described in Chapter 2 has been analyzed in this chapter. The parameters obtained from the literature for a similar generator [7] were used.

Simple but effective model analysis methods were proposed for model verification and for preliminary parameter selection in parameter estimation of the synchronous generator. It has been shown, that the proposed simple methods of the model analysis are suitable for model verification and stability analysis of the model of the synchronous generator. An initial parameter set has also been found by modifying the set in [7] in such a way, that the dynamic properties of the model shows the ones of engineering expectations.

All parameters of the system has been selected for preliminary sensitivity analysis, and the sensitivity of the state variables and outputs has been investigated for all of them. The sensitivity analysis on the partially controlled generator has been performed by simulation by using a traditional PI controllers. Based on the result of the sensitivity analysis, it is possible to define 4 groups of parameters: Not sensitive, Less sensitive, More sensitive and Critically sensitive.

Based on the results presented in Section 3.4 seven parameters of the model (L_F, r_F, r, L_d, L_q, L_{AQ}, D) and two parameters of the controllers (P, I) were selected to parameter estimation.

Chapter 4

Parameter estimation

This chapter is devoted to the parameter estimation of a synchronous generator of Paks NPP. There are different suggested ways in the literature how one can determine the model parameters of a dynamic model of a synchronous generator. One family of the methods is based on measurements using different speed and voltage values (for example Hasni et al. [43], Vas [92] or Watson and Manchur [100]) or perform short circuit tests (see Wamkeue et al. [99]). The other family of the methods is based on dynamic (possibly passive) measurements performed in an industrial environment (see: Huang et al. [45], Kyriakides and Heydt [51], Melgoza et al. [60], Mouni et al. [66], Rahman and Hiti [75] Wamkeue et al. [97]). As we could use real measured data from a synchronous generator operating in Paks NPP, the parameter estimation method described here belongs to the second group.

The developed model (Eqs. (69) and (77)) together with the model equations of the two considered PI controllers have been used for estimating the parameters using measured data from the Paks NPP obtained from load changing transients. The model is nonlinear in its parameters, therefore a special, optimization-based parameter estimation have been used that minimized the estimation error.

4.1 The measured signals and the estimation error function

There are six measured signals available from the generator: the active power (p_{out}), reactive power (q_{out}), angular velocity (ω), exciter voltage and current (v_F and i_F), and the stator current (i_{out}). The vector of measured signals is:

$$\boldsymbol{d}_d = \left[\begin{array}{cccccc} p_{out} & q_{out} & \omega & v_F & i_F & i_{out} \end{array} \right]^T, \tag{97}$$

where the output current (i_{out}) of the SG is the following:

$$i_{out} = \sqrt{i_d^2 + i_q^2} \tag{98}$$

Note that p_{out}, q_{out} and i_{out} are output variables, i_F and ω are state variables, and v_F is an input variable of the state space model (Eqs. (69) and (77)).

i	Signal	n_i	w_i
1	p_{out}	0.02152	0.5
2	q_{out}	$1.6348 \cdot 10^{-3}$	1.0
3	ω	58979.45	0.5
4	v_F	1971.391	0.2
5	i_F	$7.345 \cdot 10^{-4}$	0.2
6	i_{out}	$2.0445 \cdot 10^{-3}$	0.2

Table 4: Measured signals with their normalizing factors and weights

A six hour long measurement record has been used to estimate the parameters of the SG. Unfortunately, the quality of the measured exciter voltage and current (v_F and i_F), and that of the output current (i_{out}) signals were poor compared to the other signals, as their measurement record consisted of about 10 samples in the measurement period. In order to achieve sufficient excitation of the system that is needed for parameter estimation, we have used a measurement record containing of a load changing transient that is ***not*** a usual operation course of the power plant unit. This ensures that the measured data carry enough information for the parameters in the dynamic model so that they could be reliably estimated.

4.1.1 The estimation error

Having the measured signals $\boldsymbol{d}_d$ and their counterparts computed by the model $\tilde{\boldsymbol{d}}_d$, the estimation error can be defined as the mean-square deviation for these signals. However, because of the above mentioned signal quality problems, the estimation error has been calculated only in a ten minute neighborhood of the measured values of v_F, i_F and i_{out} (see Fig. 2 in Chapter 1 about the time plot of the measured signals).

Furthermore, the huge domain width of the signal values in the deviations (that can be as large as from $1.696 \cdot 10^{-5}$ to 1361.5) requires a normalization to transform each to the range of 1. The constant vector $\boldsymbol{n}$ was used for this purpose, the value of which is seen in the third column of Table 4.

Finally we recall, that the intended use of the model is to control the active and the reactive power, therefore we want the model to reproduce these signals in the best quality. Therefore, a signal weight vector $\boldsymbol{w}$ has been introduced, with the weights seen in the last column of Table 4.

With the above, the error function V is calculated form $\boldsymbol{d}_d$, $\boldsymbol{n}$ and $\boldsymbol{w}$ as

$$V = \sum_{t=1}^{N} \left(\sum_{i=1}^{6} w_i \cdot n_i \cdot (d_{di}(t) - \tilde{d}_{di}(t))^2 \right), \tag{99}$$

where N is the number of measurement points, and

$$\tilde{\boldsymbol{d}}_{\boldsymbol{d}} = \begin{bmatrix} \tilde{p}_{out} & \tilde{q}_{out} & \tilde{\omega} & \tilde{v}_F & \tilde{i}_F & \tilde{i}_{out} \end{bmatrix}^T$$

is the vector of model-predicted signals.

Parameter	-50%	-20%	-10%	-5%	0%	10%	20%	50%
L_{AD}	199.3	17.7	9.3	7.9	6.8	x	x	x
L_D	x	x	x	8.5	6.8	x	5.8	7.1
L_F	x	x	x	2.2	6.8	6.1	2.4	4.9
r_F	2.5	6	5.8	5.4	6.8	6.3	7.5	4.1
L_e	27.8	4.2	2.9	4	6.8	7.4	9.2	24.5
R_e	2	3.5	9.3	6.9	6.8	2.4	4.4	4.9
r	6.4	8.4	7	8	6.8	5.4	5.8	3.3
L_d	x	41.3	6.5	6.7	6.8	7.6	16.3	291
L_q	x	41.3	7.5	3.3	6.8	14.9	56.7	154.6
L_Q	x	6.2	5	7.9	6.8	5.7	x	x
L_{AQ}	3.9	5.7	7	8.1	6.8	6	x	x
l_d	6.8	6.8	6.8	6.8	6.8	6.8	6.8	6.8
l_q	6.8	6.8	6.8	6.8	6.8	6.8	6.8	6.8
l_F	6.8	6.8	6.8	6.8	6.8	6.8	6.8	6.8
l_D	6.8	6.8	6.8	6.8	6.8	6.8	6.8	6.8
l_Q	6.8	6.8	6.8	6.8	6.8	6.8	6.8	6.8
L_{MD}	6.8	6.8	6.8	6.8	6.8	6.8	6.8	6.8
L_{MQ}	6.8	6.8	6.8	6.8	6.8	6.8	6.8	6.8
r_D	7.2	6.8	6.6	6.3	6.8	7.4	3.6	9.5
r_Q	3.7	5.9	7.2	7.2	6.8	5.8	4.7	4.7
D	4.6	12.5	7.8	4.2	6.8	5.3	4.8	6.4
P	6.3	7.3	7.4	7.5	6.8	7.5	6.4	6.4
I	3.6	4.4	4.9	6.7	6.8	4.8	5.8	6.8

Table 5: Error function value with changing the parameter values

4.1.2 Sensitivity of the estimation error function

Recall, that a preliminary sensitivity analysis has already been performed and described in Section 3.4, in order to select the parameters to be estimated from the large set of all model parameters. As the model of the SG is non-linear, this set may van with the operating regime so a further refinement of the parameters to be estimated was necessary.

During this refinement, further parameters from the set of less influencing ones, including the resistances r_D and r_Q, have been excluded from the set of parameters to be estimated based on the analysis of the sensitivity of the estimation error function in Eq. (99) with respect to them.

In the first step of refinement we checked the error function using simulations. We used valid measured data from MVM Paks NPP during the simulation. In the simulation we used power changing transient data that is seen in Fig. 2 in Chapter 1. The simulations were performed with the nominal values of the parameters, and by changing them one-by-one 5%, 10%, 20% and 50% up and down from their nominal values. The simulations were repeated and the differences were observed in the outputs, and finally the error signal value were computed. In Table 5 the x

Description	Value
Apparent energy	259 MVA
Output voltage	15.75 kV
Output current	9490 A
$\cos\varphi$	0.85
Frequency	50 Hz
Excitation current	1450 A
Excitation voltage	435 V

Table 6: Nominal operating data of the SGs which work in Paks NPP

character denotes that the model is unstable. With this simulation we can set the validity domain of the parameter set.

4.2 Generator parameters and initial values

As we have seen before in Section 2.3, the developed model (Eqs. ((69) and (77)) has 23 parameters that are collected in Table 7.

The initial values of the parameters of the generator in the MVM Paks NPP used in the parameter estimation method were taken from the literature [7], where the parameters for a similar generator were given. In the case of known engineering parameters of the SG in MVM Paks NPP, the initial values of those parameters were set to their known values. In some cases, however, slight modifications of the parameters taken from the literature were made during the preliminary simulation experiments dedicated for the parameter sensitivity analysis (see earlier Section 3.4). All nominal parameters have been normalized, i.e. transformed to p.u. The resulting initial values can be seen in the second column of Table 7.

4.2.1 Choice of the base and normalized quantities

The first step in parameter estimation is to choose the basic values of the signals that are needed for computing the normalized (p.u.) values of the considered SG in the Paks NPP. For this, the nominal (original) operating values of the SG were recorded which collected in Table 6.

The base quantities were determined from the stator measured steady state value of the rated power $s_B = 259$ MVA$/3 = 86.333$ MVA, the output voltage $v_B = 15.75$ kV$/\sqrt{3} = 8.874$ kV, the output current $i_B = 9729$ A, and the angular velocity $\omega_B = 2\pi f$ rad/s, where the subscript B refers to the base value of quantities. Using the base quantities, we can calculate the base units for time, resistance and inductance, that are $t_B = 1/(2\pi 50 \text{ Hz}) = 3.183$ ms, $R_B = v_B/i_B = 0.912\ \Omega$ and $L_B = v_B/(i_B/t_B) = 2.90$ mH.

From the measured rotor signals we can calculate the rotor base current and voltage values, that are $i_{FB} = 454.625$ A and $v_{FB} = 189900$ V. Using the above rotor base values, the base units for resistance ($R_{FB} = v_{FB}/i_{FB}$), inductance ($L_{FB} =$

$v_{FB}/(i_{FB}/t_{FB})$) can be easily obtained. The normalized quantities are obtained from the original ones by dividing them with the base quantities.

4.2.2 Initial values of the parameters

The known parameters of SG operating at Paks NPP has been transformed to p.u. The resulting per unit parameters were almost equal to the parameter of the smaller SG. After a few simulations some parameters have been modified and set as the initial parameter values of the generator.

Note that the original known coils and the exciter parameters of the SG were modified because the output power of the nuclear units was increased.

Besides the model parameters and their nominal values that belong closely to the SG, the parameters (P_ω and I_ω) of the angular velocity controller (turbine speed controller), and that of the exciter voltage controller (P and I) are also given in Table 7. The parameters of the speed controller has been set to $P_\omega = 0.05$ and $I_\omega = 0.1$ and the parameters of active power controller to $P = 1.096 \cdot 10^{-3}$ and $I = 1.096 \cdot 10^{-5}$. Using this improved parameters for the speed controller the speed follows better the set points in the simulation, but the torque demand was higher than that is available from the turbine.

The results of the sensitivity analysis (see in subsection 3.4.4 before) are also indicated in the third column of Table 7 with a "y" (i.e. "yes") answer to the "est.?" (i.e. "estimated?") question.

Based on the above sensitivity analysis results, the parameters to be estimated are: L_F, r_F, r, L_d, L_q, L_{AQ}, D, P, I. The value of all the other parameters was set and held constant to its nominal value shown in Table 7. Finally, some initial values in the state equations were calculated. The measured value of the exciter voltage is $v_F(t = 0) = 0.001645$. From this, we can calculate the initial value of $\delta = 0.36$rad and obtain the d and q components of the network voltage: $v_d(t = 0) = -1.3585$, $v_q(t = 0) = 0.46$ given in p.u.

4.3 The parameter estimation method and error function minimization - APPS

With the above classification of parameters, the appropriately designed estimation error (99) can be regarded as a function of parameters to be estimated, i.e. $V(L_F, r_F, r, L_d, L_q, L_{AQ}, D, P, I)$ given the value of the measured signals. The error function (V) and its weights were selected according to the measurement and data collection properties of data in MVM Paks NPP.

A commonly accepted way of estimating the parameters is to minimize this estimation error function, that is

$$\min_{L_F, r_F, r, L_d, L_q, L_{AQ}, D, P, I} V(L_F, r_F, r, L_d, L_q, L_{AQ}, D, P, I) \tag{100}$$

and take the minimizer as an estimate.

The weights of error function have been defined considering of the different quality of the measured industrial signals.

Parameter	initial value (p.u.)	est.? (y/n)	estimated value (p.u.)	confidence (%) (for 90%)
L_{AD}	1.550	n	-	-
L_D	1.605	n	-	-
L_F	1.65	y	1.651	3
r_F	$7.4 \cdot 10^{-4}$	y	$6.305 \cdot 10^{-4}$	3
r	$1.096 \cdot 10^{-3}$	y	$1.09 \cdot 10^{-3}$	4.9
L_d	1.7	y	2.1	2.9
L_q	1.64	y	1.526	1.2
L_Q	1.526	n	-	-
L_{AQ}	1.55	y	1.527	4.8
l_d	0.150	n	-	-
l_q	0.150	n	-	-
l_F	0.101	n	-	-
l_D	0.055	n	-	-
l_Q	0.036	n	-	-
L_{MD}	0.02838	n	-	-
L_{MQ}	0.2836	n	-	-
r_D	0.0131	n	-	-
r_Q	0.054	n	-	-
D	2.004	y	2.004	2.5
P	0.03	y	0.0515	20
I	0.003	y	0.0021	14
P_ω	$1.096 \cdot 10^{-3}$	n	-	-
I_ω	$1.096 \cdot 10^{-5}$	n	-	-

Table 7: Model parameters

Minimization of the error function has been performed using the Asynchronous Parallel Pattern Search (APPS) method. APPS is a variation of parallel pattern search that uses parallel resources more efficiently by eliminating synchronization. It is important to note that the optimization problem is solvable with APPS method without explicit derivative information [50].

Other error function minimization methods (simplex, iterative) has also been tried, the APPS provide the shortest run time during the simulations because the APPS method change in parallel the values of the parameters of the synchronous generator. The APPS method can be used effectively in cascade control systems.

As the model is non-linear, the model is under closed-loop control and the input is not excited enough, the error function has a lot of local minima, while the optimization method has to search for the absolute minimum point of the error function. Figure 20 shows that the APPS method can find the absolute minimum of the error function.

Figure 17 and Figure 18 show the run of the APPS method in a two-dimensional sub-space dimensions of the parameter space. In Figure 17 the method has been started form the minimum point with $\pm 20\%$ changing of the P and I parameters. Note that one has to start the APPS method from different starting points because it is a local optimization method.

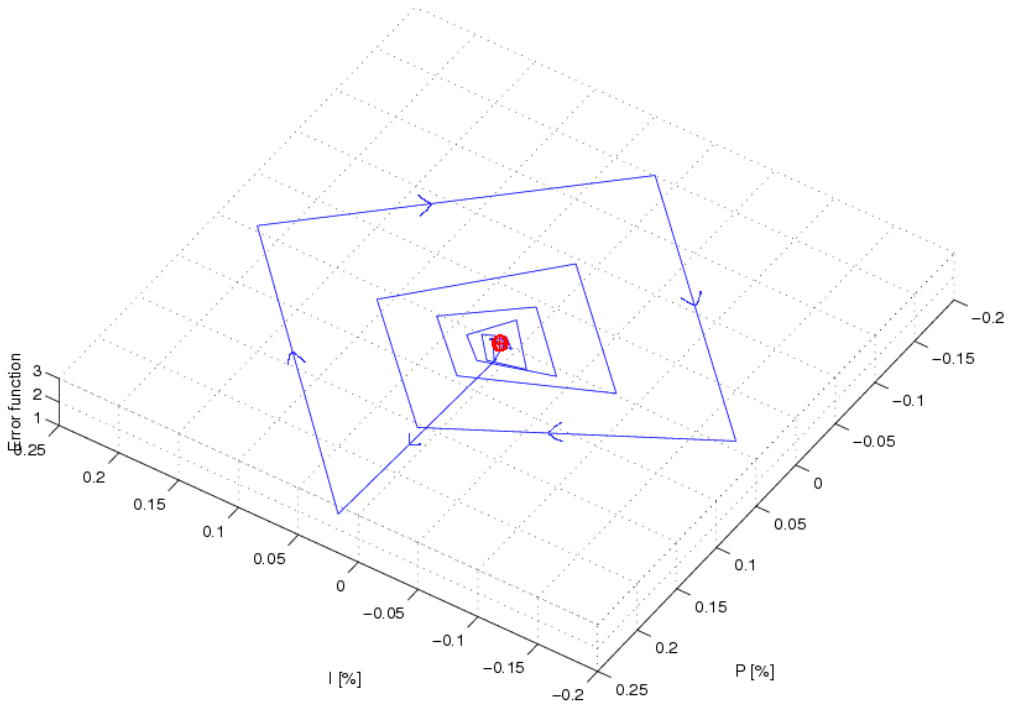

Figure 17: The operation of the APPS method. The figure shows the tested points and the value of the error function. The starting point was the same as the minimum value of the error function. The starting point is marked by a red cross, and the minimum point is marked by a red circle.

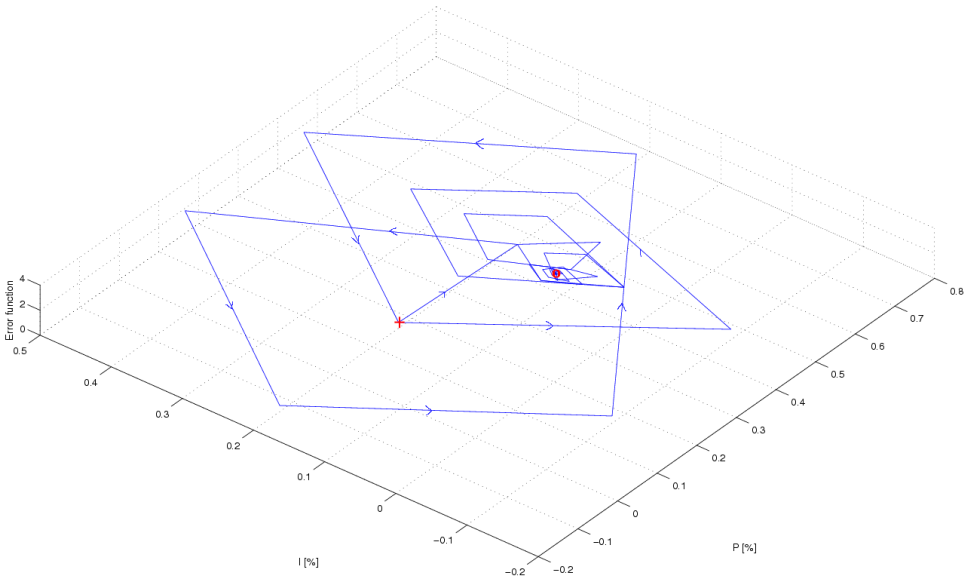

Figure 18: The operation of the APPS method. The figure shows the tested points and the value of the error function. The execution was tested by starting the method from the same starting point with different derivations. The starting point is marked by a red cross, the minimum value is marked by a red circe. The minimum point was the same point for each execution (see in Table (8)).

The dimension of the parameter space is nine, the search space has been constrained to nine-dimensional rectangle with the comer points

$$\boldsymbol{a}_{\%} = [\pm 5\% \quad \pm 20\% \quad \pm 10\% \quad \pm 5\% \quad \pm 5\% \quad \pm 5\% \quad \pm 10\% \quad \pm 80\% \quad \pm 80\%].$$

The initial point $\boldsymbol{p}_0$ was chosen as

$$\boldsymbol{p}_0 = [1.651 \quad 7.40 \cdot 10^{-4} \quad 1.096 \cdot 10^{-3} \quad 1.700 \quad 1.640 \quad 1.550 \quad 2.004 \quad 0.030 \quad 0.003],$$

where all coordinates are given in p.u. The result of the optimization i.e. the estimated parameters are given as the percent of change compared to the initial point:

$$\boldsymbol{p}_{\%} = [0 \quad -14.8\% \quad -0.5\% \quad 23.52\% \quad -6.95\% \quad 2.5\% \quad 0 \quad 71.66\% \quad -30\%].$$

Finally, the parameter values are given in p.u notation

$$\boldsymbol{p}_{p.u.} = [1.651 \quad 6.305 \cdot 10^{-4} \quad 1.09 \cdot 10^{-3} \quad 2.1 \quad 1.526 \quad 1.527 \quad 2.004 \quad 0.0515 \quad 0.0021].$$

The parameters were collected in Table 8 together with their search space, the constraints of which is given in the last column. The resulting estimated parameters are also shown in the table.

Parameter	Estimated value (p.u.)	Confidence (90%)	Domain (%)
L_F	1.651	3%	±10%
r_F	6.305 10^{-4}	3%	±40%
r	1.090 10^{-3}	4.9%	±20%
L_d	2.1	2.9%	±20%
L_q	1.526	1.2%	±15%
L_{AQ}	1.527	4.8%	±15%
D	2.004	2.5%	±45%
P	0.0515	20%	±30%
I	0.0021	14%	±30%

Table 8: Parameter estimation data

4.4 The quality of the estimated parameters

The quality of the estimated parameters were determined from the level sets of the error function, and from the quality of the fit.

4.4.1 Confidence regions in the parameter space

The quality of the estimated parameters has been examined from the shape of the estimation error function as functions of the parameters in the neighborhood of its minimum that belongs to the estimated values. The error function was plotted against two parameters with all the others fixed at their estimated values in Figs. 19, 20, 21 and 22. The dots denote the set of points where the error had been evaluated. The surface representing the error function has been fit on these points.

The confidence regions As the parameter estimation was based on optimization, no statistical properties of the estimation (e.g. covariance matrix, or confidence regions) could be obtained. However, a good approximation of the confidence region in the parameter space can be obtained by computing the $(1 + \alpha) \cdot V_{min}$ level set of the estimation error function, where V_{min} is its minimum value, and $(1 - \alpha) \cdot 100$ is the confidence level [39]. With this, a conservative approximation of the individual confidence intervals of the parameters can be obtained by projecting the confidence region to the one-dimensional parameter sub-space. The obtained approximate individual confidence intervals are also collected in Table 8 at the 90% confidence level (i.e. $\alpha = 0.1$).

It is important to note that the confidence regions carry information about the information content of the measured data that were used for the parameter estimation, i.e. about the excitation of the system. In the case of sufficient excitation (i.e. good quality data) these regions are of elliptical shape.

Fig. 19 shows the estimation error as a function of the parameters L_F and r_F, together with their level sets, and the 95% and 90% confidence regions. Note that these regions have an exotic shape, and the individual confidence intervals for L_F

and r_F were determined so wide that the resulting rectangle completely covers the confidence region. In Figs. 19, 20, 21 and 22 the dark blue color represents the 90% confidence region and the blue color shows the 80% region. The bottom subfigures of Figs. 19 and 21 show the 95% and the 90% confidence regions.

The confidence interval of L_d and L_q is small which means that the estimation is sharp, as it is apparent in Fig. 21.

4.4.2 The quality of the fit

The quality of the SG model with its estimated parameters can be evaluated in the space of the output and state variables as signals, too. As the final aim of our study is to design controllers that control both the active and the reactive power, the quality of the obtained model is evaluated by comparing these measured signals with their simulated counterparts provided by the model.

The simulation results are shown in Fig. 23, where the active (p_{out}), reactive (q_{out}) power and the torque angle (δ) are shown. It is apparent that the model has an excellent fit with both the measured active and reactive power signal.

Note that the torque angle is a non-measured state variable that provides an insight on how the active power controller operates during a load changing transient.

The controller had to decrease the exciter voltage in such a great extent so that the simulated reactive power signal could follow the measured signal. This is the reason of the undesired large variation of the torque angle.

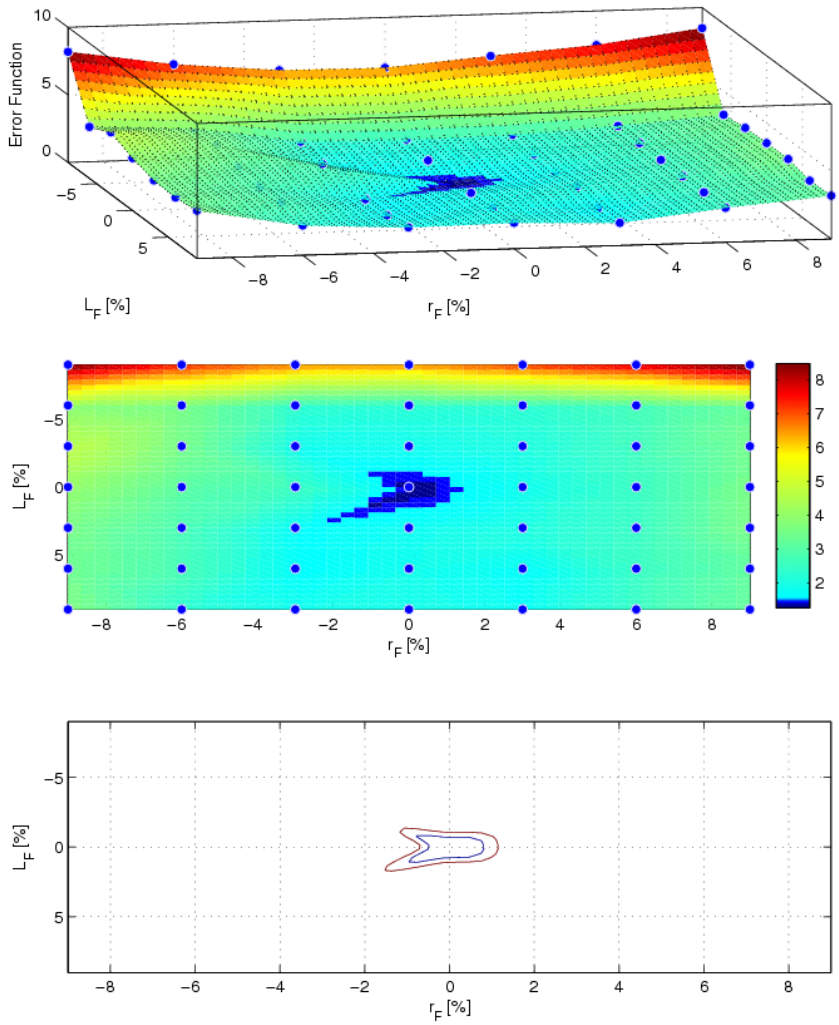

Figure 19: The value of the error function and confidence regions in the domain of ±9% changing of L_F and r_F and the confidence regions of L_F and r_F parameters. The dark blue color represents the 90% confidence region and the blue color shows the 80% region in the upper two subfigures. In the bottom figure the blue color represents the 95% confidence region and the red color shows the 90% region.

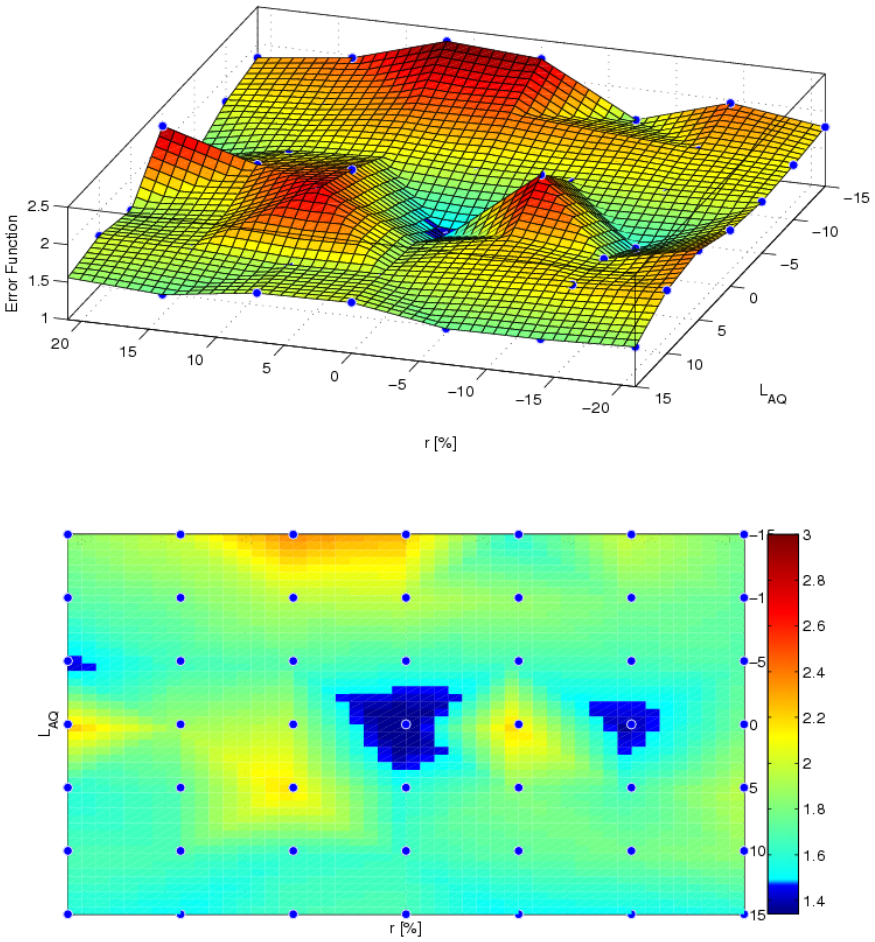

Figure 20: The value of the error function and confidence regions in the domain of $\pm 21\%$ changing of r and $\pm 15\%$ changing of L_{AQ} parameters. The dark blue color represents the 90% confidence region and the blue color shows the 80% region. As the model is non-linear, the model is under closed-loop control and the input is not excited enough the error function has a lot of local minima. The figure shows that the APPS method can find the absolute minimum of the error function.

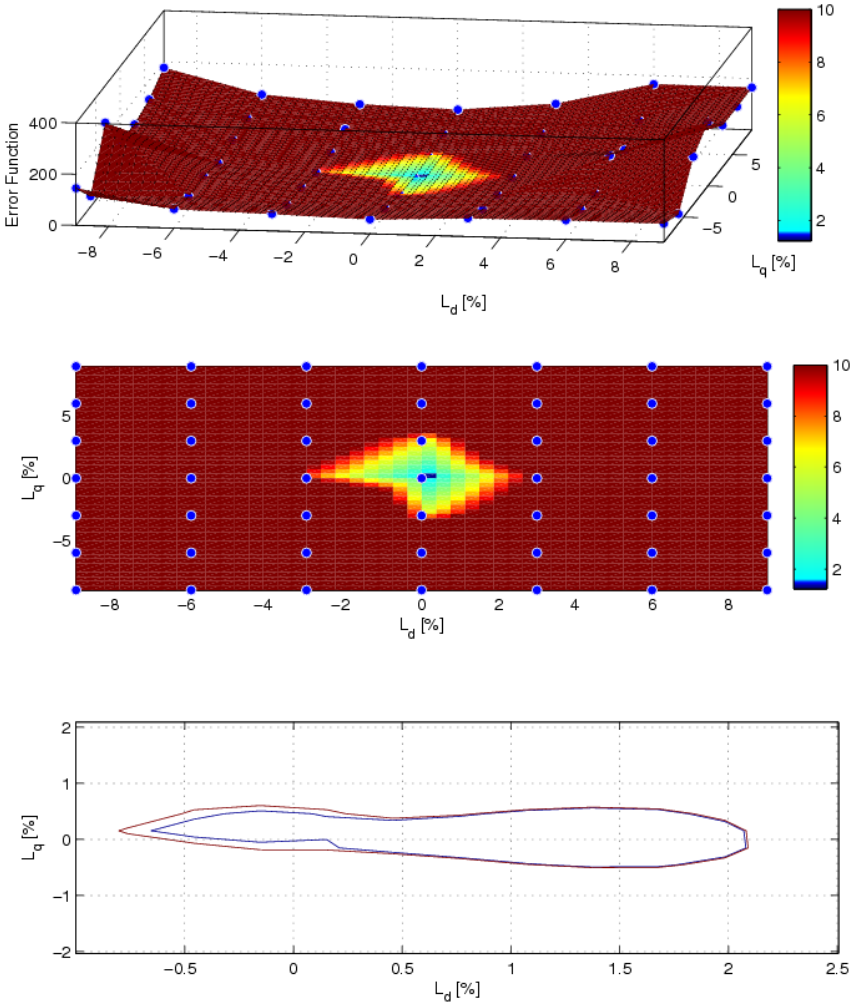

Figure 21: The value of the error function and confidence regions in the domain of ±9% changing of L_d and ±9% changing of L_q parameters. The dark blue color represents the 90% confidence region and the blue color shows the 80% region in the upper two subfigures. In the bottom figure the blue color represents the 95% confidence region and the red color shows the 90% region.

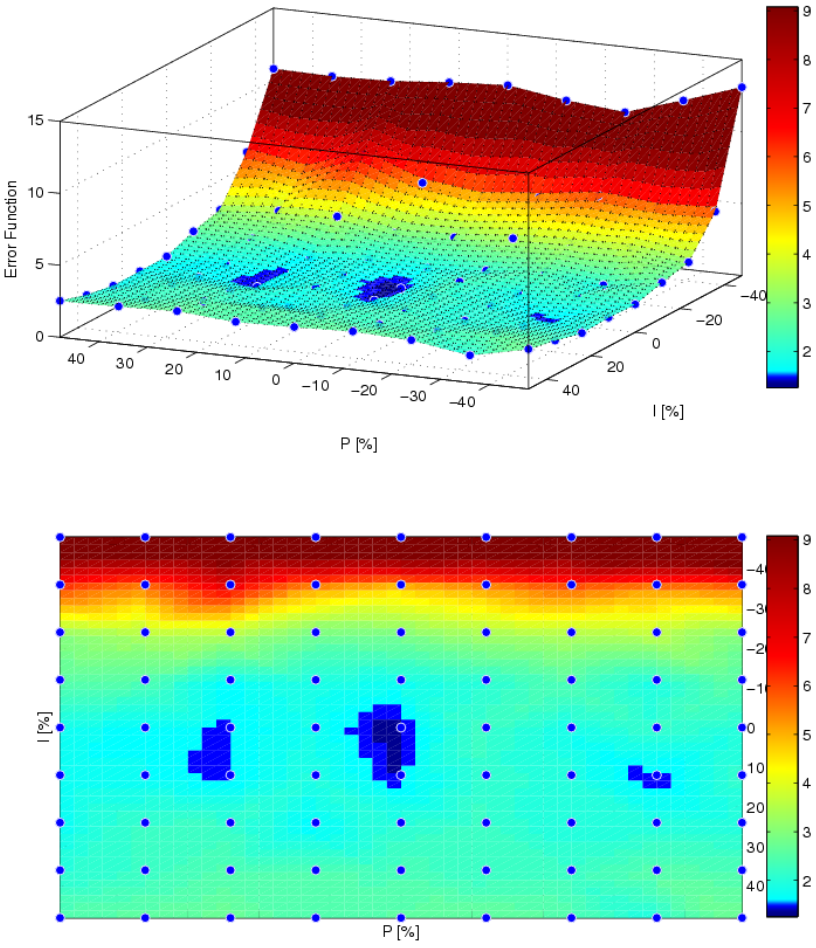

Figure 22: The value of the error function and confidence regions in the domain of $\pm 45\%$ changing of P and I parameters. The dark blue color represents the 90% confidence region and the blue color shows the 80% region.

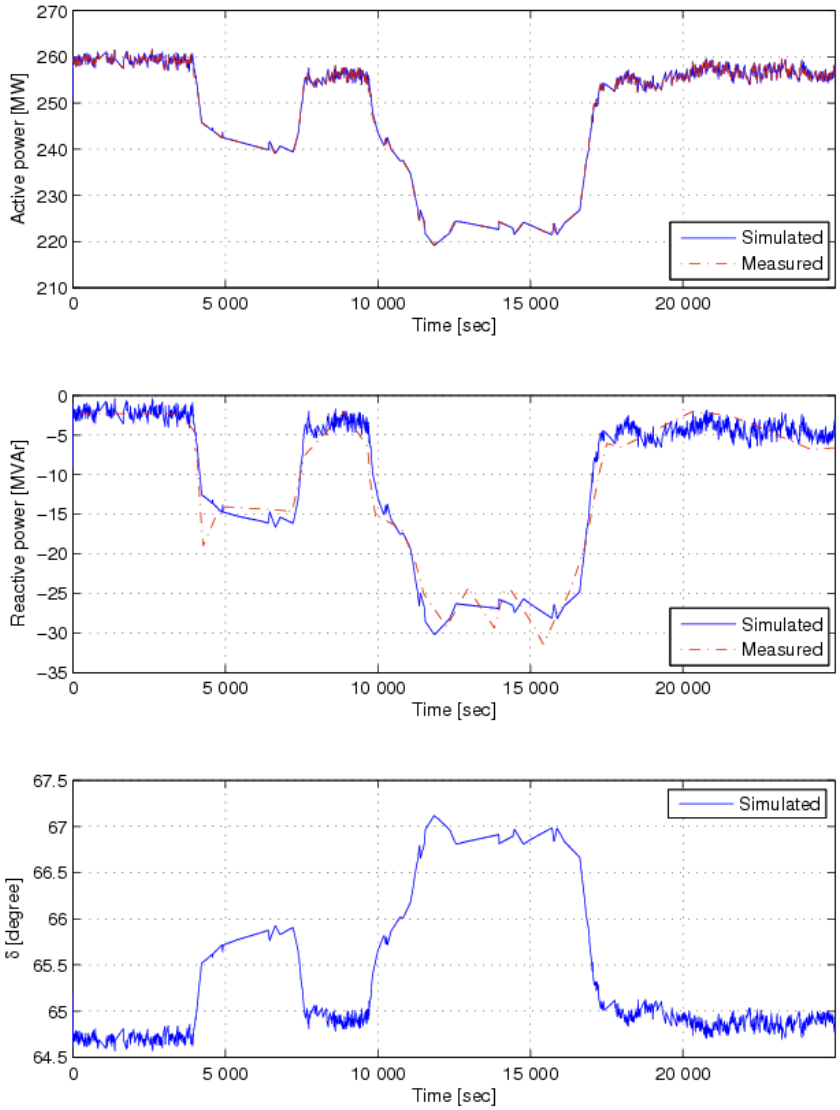

Figure 23: The simulated and measured active and reactive power, and the simulated torque angle

4.5 Summary

The new scientific results of this chapter are summarized here as follows.

A parameter estimation method using passive industrial measurement was proposed for a synchronous generator that uses passive measurement of power changing transients.

The results of the preliminary sensitivity analysis were refined by dynamical parameter sensitivity analysis.

The error function (V) and its weights were selected taking into account the measurement conditions (measurement frequency, accurancy and importance) of the involved signals in MVM Paks NPP. The quality of the error function (V) is verified by the fit of the measured and the simulated signals, as it is apparent in Fig. 23.

The parameter estimation was carried out by using the APPS method. The quality of the parameter estimation was characterized using the quality, the fit and the dependence of the error function on the parameters. The confidence region was also defined from the level sets of the error function.

Chapter 5

Observer based LQ-servo control of the synchronous generator

The advanced control design of the synchronous generators of power plants is far from being trivial because of the nonlinearity of the generator and the widely varied power demand of the consumers (see e.g. [53], [32], or [19] for recent studies).

Therefor, and because of the lack of reliable control oriented model of the industrial generators, the control studies of electrical machines are reported in the literature (Bansal [12], Basak et al. [14], Colak et al. [23], Hansen and Michalke [42], Kené et al. [49], Leon et al. [53], Lesani et al. [53], Liu et al. [54], Loukianov et al. [55], Malekpour et al. [57], de Mello et al. [25], Mi et al. [61], Mouni et al. [65], Qiao et al. [74], Rahman et al. [76], Ramtharan et al. [77], Molavi et al. [63], Verma et al. [96],), but do not deal with large synchronous generator which works in a NPP.

This chapter is denoted to the design and verification of a robust controller that is able to simultaneously control the active and reactive power even during a load changing transient.

5.1 The power control structure in MVM Paks NPP

This section describes the existing power structure in a block of MVM Paks NPP, and derives design specification of the proposed controller structure therefrom.

5.1.1 The existing controller structure

The power control of a unit in the Paks NPP is performed by three loosely coupled controllers: the power controller of the reactor, the turbine power controller and the generator exciter controller (see the technological schematic in Fig. 1 in Chapter 1 and the simplified schematic in Fig. 24). The synchronous generator has 2 controllers in Paks NPP: one PID (proportional-integral-derivative) controller regulates the speed (ω) of the axis using the manipulatable variable T_{mech} and oneother PID controller controls the active output power (p_{out}) of the generator by manipulating

the variable v_F. While the reactor power controller is mainly responsible to take care of the total power, the turbine controller regulates the frequency, and the generator exciter controller deals with maintaining the proper ratio of the active and reactive power.

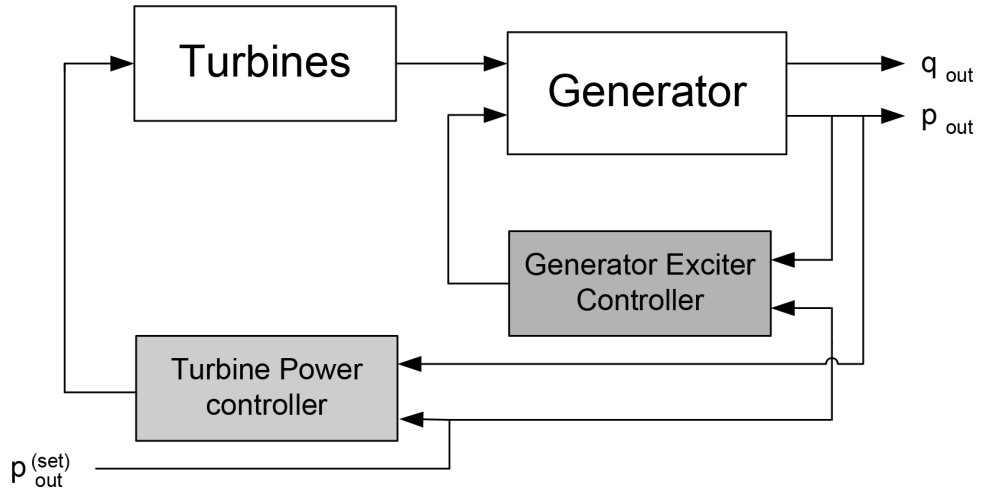

Figure 24: The simplified controller structure of the currently used controllers in MVM Paks NPP

The detailed model-based analysis of the reactor power controller of a unit in Paks NPP is reported in [35], that uses a simple dynamic model of the primary circuit based on first engineering principles.

5.1.2 Controller design specification

Despite of the conservatism in the filed of controlling safety critical systems, such as NPPs, numerous studies on advanced controllers are reported in the literature (Banavar et al. [11], Boroushaki et al. [19], Venayagamoorthy [95], Gábor et al [35]), the results indicate that advanced controllers can offer huge benefits for the controller structure of NPPs.

As the generator exciter controller operates relatively independently of the other two controllers involved in the power control, we aim at optimally re-design it using a simple control-oriented dynamic model in order to be able to maintain simultaneously the desired active and reactive power level even under power changing operation conditions (see Fig. 25).

The control aims and expectations against the controller can be summarized as follows.

- The performance output ($\boldsymbol{y}_{\text{perf}}$) of the system should follow the prescribed time varying piecewise constant reference signal, where

$$\boldsymbol{y}_{perf} = \begin{bmatrix} p_{out} \\ q_{out} \end{bmatrix}. \tag{101}$$

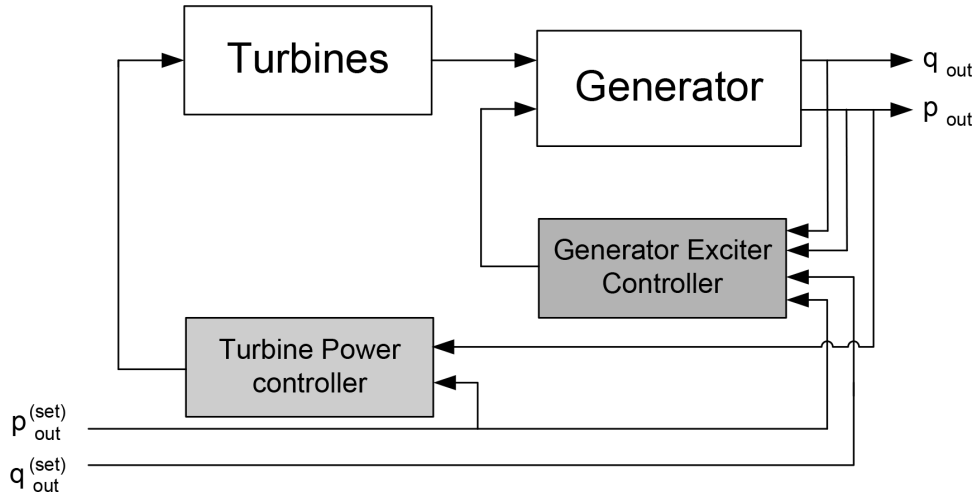

Figure 25: The simplified schematic of the redesigned new generator controller and the turbine controller

- It is convenient to define the measurable/computable state variables of the system (i_d, i_F , and i_q) to be the measured outputs of the system, i.e.

$$\boldsymbol{y}_{meas} = \begin{bmatrix} i_d \\ i_F \\ i_q \end{bmatrix}. \tag{102}$$

- The manipulated input vector ($\boldsymbol{u}$) of the generator is

$$\boldsymbol{u} = \begin{bmatrix} v_F \\ T_{mech} \end{bmatrix} \tag{103}$$

- The performance output ($\boldsymbol{y}_{\text{perf}}$) should be insensitive with respect to disturbance $\boldsymbol{d}$, where

$$\boldsymbol{d} = \begin{bmatrix} v_d \\ v_q \end{bmatrix} \tag{104}$$

  (see Eq. (73) in Chapter 2).)

- The closed loop system should be locally asymptotically stable.

The above aims suggest the use of LQ-servo technique for the controller design [10]. The choice is justified by the following properties of the LQ-servo method.

- It is a robust method, i.e. relatively insensitive for the difference between the linear and nonlinear models, moreover it performs trajectory tracking that was the primary control aim.

- It has good disturbance rejection properties.

As an additional aim, the controller designed in the sequel has to cope with industrial conditions which should be justified by controller verification using real measurement data from Paks NPP.

As an LQ-servo controller applies full state feedback and not all of the state variables are measurable, the need of designing a state observer [101], [68] also arises (see in Section 5.3).

5.2 The locally linearized model of the synchronous generator

The LQ-servo design is based on a locally linearized of the system to be controlled, this is presented here.

The steady-state values of the state variables can be obtained from the steady-state version of state equation (69) extended with the algebraic constraint defined by the steady state version of (65) using the above parameters. The equilibrium point of the system is found to be

$$\boldsymbol{x}^0 = \begin{bmatrix} i_d^0 \\ i_q^0 \\ i_F^0 \\ i_D^0 \\ i_Q^0 \end{bmatrix} = \begin{bmatrix} -1.75 \\ 0.79 \\ 2.98 \\ 1.24 \cdot 10^{-7} \\ 7.18 \cdot 10^{-8} \end{bmatrix} \tag{105}$$

The locally linearized state-space model has the form of (107), where the state vector $\boldsymbol{x}$ is the centered and truncated version of the state vector of the subset of the nonlinear model, i.e.

$$\boldsymbol{x} = \begin{bmatrix} i_d - i_d^0 \\ i_q - i_q^0 \\ i_F - i_F^0 \\ i_D - i_D^0 \\ i_Q - i_Q^0 \end{bmatrix}. \tag{106}$$

The two distinct output equations stand for the performance output and the measured output, respectively.

$$\begin{aligned} \frac{\mathrm{d}\boldsymbol{x}}{\mathrm{d}t} &= \boldsymbol{A}\,\boldsymbol{x} + \boldsymbol{B_u}\,\boldsymbol{u} + \boldsymbol{B_d}\,\boldsymbol{d} \\ \boldsymbol{y}_{\mathrm{meas}} &= \boldsymbol{C}_{\mathrm{meas}}\,\boldsymbol{x} \\ \boldsymbol{y}_{\mathrm{perf}} &= \boldsymbol{C}_{\mathrm{perf}}\,\boldsymbol{x} + \boldsymbol{D_u}\,\boldsymbol{u} + \boldsymbol{D_d}\,\boldsymbol{d}, \end{aligned} \tag{107}$$

where the matrix $\boldsymbol{A}$ is

$$\boldsymbol{A} = 10^{-3} \cdot \begin{bmatrix} -26.872 & 0.3249 & 10.564 & -2201.5 & -1947.7 \\ 9.26216 & -4.914 & 78.448 & 758.746 & 671.266 \\ 17.008 & 4.4313 & -94.124 & 1393.33 & 1232.69 \\ 11628.1 & 7836.3 & 7836.35 & -106.52 & 272.907 \\ -11635.7 & -7841.5 & -7841.5 & 106.585 & -308.47 \end{bmatrix}$$

and the $\boldsymbol{B_d}$, $\boldsymbol{B_u}$, $\boldsymbol{C}_{\mathrm{meas}}$, $\boldsymbol{C}_{\mathrm{perf}}$, $\boldsymbol{D_d}$ and $\boldsymbol{D_u}$ matrices are:

$$\boldsymbol{B_d} = \begin{bmatrix} -1.2742 & 0 \\ 0.4391 & 0 \\ 0.8064 & 0 \\ 0 & -5.0505 \\ 0 & 5.0538 \end{bmatrix} \quad \boldsymbol{B_u} = \begin{bmatrix} 0.4391 & -0.8620 \\ -6.6400 & 0.2971 \\ 5.9884 & 0.5455 \\ 0 & 1.4650 \\ 0 & -1.4659 \end{bmatrix}$$

$$\boldsymbol{C}_{\text{meas}} = \begin{bmatrix} 1 & 0 & 0 & 0 & 0 \\ 0 & 1 & 0 & 0 & 0 \\ 0 & 0 & 0 & 1 & 0 \end{bmatrix} \quad \boldsymbol{C}_{\text{perf}} = \begin{bmatrix} -0.6600 & -0.2804 \\ 0 & 0 \\ 0 & 0 \\ 0.2804 & -0.6600 \\ 0 & 0 \end{bmatrix}^T$$

$$\boldsymbol{D_d} = \begin{bmatrix} -0.8774 & 0.3927 \\ 0.3927 & 0.8774 \end{bmatrix} \quad \boldsymbol{D_u} = \begin{bmatrix} 0 & 0 \\ 0 & 0 \end{bmatrix}.$$

5.3 State observer design

The concept of state feedback controllers is a very powerful method of control of a wide class of linear or nearly linearized systems. In practice applications, however, the state variables of the system are seldom available for feedback. As, in order to implement state feedback we must somehow obtain the state variables from the input and output signals of the system [87]. The observers can reconstruct us the values of the state variables.

The primary task of the observer is to determine the estimated value of the state vector $\boldsymbol{x}_{\text{obs}}$ from the measured output $\boldsymbol{y}_{\text{meas}}$. The proposed observer is designed by pole placement technique using the system parameters $\boldsymbol{A}$, $\boldsymbol{B_u}$ and $\boldsymbol{C}_{\text{meas}}$. The poles $\boldsymbol{\lambda}_{\text{obs}}$ of the observer error dynamics are designed to be faster (108) than the locally linearized system's poles in order that the error transients decay faster than the system transients. Therefore, the poles of the observer are chosen to be

$$\boldsymbol{\lambda}_{\text{obs}} = \begin{bmatrix} -5 \\ -6 \\ -7 \\ -8 \\ -10 \end{bmatrix}. \tag{108}$$

The observer structure can be seen in Figure 26, where the observer gain matrix $\boldsymbol{L}_{\text{obs}}$ has the following value

$$\boldsymbol{L}_{\text{obs}} = \begin{bmatrix} 12.1913 & -1.4484 & -10.3415 & 8.5417 & -39.2208 \\ 0.3850 & 7.6033 & 1.1784 & 7.9901 & -5.1052 \\ 0.1961 & 0.0263 & 8.1142 & 14.9986 & -13.4230 \end{bmatrix} \tag{109}$$

5.4 LQ servo controller design

The LQ-servo control itself is based on the extension of the linear model (107) with a tracking error variable $\boldsymbol{z}$ that represents the difference between the reference input

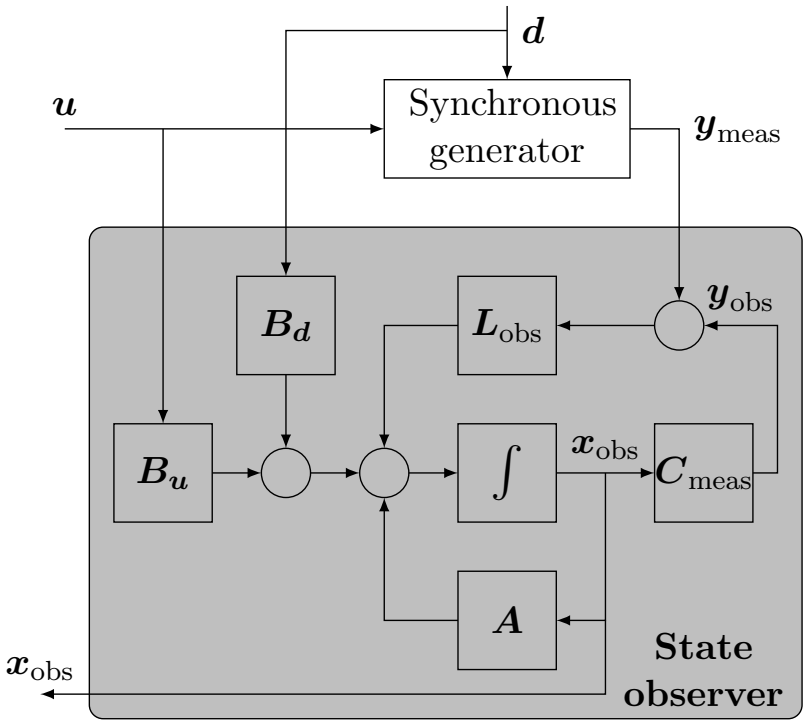

Figure 26: State observer structure for the synchronous generator

$\boldsymbol{r}_{\text{in}}$ and the performance output $\boldsymbol{y}_{\text{perf}}$. The extended state equation has the form: (110)

$$\begin{array}{rcl} \dfrac{\mathrm{d}\boldsymbol{x}}{\mathrm{d}t} & = & \boldsymbol{A}\,\boldsymbol{x} + \boldsymbol{B_u}\,\boldsymbol{u} + \boldsymbol{B_d}\,\boldsymbol{d} \\ \dfrac{\mathrm{d}\boldsymbol{z}}{\mathrm{d}t} & = & \boldsymbol{r} - \boldsymbol{y}_{\text{perf}} = \boldsymbol{r}_{\text{in}} - \boldsymbol{C}_{\text{perf}}\,\boldsymbol{x} - \boldsymbol{D_u}\,\boldsymbol{u} - \boldsymbol{D_d}\,\boldsymbol{d} \end{array} \quad . \tag{110}$$

The extended state equation in block matrix form is given by equation (111) below where $\tilde{\boldsymbol{x}} = \left[\begin{array}{c|c} \boldsymbol{x} & \boldsymbol{z} \end{array}\right]^T$

$$\frac{\mathrm{d}\tilde{\boldsymbol{x}}}{\mathrm{d}t} = \left[\begin{array}{c|c} \boldsymbol{A} & \boldsymbol{0} \\ \hline -\boldsymbol{C}_{\text{perf}} & \boldsymbol{0} \end{array}\right] \tilde{\boldsymbol{x}} + \left[\begin{array}{c} \boldsymbol{B_u} \\ \hline -\boldsymbol{D_u} \end{array}\right] \boldsymbol{u} + \left[\begin{array}{c} \boldsymbol{B_d} \\ \hline -\boldsymbol{D_d} \end{array}\right] \boldsymbol{d} + \left[\begin{array}{c} \boldsymbol{0} \\ \hline \boldsymbol{I} \end{array}\right] \boldsymbol{r}_{\text{in}} \ . \tag{111}$$

The structure of the LQ-servo control loop can be seen in Figure 27, where the inner loop is the stabilizing state feedback controller, and the outer integrating loop implements the reference tracking (servo) control.

As in the case of LQR design, the objective function to be minimized with respect to (111) is a functional of the form

$$J(\tilde{\boldsymbol{x}}, \boldsymbol{u}) = \int_0^\infty (\tilde{\boldsymbol{x}}^T\,\boldsymbol{Q}\,\tilde{\boldsymbol{x}} + \boldsymbol{u}^T\,\boldsymbol{R}\,\boldsymbol{u})\,\mathrm{d}t. \tag{112}$$

The design parameters of the LQ controller design method are the positive definite symmetric quadrature matrices $\boldsymbol{Q}$ and $\boldsymbol{R}$, where $\boldsymbol{Q}$ penalizes the state, and $\boldsymbol{R}$ penalizes the input variable. Of course, the compromise between the state signal

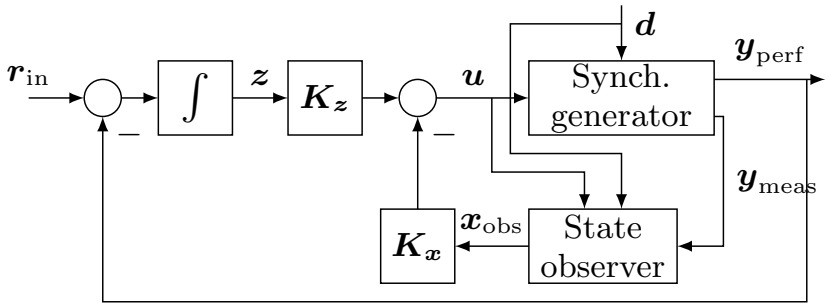

Figure 27: Observer based LQ-servo controller structure

norm (tracking quality of the control) and the input signal norm (cheapness of the control) has to be found. The state and input penalty factors were chosen to be

$$\boldsymbol{Q} = 100 \cdot \begin{bmatrix} 1 & 0 & 0 & 0 & 0 & 0 & 0 \\ 0 & 1 & 0 & 0 & 0 & 0 & 0 \\ 0 & 0 & 1 & 0 & 0 & 0 & 0 \\ 0 & 0 & 0 & 1 & 0 & 0 & 0 \\ 0 & 0 & 0 & 0 & 1 & 0 & 0 \\ 0 & 0 & 0 & 0 & 0 & 100 & 0 \\ 0 & 0 & 0 & 0 & 0 & 0 & 10 \end{bmatrix},$$

$$\boldsymbol{R} = \begin{bmatrix} 1 & 0 \\ 0 & 1 \end{bmatrix}. \tag{113}$$

The last two diagonal elements of $\boldsymbol{Q}$ in (113) are the penalties of the tracking error variable $\boldsymbol{z}$. The feedback gain that minimizes (112) with respect to (111) and governs the extended system to its equilibrium is in block matrix form $\boldsymbol{K} = \left[\begin{array}{c|c} \boldsymbol{K_x} & \boldsymbol{K_z} \end{array}\right]$ with numerical values (114):

$$\begin{aligned} \boldsymbol{K_x} &= \begin{bmatrix} -401.3310 & -378.4688 & -375.2029 & 119.7380 & 138.7553 \\ -252.8653 & -174.3798 & -174.6745 & 38.8057 & 68.5166 \end{bmatrix}, \\ \boldsymbol{K_z} &= \begin{bmatrix} -99.6438 & -2.6667 \\ -8.4329 & 31.5101 \end{bmatrix}. \end{aligned} \tag{114}$$

5.5 LQ servo controller verification

In order to verify the designed controller the transient response and the tracking properties have been checked.

5.5.1 Verification using step signals

During the normal operation of the NPP, step-type reference changes are used according to the load changes between day and night operation. Therefore the active power reference tracking experiments have been performed using step signals. The result of the time domain analysis can be seen in Figure 28, where the transient response and reference tracking of p_{out}, and q_{out} is apparent. The reference of q_{out}

was chosen to be constant zero. It can be clearly seen that the MIMO controller enables the treatment of active and reactive power independently (to some extent), as opposed to the original PI control scheme (Figure 2). The controller's robustness with respect to realistic (step-type) changes in the disturbance signal $\boldsymbol{d}$ (Eq. (104)) has also been examined; the LQ-servo compensates the step-type disturbances at time 250 and time 450 satisfactorily. The closed loop system's local asymptotic stability is guaranteed by the LQ method.

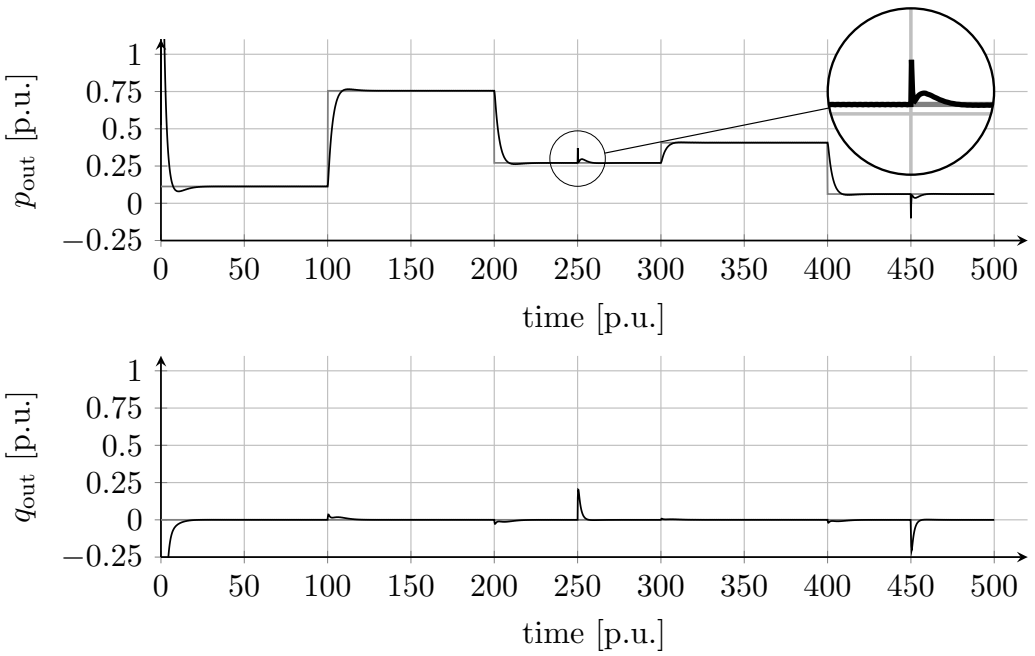

Figure 28: Transient response and reference tracking of active and reactive power. The disturbance rejection properties have also been examined using step-like changes of the disturbances v_d and v_q at time 250 (highlighted) and time 450, respectively.

5.5.2 Verification using measured data

The measured data of the generator #1 in Figure 2 (see in Chapter 1) were used for verification in such a way that the active power reference signal was set equal to the measured one, and the reactive power reference was to be zero.

The simulation results using measured data are shown in Figure 29, where the controller generated active (p_{out}) and reactive (q_{out}) power are shown. It is apparent that the designed controller has an excellent fit with both the simulated active and reactive power signal. The measured input data of the generator contains the effect of the disturbance by the infinite huge electrical network, but this disturbance apparently does not influence the stability of the designed LQ controller.

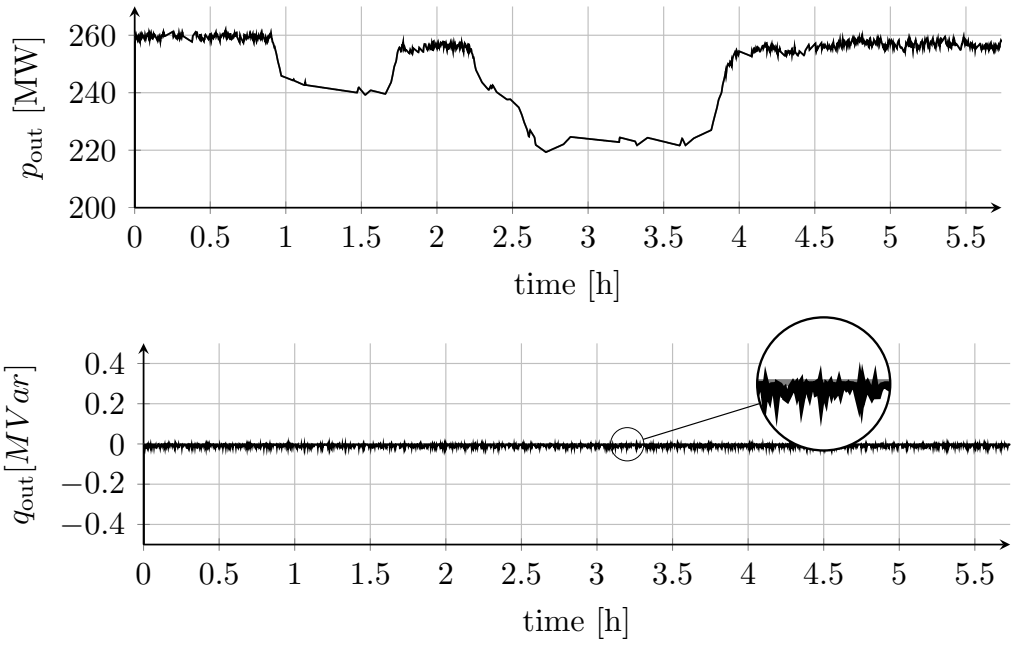

Figure 29: Transient response and reference tracking of active and reactive power on valid data from Paks NPP.

5.6 Summary

The servo version of a Linear Quadratic Regulator (LQR) has been proposed for control of the industrial synchronous generator operating in MVM Paks NPP.

The linearized version of the generator model was used for the design in a predefined operating point.

A state observer has also been designed for the controller using the pole placement design technique. The proposed LQ-servo controller was verified by simulation using step changes in active power and a good tracking property was observed in a wide operating region. The controller is also robust against step-like disturbances arising from the wide area network.

Chapter 6

Conclusion and further work

A simple bi-linear dynamic model of an industrial size SG operating in a nuclear power plant is proposed in this dissertation. The simple dynamic model is based on first engineering principles that describes the mechanical phenomena together with the electrical model.

The developed model has been verified under the usual controlled operating conditions when the angular speed and the effective power are controlled. A preliminary sensitivity analysis augmented by the sensitivity analysis of the estimation error has been applied to determine the model parameters to be estimated out of the possible 23 model parameters.

The selected model parameters have been estimated using measured data from an industrial generator operating in a nuclear power plant applying the asynchronous parallel pattern search method that minimizes the estimation error as a function of the parameters. The confidence regions in the parameter space have been analyzed by investigating the geometry of the estimation error function. The quality of the model has been evaluated by the fit in the effective and reactive power, and a good fit could be achieved.

Furthermore, an LQ-type multiple-input multiple-output controller has also been presented that does not only control active power of a synchronous generator, but can follow the reactive power demand, as well. This fits well into the recent trends in electrical energy market, where it is more widely accepted that consumers pay for the reactive power support service.

The developed controller is based on a locally linearized model of the SG operating in the MVM Paks NPP, and applies a state observer for its realization. The proposed controller was verified by simulation using artificial step changes and real load changing signals, and good tracking and robustness properties were observed.

The proposed approaches and methods can easily be applied to any industrial power plant generator connected to the electrical grid, if one follows the parameter estimation procedure suggested in [O5] that only uses passive transient measured data.

6.1 New scientific results

Model analysis, verification, parameter estimation and control methods were developed and presented in this work for an industrial synchronous generator that operates in MVM Paks Nuclear Power Plant. The new scientific results presented in this work are summarized in this section. They are arranged in three thesis points as follows.

Thesis 1. I have proposed simple but effective model analysis methods for model verification and for preliminary parameter selection for the parameter estimation of the investigated synchronous generator ([O1], [O2], [O3] and [O5], Chapter 3).

(i) I have proposed simple step changes in exciter voltage, in active power and in the network disturbances together with local stability analysis for model verification. It was shown, that the proposed simple methods of the model analysis are suitable for model verification.

(ii) I have selected all parameters of the developed dynamic model of the generator for sensitivity analysis, where I have investigated the sensitivities of both state variables and outputs. Based on the result of the sensitivity analysis I have defined 4 groups of parameters: Not sensitive, Less sensitive, More sensitive and Critically sensitive. I have selected seven parameters of the model (L_F, r_F, r, L_d, L_q, L_{AQ}, D) and two parameters of the controllers (P, I) to parameter estimation based on the results of this analysis.

Thesis 2. I have proposed a parameter estimation method using passive industrial measurements of a load changing transient for the synchronous generator. ([O5] and Chapter 4).

(i) I have refined the results of the preliminary sensitivity analysis based on dynamical parameter sensitivity analysis using passive measurement of one power changing transient and I have selected nine parameters (L_F, r_F, r, L_d, L_q, L_{AQ}, D, P and I) for estimation.

(ii) I have selected the error function (V) and its weights according to the measurement and data collection properties of data in MVM Paks NPP. The quality of the error function (V) resulted in a good fit of the measured and the simulated signals.

(iii) The parameter estimation was carried out by using the APPS method. I have characterized the quality of the parameter estimation using the quality of the fit and the dependence of the error function on the parameters. I have estimated also the confidence region from the level sets of the error function.

Thesis 3. I have proposed a suitably designed observer-based LQ-servo controller for controlling both the active and reactive power of the synchronous generator of MVM Paks Nuclear Power Plant (NPP) ([O8], [O6] and Chapter 5).

(i) The design has been based on locally linearized version of the nonlinear state space model of the SG. I have designed also a state observer for the controller using the pole placement design technique.

(ii) I have verified the proposed LQ-servo controller based on simulation using step changes in active power and I have observed a good tracking property in a wide operating region. The controller is also robust against step-like disturbances arising from the wide area network.

6.2 Further work

The work presented in this thesis has opened the door for improving and extending the model analysis and control design of synchronous machines in the following important directions.

The first direction for further work includes the investigation of the effect of the synchronous generator and its re-designed exciter controller in MVM Paks NPP as a fundamental part of the overall control scheme of a NPP block (or unit). For this purpose, the dynamic model of the SG should be integrated with the already existing control-oriented model of the primary circuit, and a simple dynamic model of the turbine and its controller should also be developed.

The other future research direction would be the extension of the dynamic model of the SG with failure mode description, and investigate the possibility to design advanced fault sensitive observers for fault detection and diagnosis purposes.

The proposed model analysis, parameter estimation and control design tools can also be relatively easily generalized to other types of electrical machines, such as synchronous motors, and asynchronous generators and motors, as well. Further work along this line is already in progress (see [O10]).

Finally, the proposed controller design was based on a locally linearized model of the SG, that has limited the operation domain and robustness of the developed controller. The use of the original bi-linear state space model of the SG could open the possibility to apply advanced nonlinear feedback design approaches, such as passivity or control Lyapunov function based controllers (see [O7]).

6.3 Own Papers

Bibliography

[O1] Attila Fodor, Attila Magyar, and Katalin M. Hangos. Dynamic modeling and analysis of a synchronous generator in a nuclear power plant. *International PhD Workshop on Systems and Control, Hluboka nad Vltavou, Czech Republic, ISBN: 978-80-903834-3-2*, 91–96, 2009.

Cited by:

B. Pan, J. Sun, and L. F. Lou. Dynamic modeling, simulation and test verification for a drive mechanism of a generator. *Zhendong yu Chongji/Journal of Vibration and Shock 30(5):236–241, 2011.*

D-H. Wang and X-D. Shi. System performance analysis for a metal plate spring vibration isolator. Zhendong yu Chongji/Journal of Vibration and Shock 30(5):263–266, 2011.

T. Lin and L. Lou. Research on the Testing Experiment of Torsion Vibration of Transmission Shaft Aviation Generator. *Zhendong yu Chongji/Journal of Vibration and Shock 30(5):40–43, 2010.*

[O2] Attila Fodor, Attila Magyar, and Katalin M. Hangos. Dynamic modeling and model analysis of a large industrial synchronous generator. *Proc. of Applied Electronics 2010, Pilsen, Czech Republic, ISBN 978-80-7043-865-7, ISSN: 1803–7232*, 91–96, 2010.

[O3] Attila Fodor, Attila Magyar, and Katalin M. Hangos. Parameter sensitivity analysis of a synchronous generator. *Hungarian Journal of Industrial Chemistry, ISSN: 0133-0276*, 38(1):21–26, 2010.

[O4] Attila Fodor, Attila Magyar, and Katalin M. Hangos. Parameter sensitivity analysis of an industrial synchronous generator. *11th International PhD Workshop on Systems and Control 2010, Veszprém, Magyarország, ISBN: 978-615-5044-00-7*, 2010.

[O5] Attila Fodor, Attila Magyar, and Katalin M. Hangos. Control-oriented modeling of the energy-production of a synchronous generator in a nuclear power plant. *Energy, **IF 3.565***, 39:135–145, DOI = 10.1016/j.energy.2012.01.054, 2012.

Cited by:

R. A. Jouneghani. Distributed Energy Storage Systems: Microgrid Application, Market-Based Optimal Operation and Harmonic Analysis PhD Dissertation *Virginia Polytechnic Institute and State University*, 2013

[O6] Attila Fodor, Attila Magyar, and Katalin M. Hangos. MIMO LQ control of the energy production of a synchronous generator in a nuclear power plant. *Chemical Engineering Transactions (ISSN 1974-9791)*, 29:361–366, 2012.

Cited by:

Y. Langeron, A. Grall, and A. Barros A. Actuator health prognosis for designing LQR control in feedback systems. *Chemical Engineering Transactions* 33:979–984, 2013

[O7] Attila Magyar and Attila Fodor. Quasi-polynomial control of a synchronous generator. *Hungarian Journal of Industry and Chemistry, ISSN: 0133-0276*, 41(1):51–57, 2013.

[O8] Attila Fodor, Attila Magyar, and Katalin M. Hangos. MIMO LQ control of the energy production of a synchronous generator in a nuclear power plant. *Electric Power Components and Systems,* ***IF: 0.62***, 42(15):1673–1682, DOI = 10.1080/15325008.2014.950359, 2014.

[O9] Péter Görbe, Attila Magyar, Attila Fodor, and Katalin M. Hangos. Experimental study of the nonlinear distortion caused by domestic power plants. *Applied Thermal Energy,* ***IF: 3.107***, 70(2):1288–1293, DOI = 10.1016/j.applthermaleng.2014.05.072, 2014.

Cited by:

H.L. Lam, P.S. Varbanov, J.J. Klemes Applied Thermal Engineering towards sustainable development *Applied Thermal Energy* 70(2):1051–1055, 2014

[O10] Attila Fodor, Roland Bálint, Attila Magyar and Gábor Szederkényi. Stability and Parameter Sensitivity Analysis of an Induction Motor. *Hungarian Journal of Industry and Chemistry, ISSN: 0133-0276*, 42(2):109–113, 2014.

Chapter 7

Appendix

7.1 Abbreviations

APPS	Asynchronous Parallel Pattern Search
BDF	Backwards Differentiation Formula
CCS	Computer Control System
EMF	Electromagnetic Field
IM	Induction Motor
LQ	Linear-Quadratic
LQR	Linear-Quadratic Regulator
MIMO	Multiple-Input Multiple-Output
NPP	Nuclear power plant
PID	Proportional-Integral-Derivative
p.u.	Per Unit, Base quantities
RMS	Root Mean Square
SG	Synchronous generator
SM	Synchronous machine

7.2 Notation list

The vectors by boldface, the matrices with capital boldface letters are denoted.

$\boldsymbol{A}$, $\boldsymbol{B}_u$ and $\boldsymbol{C}_{\text{meas}}$	Controlled system parameters
$\boldsymbol{a}_{\%}$	The boundaries of the parameter space
C_{Speed}	Normalized cost function value of the speed controller
$C_{ActivePower}$	Normalized cost function value of the active power controller
$\tilde{\boldsymbol{d}}_d$	Vector of measured signals
$\boldsymbol{d}_d$	Vector of simulated signals
D	Damping constant
H	Inertia constant
i_0	Zero-sequence current of the stator
$\boldsymbol{I}_3$	3x3 unit matrix
i_a, i_b and i_c	Stator phase currents
$\boldsymbol{i}_{0dq}$ and $\boldsymbol{i}_{dq}$	Stator current vectors
$\boldsymbol{i}_{abc}$	Stator phase current vector

i_d and i_q	Stator current d and q component
i_D and i_Q	Currents of amortisseur winding
$\boldsymbol{i}_{FDQ}$	Rotor current vector
i_F	Exciter (field) current
$\tilde{i_F}$	Measured exciter (field) current
i_{out}	Stator current
$\tilde{i_{out}}$	Measured stator current
J	LQ controller error function
$k = \sqrt{3/2}$	
$\boldsymbol{K}$	Controller feedback gain matrix
$\boldsymbol{K}_x$	Controller feedback gain submatrix
$\boldsymbol{K}_z$	Controller feedback gain submatrix
$\boldsymbol{L}$	Inductance matrix of the SG model
$\tilde{\boldsymbol{L}}$	Inductance matrix of the SG model which connected to an infinitely large network
$L_{AD} = kM_D$	Amortisseur winding linkage inductances
$L_{AF} = kM_F$	Field linkage inductance
$L_{AQ} = kM_Q$	Amortisseur winding linkage inductances
L_{AD} and L_{AQ}	Mutual inductances
L_d and L_q	d and q component of stator inductance
$\tilde{L_d}$ and $\tilde{L_q}$	d and q component of modified stator inductance
L_D and L_Q	Inductances of amortisseur winding
l_d and l_q	Linkage inductances
l_F, l_D and l_Q	Linkage inductances
L_F	Rotor inductance
L_{FB}	Rotor inductance, base unit
L_n	Inductance of the neutral point
L_m, L_{MD} and L_{MQ}	Mutual inductances
$\boldsymbol{L}_{\text{obs}}$	Observer gain matrix
L_{RR}, L_{ss}	Rotor-rotor, stator-stator self inductances
L_{Rs}, L_{sR}	Rotor-stator, stator-rotor, inductances
M_D, M_Q, M_F and M_s	Mutual inductances
$\boldsymbol{n}$	Signal normalization vector
N	Number of measurement points
$\boldsymbol{n}_{0dq}$ and $\boldsymbol{n}_{dq}$	Neutral voltage vectors
r	Stator resistance
n_{sample}	Number of the sample points of the simulation
$\boldsymbol{R}$	Input penalty factors
$\boldsymbol{R}_{abc}$	Stator phase resistance matrix
R_B and L_B	Base resistance and inductance
R_e and L_e	Line resistance and inductance
r_F, r_D and r_Q	Rotor resistances
R_{FB}	Rotor base resistance
$\boldsymbol{R}_{FDQ}$	Rotor resistance matrix

$\boldsymbol{r}_{\text{in}}$	Reference input of the LQR
r_n	Resistance of the neutral point
$\boldsymbol{R}_{RS\omega}(\omega)$	Submatrix of SG model
$\tilde{\boldsymbol{R}}_{RS\omega}(\omega)$	Submatrix of SG model which connected to an infinitely large network
$\boldsymbol{P}$	Park Transformation Matrix
P, I	Active power controller parameters
$\boldsymbol{p}_0$	Initial point of the parameter estimation
P_ω, I_ω	Speed controller parameters
p_{out}	Active power
$\tilde{p_{out}}$	Measured active power
$\boldsymbol{p}_{p.u.}$	Vector of the values of parameters
$\boldsymbol{p}_{\%}$	Vector of the percent change parameters
$\boldsymbol{Q}$	State penalty factors
q_{out}	Reactive power
$\tilde{q_{out}}$	Measured reactive power
S_B	Rated power, base quantity
t_B	Time, base
T_{Damp}	Damping torque
T_{Electr}	Electrical torque
T_{Mech}	Mechanical torque
$\boldsymbol{y}_{perf}$	Performance output vector
Θ	Angle between the phase axis a and the axis d
V	Error function for parameter estimation
v_0	Zero-sequence voltage of the stator
$\boldsymbol{v}_{0dq}$ and $\boldsymbol{v}_{dq}$	Stator voltage vectors
v_a, v_b and v_c	Phase stator voltages
$\boldsymbol{v}_{abc}$	Phase stator voltage vector
V_B and I_B	Stator voltage and current, base
v_d and v_q	Stator voltage, d and q component
v_F	Exciter (field) voltage
$\tilde{v_F}$	Measured exciter (field) voltage
$\boldsymbol{v}_{FDQ}$	Rotor voltage vector
V_{FB} and I_{FB}	Rotor voltage and current, base
V_{min}	Minimum value of the error function
$\boldsymbol{v}_n$	Neutral voltage
v_∞	Voltage of the network
$\boldsymbol{v}_{\infty abc}$ and $\boldsymbol{v}_{\infty 0dq}$	Voltage of the network
$\boldsymbol{w}$	Signal weight vector
$\boldsymbol{x}$	Vector of state variables
$\tilde{\boldsymbol{x}}$	Extended vector of state variables
$\boldsymbol{x}_{\text{obs}}$	State vector of the observer
$\boldsymbol{y}_{\text{meas}}$	Measured output
$\boldsymbol{z}$	Tracking error variable
δ	Torque angle
λ_0	Zero-sequence stator flux

$\boldsymbol{\lambda}_{0dq}$ and $\boldsymbol{\lambda}_{\boldsymbol{dq}}$	Stator flux vectors
λ_a, λ_b and λ_c	Stator phase fluxes
$\boldsymbol{\lambda}_{abc}$	Stator phase flux vector
λ_d and λ_q	d and q component of stator flux
λ_D and λ_Q	d and q component of the flux of amortisseur winding
λ_F	Flux of the exciter winding
$\boldsymbol{\lambda}_{FDQ}$	Rotor flux vector
$\boldsymbol{\lambda}_{\text{obs}}$	Poles of the observer
$\tau_j = 2H\omega_B$	
ω	Angular velocity
$\tilde{\omega}$	Measured angular velocity
ω_B	Angular velocity, base
ω_{pv}	Process value of the angular velocity
ω_r	Rated synchronous angular velocity
ω_{sv}	Set value of the speed controller

Bibliography

[1] KFKI Verona System. http://www.kfki.hu/~aekihp/arlhome/html/verona-1.html/.

[2] MVM Paks Nuclear Power Plant. http://paksnuclearpowerplant.com/, http://www.atomeromu.hu/.

[3] S. Achilles and M. Pöller. Direct drive synchronous machine models for stability assessment of wind farms. *Proceedings of 4th International Workshop Large Scale Integration of Wind Power and Transmission Networks for Offshore Windfarms*, 2003.

[4] J. Alvarez-Ramirez, H. Puebla, and G. Espinosa. A cascade control strategy for a space nuclear reactor system. *Annals of Nuclear Energy*, 28:93–112, 2001.

[5] H. Amaris and M. Alonso. Coordinated reactive power management in power networks with wind turbines and facts devices. *Energy Conversion and Management*, 52(7):2575–2586, 2011.

[6] P. M. Anderson, B. L. Agrawal, and J. E. Van Ness. *Subsynchronous Resonance in Power Systems*. IEEE Press, New York, 1990.

[7] P. M. Anderson and A. A. Fouad. *Power Systems Control and Stability*. The IOWA State University Press, Ames Iowa, 1977.

[8] M. A. Arjona, R. Escarela-Perez, G. Espinosa-Perez, and J. Alvarez-Ramirez. Validity testing of third-order nonlinear models for synchronous generators. *Electronic Power System Research*, 79:953–958, 2009.

[9] K. J. Aström and B. Wittenmark. *Computer-Controlled Systems Theory and Design*. Tsinghua University Press, Prentice Hall, 1994.

[10] M. A. Athans and P. L. Falb. *Optimal Control*. McGraw-Hill, New York, 1966.

[11] R. N. Banavar and U. V. Deshpande. Robust controller design for a nuclear power plant using h-infinity optimization. *Proc. of the 35th Conference on Decision and Control, Kobe, Japan*, pages 4474–4479, 1996.

[12] R. C. Bansal. Automatic reactive-power control of isolated wind-diesel hybrid power systems. *IEEE Transaction on Industrial Electronics*, 53:1116–1126, August 2006.

[13] A. Barakat, S. Tnani, G. Champenois, and E. Mouni. Analysis of synchronous machine modeling for simulation and industrial applications. *Simulation Modelling Practice and Theory*, 18(9):1382–1396, 2010.

[14] P. Basak, S. Chowdhury, S. Halder nee Dey, and S. P. Chowdhury. A literature review on integration of distributed energy resources in the perspective of control, protection and stability of microgrid. *Renewable and Sustainable Energy Reviews*, 16(8):5545–5556, 2012.

[15] Gy. Bebesi. *A hosszú 19. század rövid története.* Pácsi Tudományegyetem, Pécs, 2010.

[16] W. Böhm. *Villamos hajtások.* Műszaki Könyvkiadó, Budapest, 1982.

[17] I. Boldea. *Synchronous generators.* CRC Press Taylor & Francis Group, 2006.

[18] Oskar Bolza. *Vorlesungen über Variationsrechnung.* BoD–Books on Demand, 2013.

[19] M. Boroushaki, M. B. Ghofrani, C. Lucas, and M. J. Yazdanpanah. An intelligent nuclear reactor core controller for load following operations, using recurrent neural networks and fuzzy systems. *Annals of Nuclear Energy*, 30:63–80, 2003.

[20] Yang Cao, Shengtai Li, Linda Petzold, and Radu Serban. Adjoint sensitivity analysis for differential-algebraic equations: The adjoint dae system and its numerical solution. *SIAM Journal on Scientific Computing*, 24(3):1076–1089, 2003.

[21] M. Caracotsios and W. E. Stewart. Sensitivity analysis of initial value problems with mixed ode's and algebraic equations. In *Mathematics Research Center Report No 2777, University of Wiscosin, Madison*, 1984.

[22] Makis Caracotsios and Warren E Stewart. Sensitivity analysis of initial value problems with mixed odes and algebraic equations. *Computers & Chemical Engineering*, 9(4):359–365, 1985.

[23] I. Colak, R. Bayindir, and O. Bay. Reactive power compensation using a fuzzy logic controlled synchronous motor. *Energy Conversion and Management*, 44:2189–2204, 2003.

[24] M. E. Coultes and W. Watson. Synchronous machine models by standstill frequency response tests. *IEEE Transactions on Power Apparatus and Systems*, PAS-100:1480–1489, 1981.

[25] F. P. de Mello and C. Concordia. Concepts of synchronous machine stability as affected by excitation control. *IEEE Transaction on Power Apparatus and Systems*, PAS-88:316–329, 1969.

[26] S. E. M. de Oliveira and J. A. de Souza. Effect of field-voltage source impedance on load-rejection test results of large-rating synchronous generators. *IEEE Transactions on Energy Conversion,*, 26(1):30–35, 2011.

[27] M. Dehghani and S. K. Y. Nikravesh. Nonlinear state space model identification of synchronous generators. *Electronic Power System Research*, 78:926–940, 2008.

[28] A. B. Dehkordi, A. M. Gole, and T. L. Maguire. Permanent magnet synchronous machine model for real-time simulation. In *International Conference on Power Systems Transients (IPST' 05) in Montreal, Canada*, June 19-23, 2005.

[29] M. Dittmar. Nuclear energy, status and future limitations. *Energy*, 37(1):35–40, 2012.

[30] S. O. Emeka. Dynamics of a turbo-generator driven by dc motors during off-line three-phase sudden short circuit. *Electric Power Components and Systems*, 39:16:1828–1844, 2011.

[31] Cs. Fazekas, G. Szederkényi, and K. M. Hangos. A simple dynamic model of the primary circuit in vver plants for controller design purposes. *Nuclear Engineering and Design*, 237:1071–1087, 2007.

[32] L. Fernandez, C. Garcia, and F. Jurado. Comparative study on the performance of control systems for doubly fed induction generator (dfig) wind turbines operating with power regulation. *Energy*, 33 (9):1438–1452, 2008.

[33] L. M. Fernandez, C. A. Garcia, and F. Jurado. Operating capability as a pq/pv node of a direct-drive wind turbine based on a permanent magnet synchronous generator. *Renewable Energy*, 35(6):1308–1318, 2010.

[34] Santos Galán, William F Feehery, and Paul I Barton. Parametric sensitivity functions for hybrid discrete/continuous systems. *Applied Numerical Mathematics*, 31(1):17–47, 1999.

[35] A. Gábor, I. Sonnevend, and T. Bartha. Control-oriented modelling of the primary circuit and its controllers of a PWR nuclear power plant. *9th European Workshop on Advanced Control and Diagnosis, ACD*, 2011.

[36] F. M. Gonzalez-Longatt, P. Wall, and V. Terzija. A simplified model for dynamic behavior of permanent magnet synchronous generator for direct drive wind turbines. *PowerTech, 2011 IEEE Trondheim*, pages 1–7, 2011.

[37] S. Halász. *Villamos hajtások*. Rotel, Budapest, 1993.

[38] K. M. Hangos, J. Bokor, and G. Szederkényi. *Analysis and Control of Nonlinear Process Systems*. Springer, 2004.

[39] K. M. Hangos and I. T. Cameron. *Process Modelling and Model Analysis*. Academic Press, London, 2001.

[40] K. M. Hangos, R. Lakner, and M. Gerzson. *Intelligent Control Systems: An Introduction with Examples*. Kluwer Academic Publisher, 2001.

[41] Ralf Hannemann-Tamás. *Adjoint Sensitivity Analysis for Optimal Control of Non-Smooth Differential-Algebraic Equations*. Shaker Varlag, 2012.

[42] A. D. Hansen and G. Michalke. Modelling and control of variable-speed multi-pole permanent magnet synchronous generator wind turbine. *Wind Energy*, 11(5):537–554, 2008.

[43] M. Hasni, O. Touhami, R. Ibtiouen, M. Fadel, and S. Caux. Synchronous machine parameter estimation by standstill frequency response tests. *Journal of Electrical Engineering*, 59(2):75–80, 2008.

[44] Edward J Haug and Paul E Ehle. Second-order design sensitivity analysis of mechanical system dynamics. *International Journal for Numerical Methods in Engineering*, 18(11):1699–1717, 1982.

[45] M. Huang, W. Li, and W. Yan. Estimating parameters of synchronous generators using square-root unscented kalman filter. *Electronic Power System Research*, 80:1137–1144, 2010.

[46] IAEA. Pressurized water reactor simulator. *IAEA-TCS-22, ISSN 1018-5518, IAEA, Vienna*, 2003.

[47] Magyar Villamosenergia ipari Átviteli Rendszerirányító ZRt. (MAVIR). A Magyar Villamosenergia-rendszer Forrásoldali Kapacitáselemzése. Online: http://www.mavir.hu/c/document_library/get_file?uuid=9947ea21-a555-4c17-986b-ba9d5be91d6e&groupId=10258, 2011.

[48] Á. Jamniczky. *Villamos gépek üzemtana*. Veszprémi Egyetem, Veszprém, 1984.

[49] G. Kenné, R. Goma, H. Nkwawo, F. Lamnabhi-Lagarrigue, A. Arzandé, and J. C. Vannier. Real-time transient stabilization and voltage regulation of power generators with unknown mechanical power input. *Energy Conversion and Management*, 51(1):218–224, 2010.

[50] T. G. Kolda. Revisiting asynchronous parallel pattern search for nonlinear optimization. *SIAM Journal on Optimization*, 16(2):563–586, 2005.

[51] E. Kyriakides and G. T. Heydt. Estimation of synchronous generator parameters using an observer for damper currents and a graphical user interface. *Electronic Power System Research*, 69:7–16, 2004.

[52] R. Leine and H. Nijmeijer. *Dynamics and bifurcations of non-smooth mechanical systems*, volume 18. Springer Science & Business, 2013.

[53] A. Leon, J. Solsona, J. Figueroa, and M. Valla. Optimization with constraints for excitation control in synchronous generators. *Energy*, 36 (8):5366–5373, 2011.

[54] W. Liu, G. K Venayagamoorthy, and D. C. Wunsch. A heuristic-dynamic-programming-based power system stabilizer for a turbogenerator in a single-machine power system. *IEEE Transaction on Industry Applications*, 41(5):1377–1385, 2005.

[55] A. Loukianov, J. M. Canedo, V. I. Utkin, and J. Cabrera-Vazquez. Discontinuous controller for power systems: sliding-mode bock control approach. *IEEE Transactions on Industrial Electronics*, 51:340–353, 2004.

[56] S. H. Shin J. W. Jang K. B. Lee M. G. Na, D. W. Jung and Y. J. Lee. A model predictive controller for loadfollowing operation of pwr reactors. *IEEE Transactions on Nuclear Science*, 52:1009–1020, 2005.

[57] A. R. Malekpour and T. Niknam. A probabilistic multi-objective daily volt/var control at distribution networks including renewable energy sources. *Energy*, 36(5):3477–3488, 2011.

[58] Timothy Maly and Linda R Petzold. Numerical methods and software for sensitivity analysis of differential-algebraic systems. *Applied Numerical Mathematics*, 20(1):57–79, 1996.

[59] V. Mehrmann and L. Wunderlich. Hybrid systems of differential-algebraic equations–analysis and numerical solution. *Journal of Process Control*, 19(8):1218–1228, 2009.

[60] J. J. R. Melgoza, G. T. Heydt, A. Keyhani, B. L. Agrawal, and D. Selin. Synchronous machine parameter estimation using the hartley series. *IEEE Transactions on Energy Conversion*, 16(1):49–54, 2001.

[61] C. Mi, M. Filippa.and J. Shen, and N. Natarajan. Modeling and control of a variable-speed constant-frequency synchronous generator with brushless exciter. *IEEE Transactions on Industry Applications*, 40(2):565–573, 2004.

[62] F. Milano. *Power System Modelling and Scripting*. Springer, ISBN: 978-3-642-13668-9 (Print), 978-3-642-13669-6 (Online), 2010.

[63] R. Molavi and D. A.. Khaburi. Optimal control strategies for speed control of permanent-magnet synchronous motor drives. *Proceedings of World Academy of Science*, 34:428–462, 2008.

[64] T. W. Mon and M. M. Aung. Simulation of synchronous machine in stability study for power system. *World Academy of Science, Engineering and Technology*, 39:128–133, 2008.

[65] E. Mouni. and S. Tnani.and G. Champenois. Synchronous generator output voltage real-time feedback control via H_∞ strategy. *IEEE Transactions on Energy Conversion*, 24(2):329–337, 2009.

[66] E. Mouni, S. Tnani, and G. Champenois. Synchronous generator modelling and parameters estimation using least squares method. *Simulation Modelling Practice and Theory*, 16(6):678–689, 2008.

[67] S. Nanou, G. Tsourakis, and C. D. Vournas. Full-converter wind generator modelling for transient stability studies. *PowerTech, 2011 IEEE Trondheim*, pages 1–7, 2011.

[68] R. Neimeier, G. Schulz-Ekloff, T. Vielhaben, and G. Thiele. A nonlinear observer for the iron-catalysed hydrogen peroxide decomposition in a continuous stirred tank reactor. *Chemical Engineering and Technology*, 20(6):391–395, 1997.

[69] Gy. Németh and Gy. W. Hegyi. *Görög-római történelem.* Osiris Kiadó, Budapest, 2011.

[70] R. H. Park. Two-reaction theory of synchronous machines generalized method of analysis-part I. *Transactions of the American Institute of Electrical Engineers*, 48(3):716–727, 1929.

[71] A Perdana. *Dynamic Models of Wind Turbines (Degree of Doctor of Philosophy).* Chalmers University of Technology, ISBN: 978-91-7385-226-5, 2008.

[72] P. Prempraneerach, F. S. Hover, M. S. Triantafyllou, C. Chryssostomidis, and G. E. Karniadakis. Sensitivity analysis and low-dimensional stochastic modeling of shipboard integrated power systems. *IEEE Power Electronics Specialists Conference, 2008. PESC 2008.*, pages 1999–2003, 2008.

[73] P. Prempraneerach, F. S. Hover, M. S. Triantafyllou, C. Chryssostomidis T. J. Mccoy, and G. E. Karniadakis. Sensitivity analysis of the shipboard integrated power system. *Naval Engineers Journal*, 120(1):109–121, 2008.

[74] W. Qiao, L. Qu, and R. G. Harley. Control of IPM Synchronous Generator for Maximum Wind Power Generation Considering Magnetic Saturation. *42nd IAS Annual Meeting Industry Applications Conference Conference Record of the 2007 IEEE*, pages 1265–1272, 2007.

[75] K. M. Rahman and S. Hiti. Identification of machine parameters of a synchronous motor. *IEEE Transactions on Industry Applications*, 41(2):557–565, 2005.

[76] M. F. Rahman, Md. E. Haque, Lixin Tang, and Limin Zhong. Problems associated with the direct torque control of an interior permanent-magnet synchronous motor drive and their remedies. *IEEE Transactions on Industrial Electronics*, 51(4):799–809, 2004.

[77] G. Ramtharan, N. Jenkins, and O. Anaya-Lara. Modelling and control of synchronous generators for wide-range variable-speed wind turbines. *Wind Energy*, 10(3):231–246, 2007.

[78] H. Raoufi and M. Kalantar. Reactive power rescheduling with generator ranking for voltage stability improvement. *Energy Conversion and Management*, 50(4):1129–1135, 2009.

[79] James D Riley, Morris M Bennett, and Emily McCormick. Numerical integration of variational equations. *Mathematics of Computation*, pages 12–17, 1967.

[80] Sz. Rozgonyi and K. M. Hangos. Domain of attraction analysis of a controlled hybrid reactor model. *Annals of Nuclear Energy*, 38:969–975, 2011.

[81] AI Ruban. Sensitivity coefficients for discontinuous dynamic systems. *Journal of Computer and Systems Sciences International*, 36(4):536–542, 1997.

[82] Adrian Sandu. Reverse automatic differentiation of linear multistep methods. In *Advances in Automatic Differentiation*, pages 1–12. Springer, 2008.

[83] Adrian Sandu and Philipp Miehe. Forward, tangent linear, and adjoint runge–kutta methods for stiff chemical kinetic simulations. *International Journal of Computer Mathematics*, 87(11):2458–2479, 2010.

[84] Martin Schlegel, Wolfgang Marquardt, Rainald Ehrig, and Ulrich Nowak. Sensitivity analysis of linearly-implicit differential–algebraic systems by one-step extrapolation. *Applied Numerical Mathematics*, 48(1):83–102, 2004.

[85] A. Semlyen, J. F. Eggleston, and J. Arrillaga. Admittance matrix model of a synchronous machine for harmonic analysis. *IEEE Transactions on Power Systems*, 2(4):833–839, 1987.

[86] S.-H. Seong and S.-O. Kim. Performance evaluation of control strategies for power maneuvering event of the KALIMER-600. *Annals of Nuclear Energy*, 42:50–62, 2012.

[87] N. K. Sinha. *Control Systems*. CBS College Oublishing, New York, 1986.

[88] A. Soto-Cota, A. G. Loukianov, J. M. Canedo, and L. M. Fridman. Variable structure control of synchronous generator: singularly perturbed analysis. *International Journal of Control*, 79(1):1–13, 2006.

[89] X. Tu, L. A. Dessaint, M. E. Kahel, and A. Barry. Modeling and experimental validation of internal faults in salient pole synchronous machines including space harmonics. *Mathematics and Computers in Simulation*, 71(4-6):425–439, 2006. Modeling and Simulation of Electric Machines, Converters and Systems.

[90] P. Vas. *Vector Control of a.c. machines*. Oxford University Press, 1990.

[91] P. Vas. *Electrical machines and drives: a space-vector theory approach*. Oxford University Press, 1992.

[92] P. Vas. *Parameter estimation, condition monitoring and diagnosis of electical machines*. Oxford University Press, 1993.

[93] P. Vas. *Sensorless Vector and Direct Torque Control*. Oxford University Press, 1998.

[94] P. Vas. *Artifical-intelligence-Based Electrical Machines and Drives*. Oxford University Press, 1999.

[95] G. K. Venayagamoorthy and R. G. Harley. Two separate continually online-trained neurocontrollers for excitation and turbine control of a turbogenerator. *IEEE Transactions on Industry Applications*, 38(3):887–893, 2002.

[96] K. Verma and K. Niazi. A coherency based generator rescheduling for preventive control of transient stability in power systems. *International Journal of Electr Power and Energy Systems*, 45:10–18, 2013.

[97] R. Wamkeue, F. Baetscher, and I. Kamwa. Hybrid-state-model-based time-domain identification of synchronous machine parameters from saturated load rejection test records. *IEEE Transactions on Energy Conversion*, 23(1):68–77, 2008.

[98] R. Wamkeue, C. Jolette, and I. Kamwa. Advanced modeling of a synchronous generator under line-switching and load-rejection tests for isolated grid applications. *IEEE Transactions on Energy Conversion*, 25(3):680–689, 2010.

[99] R. Wamkeue, I. Kamwa, and X. Dai-Do. Short-circuit test based maximum likelihood estimation of stability model of large generators. *IEEE Transactions on Energy Conversion*, 14(2):167–174, 1999.

[100] W. Watson and G. Manchur. Synchronous machine operational impeadances from low voltage measurements at the stator terminals. *IEEE Transactions on Power Apparatus and Systems*, PAS-93:777–784, 1973.

[101] G. Wozny, G. Fieg, L. Jeromin, and H. Gülich. Design and analysis of a state observer for the temperature front of a retification column. *Chemical Engineering and Technology*, 12(1):339–344, 1989.

[102] H. Xiong, H. Cheng, and H. Li. Optimal reactive power flow incorporating static voltage stability based on multi-objective adaptive immune algorithm. *Energy Conversion and Management*, 49(5):1175–1181, 2008.

[103] W. Xiu and Y. Liao. Accurate transmission line fault location considering shunt capacitances without utilizing line parameters. *Electric Power Components and Systems*, 39:16:1783–1794, 2011.